Final Technical Report

to

National Aeronautics and Space Administration

NASA Grant No. NAG 5-919

Remote Measurement of Soil Moisture Over Vegetation Using Infrared Temperature Measurements

Submitted by:

Dr. Toby N. Carlson

Department of Meteorology
The Pennsylvania State University
University Park, PA 16802

January 1991

1. Introduction

This final report summarizes research work performed between the inception of this grant in 1986 and the present. The underlying motivation for all the work was to develop better methods for remote sensing of surface evapotranspiration, soil moisture and fractional vegetation cover. Details and results are to be found in several journal articles and four theses. In the interest of brevity, we will refer directly to these publications, which are attached as appendices, and to their figures. These papers are, respectively: Appendix A (Carlson and Buffum, 1989); Appendix B (Lynn and Carlson, 1990); Appendix C (Carlson et al., 1990); Appendix D (Carlson et al., 1991). Additional publications generated by this grant and referred to in subsequent sections consist of reviewed publications (Carlson and Lynn, 1991; Carlson, 1991; Andre et al., 1988), one publication under review (Carlson and Lynn, 1991) and theses (Buffum, 1988; Lynn, 1989; Belles, 1990).

Objectives of our research were (1) to further develop a model of water movement through the soil\plant\atmosphere system, (2) to use this model, in conjunction with measurements of infrared surface temperature and vegetation index, to calculate soil water content and vegetation fraction, (3) to determine the magnitude of radiometric temperature response to water stress in vegetation, (4) to show at what point one can detect that sensitivity to water stress, and (5) to determine the practical limits of the methods. A new approach, undertaken during this past year, was to develop a hydrological model that can be used to calculate soil water content versus depth given conventional meteorological records and observations of vegetation cover. We will now outline the results of these initiatives.

2. Projects Undertaken

(a) Large-scale evapotranspiration measurements

We investigated the method developed by Jackson et al. (1977) to determine daily evapotranspiration from a single radiometric surface temperature made near mid day. The idea was to use our plant/soil/atmosphere model to simulate radiometric surface temperatures and to see if we could reproduce the experimental results and find the same numerical values for the coefficients in the formulae given in the literature (Jackson, 1977; Seguin and Itier, 1983). Our results (summarized in Appendix A (Carlson and Buffum, 1989) and in Buffum (1988) show that the model yields very similar coefficients to that of Jackson et al. (1977) for vegetation and Seguin and Itier (1983) for bare soil. Surface roughness and wind speed also exert an important effect on the coefficients.

We show, however, that it is not necessary to specify more than two or three wind speed and roughness categories in order to achieve a useful accuracy. The method confirms that it is theoretically possible to determine the net soil water loss by evapotranspiration using a midday radiometric surface temperature. However, since the coefficients for vegetation and bare soil are so different, one should also have knowledge of the vegetation fraction. Carlson and Buffum (1989) also present a variation of the method which does not require air temperature. In it, one substitutes for the air

temperature a second surface radiometric temperature during the morning to obtain a rate of morning increase in temperature.

b) Modeling the plant canopy

Much of our modeling effort has been devoted to improving the vegetation component of the model. A serious deficiency in using radiometric temperature to infer soil water content in the presence of vegetation is that, according to both observations and simulations, the radiometric surface temperature of a vegetation canopy tends to vary only slightly as a function of soil water content over a wide range of the latter. Typically, vegetation canopies appear "cool" (within a couple degrees centigrade of air temperature) until some low value of soil water content is reached, below which the leaves may warm rapidly with decreasing soil water content. This suggests, that plants may transpire at nearly an optimum rate until urgent water stress signals are received from the roots.

In order to approach this problem it was necessary to rethink our parameterization of stomatal resistance. Many stomatal resistance models, such as the one we had previously used, either fail to account for the lack of sensitivity of stomatal behavior to soil water content or are unable to describe the effects of transient stress in which leaf temperature can temporarily rise in response to excessive atmospheric demand in the face of reduced soil moisture.

Our present plant model incorporates a more mechanistic approach than before. By mechanistic we mean that the model accounts for internal plant mechanisms, rather than simply calculating the surface energy fluxes, as in some of the bulk evapotranspiration methods. At the same time we have made the model as deterministic as possible. By deterministic, we mean a mathematical description of the evapotranspiration as a function of external conditions or internally calculable or prescribed variables. To some extent, the idea of a mechanistic model is an elusive one, since any model must inevitably simplify the infinitely complex biochemical processes that constitute the plant mechanisms. Nevertheless, there is at present a hierarchy of mechanistic complexity in plant models, extending from simple turbulent transfer equations that take no account of the water supply in plants to ones which treat the biological functions of the leaves, stem and roots.

The new stomatal resistance model reported by Lynn and Carlson (1990; Appendix B) simulates a rich variety of plant behavior, including transient effects of water stress caused by a excess atmospheric demand. It does this by allowing stomatal resistance to depend on the (epidermal) leaf water potential, subject to a threshold leaf water potential below which the stomatal resistance increases rapidly with decreasing leaf water potential. Although the dependence of stomatal resistance on leaf water potential is questioned by many plant scientists, there is considerable experimental evidence to suggest that the loss of turgor pressure in the leaf epidermis (guard cells) causes a rapid increase in stomatal resistance with decreasing epidermal water potential below a threshold epidermal water potential and a corresponding decrease in transpiration on the scale of a field (Federer, 1980; Nizinski and Saugier, 1989; Katerji, 1990; Carlson et al., 1991; Appendix C). Our simulations (Figure 1) show that the epidermal water potential and vapor pressure deficit effects on stomatal resistance are intertwined.

Inclusion of the threshold leaf water potential in the stomatal resistance model allows the latter to simulate transient periods of plant water stress, which can occur even when the soil is well watered provided that the atmospheric demand is large. Figure 14 in Appendix B shows two evapotranspiration curves made over adjacent corn fields, one irrigated and the other non-irrigated. Neither soil was excessively dry. Both evapotranspiration curves are identical except during a few hours when the evapotranspiration over the dry field exhibited a plateau (or"hat"), signifying a limitation in the plant's rate of water loss. The hat can be simulated by imposing a threshold epidermal water potential (ψ_c), in this case of -13 bars. Figure 9 in Appendix B shows the sensitivity of stomatal resistance and transpiration to the choice of threshold leaf water potential. (Henceforth, unless otherwise stated, we will interchange the terms, evapotranspiration and transpiration, realizing that the two are similar over dense vegetation.) Not surprisingly, the threshold leaf water potential is a crucial parameter in the model. Typically, this value of ψ_c is about -15 bars in most temperate crops, but it can vary from -9 bars to -25 bars, depending on species.

The transpiration plateau occurs as follows: a decrease of the epidermal leaf water potential (to more negative values) occurs during the morning because the transpiration is increasing. Depending on atmospheric demand (essentially solar flux and vapor pressure deficit) and the soil water content, the epidermal leaf water potential may reach the threshold value. The greater the atmospheric demand, the larger the threshold water potential or the lower the soil moisture the more likely it is that the leaf water potential will reach the threshold and the longer the threshold will last.

When the epidermal water potential reaches the threshold, stomatal resistance increases rapidly with a further decrease in leaf water potential (reversing a decrease with time); this may lead to a "bump" in the stomatal resistance, as shown by both the (HAPEX) measurements and the simulations in Figure 12 of Appendix B. Because of a concomitant increase in vapor pressure deficit (between the leaf and its surroundings), due to the warming of the leaves, the increase in stomatal resistance is offset by an increase in atmospheric demand; the resultant effect of reaching the threshold leaf water potential on transpiration is a plateau rather than a collapse of the transpiration or even a decrease; the complex feedback between various mechanisms is captured by the model, showing that the plant makes optimum use of water in order to avoid becoming desiccated with increasing atmospheric demand.

The point to be made here is that water stress is relative, and the rise in leaf (and therefore canopy) temperature depends as much on atmospheric demand in the face of plant constraints as on the soil water content. Before complete wilting occurs, however, the transient stress, manifested by the "hat" results in an augmentation in the increase of leaf temperature, thereby affording an early warning of plant water stress through its detection by radiometer; this subject is addressed in the paper by Carlson et al. (1991; Appendix D).

A unique feature of the stomatal resistance model is the way in which vapor pressure deficit is specified. Without going into detail, we refer the reader to Eqn. (9) in Appendix B. Briefly, this equation relates the vapor pressure deficit to the difference

in water potential between the mesophyll and the epidermis. This formalism allows the epidermal and mesophyll leaf water potentials to vary in the opposite sense, as shown in Figure 1. It also allows transpiration to begin decreasing with increasing vapor pressure deficit as the latter becomes large; this is known as the feedforward effect (Farquhar, 1978). Inclusion of a large vapor pressure deficit sensitivity, as in the case of soybeans, results in the evapotranspiration plateau becoming concave. This is shown in the results of simulations and measurements of evapotranspiration made at Penn State (Figure 2). Further details are contained in a thesis by Lynn (1989).

i) Stomatal resistance workshop

A workshop conceived and organized by the PI on the subject of stomatal resistance was held at Penn State, 10 - 13 April, 1989. Partially funded by this grant, the workshop hosted about 35 invitees for the purpose of discussing methodology and need for improved measurement and modeling of stomatal resistance. Besides the intensive and lively discussions, the workshop resulted in a set of proceedings (available on request) and a collection of 13 reviewed articles to be published during 1991 in Agricultural and Forest Meteorology. While not contributing directly to these articles, the PI served as acting editor and has written a preface to the volume.

c) Partial vegetation cover

Spatial variations in surface radiometric temperature may be due to spatial variations in vegetation cover, rather than in soil water content. The reason is that upwelling thermal radiance is emitted from an arbitrary mix of warm, dry soil and cooler vegetation. Thus, remote radiometric surface temperature measurements can yield misleading information on the horizontal distribution of soil water content, depending on the amount of bare soil visible to the radiometer, because the vertical variation of soil water content becomes artificially mapped onto the horizontal.

The problem is to devolve both the vegetation fraction and the horizontal soil water content from remote measurements. To this end we have made use of radiance measurements at solar wavelengths, specifically the normalized difference vegetation index (NDVI). We were obliged to spend a considerable amount of time developing a partial vegetation canopy component in the boundary layer model, where bare soil and vegetation modes meld within a framework of a common mixing layer and substrate.

Our method of analysis is as follows: we first determine asymptotic surface temperatures (the extrema) for sunlit bare soil and sunlit vegetation by plotting the NDVI versus the radiometric surface temperature. In many cases this variation shows a narrow band of data points extending from high NDVI and low radiometric surface temperature to low NDVI (close to zero) and high surface temperature, as shown in Figure 6 of Appendix C. We call this narrow strip of data points the "axis of variation". The end points of the axis of variation correspond approximately to values for sunlit bare soil and a full, sunlit vegetation cover. Note that the variation of NDVI versus radiometric surface temperature flattens at high NDVI, signifying that at some point the variation ceases to increase significantly with increasing vegetation amount. Carlson et al. (1990; Appendix C) discuss the fact that NDVI increases with increasing vegetation amount, but effectively saturates (increases insignificantly) with increasing vegetation amount above a leaf area index of about 3 for many vegetation types.

We next assume that the lower temperature extremum, where NDVI no longer significantly increases with decreasing surface temperature, corresponds to a leaf area index of 3 and to 100% vegetation cover. The high temperature extremum corresponds to sunlit bare soil. Accordingly, we deduce the bare soil (surface) water content and the vegetation (root zone) water content with the aid of the aforementioned boundary layer model, by forcing the simulated temperatures to match measured temperature extrema in two simulations; these extrema correspond to that for bare soil and that for full vegetation cover (leaf area index = 3), for which we derive the root zone water content.

The next step in the analysis is to simulate the radiometric surface temperature in which we vary vegetation fraction but keep the substrate water contents (for surface and root zone) equal to the values derived in the previous step. The result is an estimate of surface radiometric temperature versus vegetation fraction, from which we derive the relationship between NDVI and vegetation fraction from the axis of variation. In principle, we can then produce a map of vegetation fraction and the surface energy fluxes.

Although there is some artistry and guesswork involved, the method offers some prospect for remotely measuring soil water content at two levels (surface and root zone), vegetation fraction and surface energy fluxes over sparse or partial vegetation cover. The method is currently being tested by our co-worker, Rob Gillies, using AVHRR satellite images of an urban area in Britain (see below).

d) Radiometric detection of transient water stress in vegetation

A question posed in our most recent paper (Carlson et al., 1991; Appendix D) is whether transient water stress associated with the transpiration plateau can be detected radiometrically. Since the onset of the hat signifies a period of plant water stress and may presage a later collapse of transpiration with further soil drying, detection of its effect on radiative surface temperature is of some interest. We began this project by using micrometeorological measurements (surface energy fluxes, radiometric temperature, soil moisture) taken during two growing seasons (one in corn and the other in soybeans) at Rock Springs, a Penn State University agricultural site. We confined our attention to days in which there was (1) dense vegetation (evapotranspiration approximately equals transpiration), (2) clear skies, and (3) functioning instruments. In

the end, we found only one period meeting these criteria that lasted more than one day; the measurements pertain to corn during July 1987.

Evapotranspiration measurements during this period show a plateau which lengthened from about two hours on the first day to about 5 hours after 3 days of soil drying. A comparison of measurements and simulations are shown in Figure 1 of Appendix D. The model was capable of simulating the transpiration plateau, including its increase in duration and the decrease in maximum evapotranspiration during the period; the threshold water potential in the model was set at -15 bars.

Having successfully simulated the behavior of the hat, we proceeded to make additional simulations that suggest how the hat may have evolved with time. We wanted to show how well the rise in canopy temperature could be detected radiometrically. Figure 9a (Appendix D) shows the simulated change in radiometric surface minus air temperature differences at 1300 local time as a function of plateau length and date in July 1987 (numbers above curve). Let us assume that the basic uncertainty in measuring a change in surface minus air temperature due to soil water content at a single point is about two decrees C. Since the soil was almost at field capacity on July 4th (the last day with significant rain before the end of the month), the departure of the canopy radiometric temperature from that for a soil at field capacity would not have exceeded two degrees C until about July 22. Therefore, the period of stress marked by the plateau would not have been detectable until a period of more than two weeks of drying had passed. By that time the soil water content would have decreased to less than 50% of field capacity and the length of the plateau exceeded 3 hours. Interestingly, however, simulations suggest that the plateau begins to form after just a few days when the soil water content was still rather high, about 70% of field capacity. This early evidence of water stress occurs because of high atmospheric demand rather than low soil moisture.

Another interesting conclusion suggested by these simulations is that the plateau would not occur if the atmospheric forcing were decreased by the reduction of sunlight associated with cloud cover (Figure 13 in Appendix D). When the net radiation was diminished to that of a broken cloud cover, the plateau vanished completely. Moreover, we also found that the plateau was effectively masked when the fractional vegetation cover was reduced to about 50% (Figure 11a in Appendix D). This suggests that detection of plant water stress using radiometric temperatures is dependent on a premise of clear skies and dense vegetation; variations with time in cloudiness or in space of vegetation fraction can completely obscure the water stress signal. In such cases of low atmospheric demand, the radiometric surface temperature is more likely responding to variations in surface (rather than root zone) soil water content.

The results of this study are very intriguing. They suggest, as has Katerji (1990), that the threshold leaf water potential can be inferred from evapotranspiration measurements by observing the plateau and then simulating the length of the plateau and the evapotranspiration level during the plateau. Further details of the field experiment are contained in a thesis by Belles (1990).

e) The effects of plant capacitance

A paper by Carlson and Lynn (1991) discusses the effect of including plant capacitance (water storage) in the model reported by Lynn and Carlson (1990). We show that the transpiration plateau can be mitigated or even removed by the effects of capacitance. Surprisingly, our results show that the effects of capacitance on either transpiration or stomatal resistance is negligible except when there would otherwise be a transpiration plateau. We also show that capacitance may constitute an important effect in the field- scale transpiration, but probably only for large vegetation (e.g. trees). Thus, trees and other large plants may have the capability of eliminating the transpiration plateau as the result of internal water storage. This paper is currently under review. A brief discussion of the this paper and those contained in appendices A, B and C are contained in a short review paper by Carlson (1991).

f) Other projects

i) A "bottom up" method for calculating soil water content

As we have discussed above, radiometric temperature measurements over vegetation can not detect deep soil drying until the soil water content has decreased below about 50% of field capacity. Nevertheless, variations in soil water content between 50 and 100% of field capacity are important for water budget analyses and for initializing regional and climate prediction models. Because of limitations in the radiometric method, we have taken a complimentary approach, which we refer to as the "bottom up" method, as opposed to the radiometric approach, which we refer to as the "top down" method.

The bottom up method uses routine meteorological and surface observations in conjunction with a simple hydrological model to calculate soil water content. The model takes precipitation, cloud cover, vegetation height and fractional cover, maximum and minimum temperature, the depth of the water table and some knowledge of the soil type and it calculates evapotranspiration, runoff, diffusion of water in the soil, and infiltration in the process of determining the vertical profile of water content in the soil. This model will be reported in a forthcoming MS thesis by William Capehart.

Figure 3 shows some preliminary results with this model, specifically the surface volumetric water content simulated for the same Penn State agricultural site referred to in Carlson et al. (1991). We wanted to find out how long it took for the simulations to "forget" the initial conditions, which are usually not known. We started the simulations with three differing soil water content profiles on 1 January 1987, By July, 1987, the 0 - 10 cm values have merged, indicating that the model is no longer sensitive to the choice of initial conditions after several months. The significance of these results is that one can simulate the substrate water contents by starting the model with any reasonable substrate water profile several months before the target date. The bottom up method is being tested against measurements of soil water content using data collected via gypsum blocks during the 1987-88 Penn State field program and with measurements made during the recent MAC Hydro experiment (referred to below). (At present we are conducting sensitivity tests to investigate the impact of initial conditions on the results, as well as

the effects of the water table level, the soil type, and the vegetation height and fractional vegetation cover on the vertical profile of soil water content.)

ii) Testing the partial vegetation cover analysis

We are currently analyzing images of radiometric surface temperature and NDVI over Newcastle, England, in order to derive patterns of vegetation fraction and surface energy fluxes. This project will test our method of estimating partial vegetation fraction, in this case over a region where vegetation fraction and therefore the evapotranspiration has been modified substantially by urbanization. The technique to be applied is identical to that referred to above in section (c). Results using AVHRR imagery are remarkably similar to those for HAPEX, which pertain to a small-scale agricultural area. Figure 4 shows the variation of radiometric surface temperature versus NDVI for the Newcastle area on 21 May, 1989. Note that the configuration of data points closely resembles that in Figure 6 in Appendix C. The warm temperature extremum, about 34^{0}C pertains to a pure urban surface and to a very low surface soil water content. At the cool end, the variation bends to the left below about 23^{0}C, approximately where the vegetation fraction reaches 100%. Accordingly, we can map the vegetation fraction as a function of NDVI between 0 and 100% percent, assuming that the vegetated fraction up to 100% corresponds to a leaf area index of 3.0.

iii) Mahantango field program (MAC Hydro experiment)

The Mahantango Watershed field program was conducted by the Agricultural Research Service, USDA (Beltsville, MD) and by NASA at Goddard Space Flight Center for the purpose of evaluating the usefulness of microwave remote measurements of soil water content and the modeling of hydrologic and biogeochemical processes. Mahantango Creek watershed, located in central Pennsylvania, is an instrumented research basin managed by the USDA, Agricultural Research Service, Northeast Watershed Research Center at University Park, PA. We are using the remote measurements of surface radiometric temperature and NDVI taken from aircraft and the in-situ measurements of vegetation height and fraction and surface meteorological data in order to calculate soil water content from the bottom-up and top-down methods referred to above. Specifically, we use the remote measurements and our hydrology model to calculate soil water content and vegetation fraction. These results will be compared with in situ measurements of soil water content and vegetation fraction and with soil water content measurements obtained from microwave data; the latter are currently being analyzed by the USDA. Preliminary data processing has only just begun; further efforts will be made in conjunction with scientists at USDA and at Penn State.

3. Synthesis and future work

Sensitivity tests with our vegetation model suggest that water stress in vegetation may be detectable for a period of a few days prior to wilting, provided that the atmospheric demand is large, an appropriate threshold leaf water potential exists and plant storage capacity is not large. What is commonly measured by radiometer are variations in the soil surface temperature, depending on the density of the vegetation canopy. On the other hand, horizontal variations in radiometric surface temperature over sparse vegetation may simply reflect horizontal variations in canopy density rather than horizontal variations in soil water content. This variation can be used to map the vegetation fraction, rather than the soil water content.

In the figure, we hope to clarify the issue of radiometric measurement of soil drying and to show how it can be applied over sparse vegetation. To do this it is necessarq to spend some time testing our present methods using available field measurements. The MAC-Hydro experiment offers the best opportunity to do so, using data obtained over a typical watershed. We will also analyze vegetation fraction for Newcastle, England. The latter analyses will be compared with available land use information. Modeling efforts will be confined to making the boundary layer-plant model user friendly and to include carbon dioxide fluxes in the plant component.

List of Figure Captions

Figure 1. Simulated mesophyll leaf water potential (ψ_l) (bar; crosses) and epidermal leaf water potential (ψ_e) (plus signs) versus time for soybean simulations presented in Figure 2. Vertical arrows denote duration of evapotranspiration plateau. Horizontal dashed line labeled ψ_c denotes the threshold epidermal leaf water potential.

Figure 2. Simulated transpiration ($L_e E_f$; solid line labeled in Wm^{-2}) and evapotranspiration ($L_e E$; crosses) and measured evapotranspiration (MEASURED; triangles) versus time for soybeans on 6 July, 1988, at the Penn State agricultural field site. Vertical arrows denote the duration of the evapotranspiration plateau in the simulations.

Figure 3. Simulated surface (0 - 10 cm) volumetric water content versus date (1987) using meteorological observations taken at Rock Springs for three differing initial soil water profiles, 20, 44 and 60% of field capacity (0.34 by volume).

Figure 4. Variation of NDVI versus radiometric surface temperature (^oC) for area around Newcastle, England, 21 May, 1989, from AVHRR of NOAA-11 satellite; the footprint for each data point is about 1.1 km.

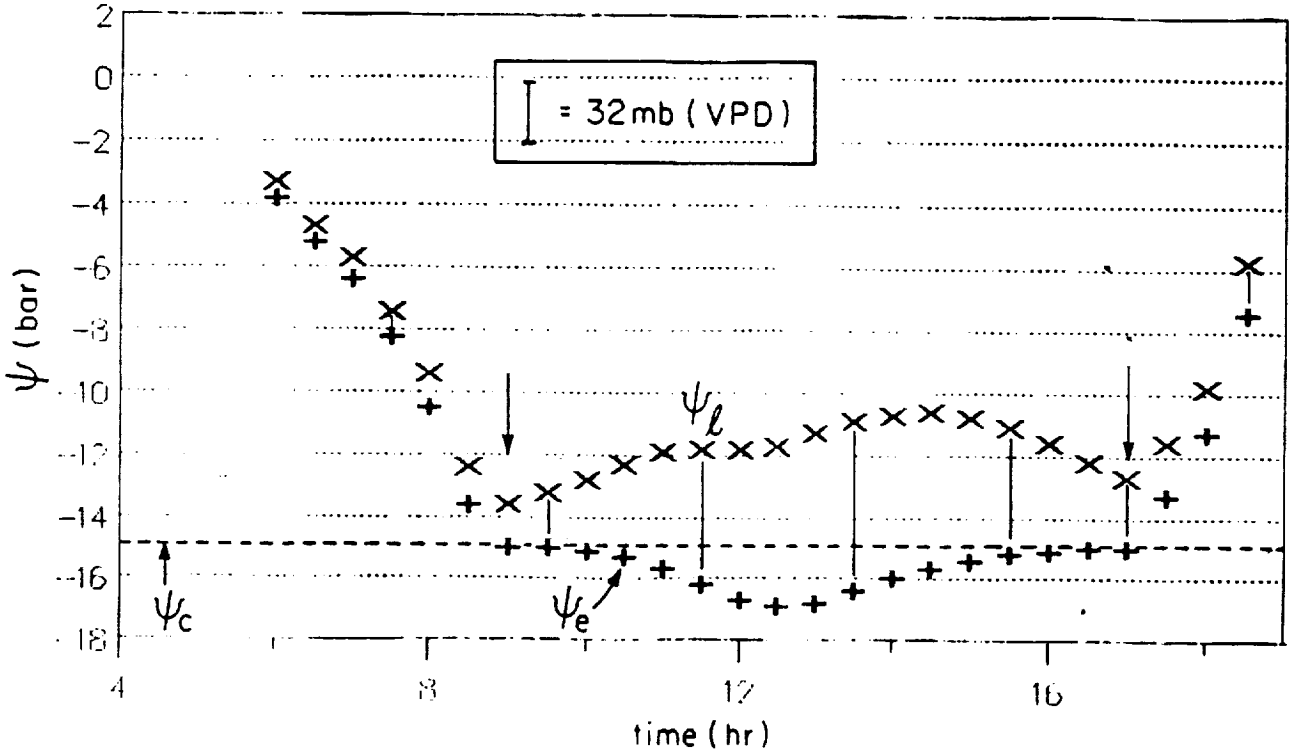

Figure 1. Simulated mesophyll leaf water potential (ψ_l) (bar; crosses) and epidermal leaf water potential (ψ_e) (plus signs) versus time for soybean simulations presented in Figure 2. Vertical arrows denote duration of evapotranspiration plateau. Horizontal dashed line labeled ψ_c denotes the threshold epidermal leaf water potential.

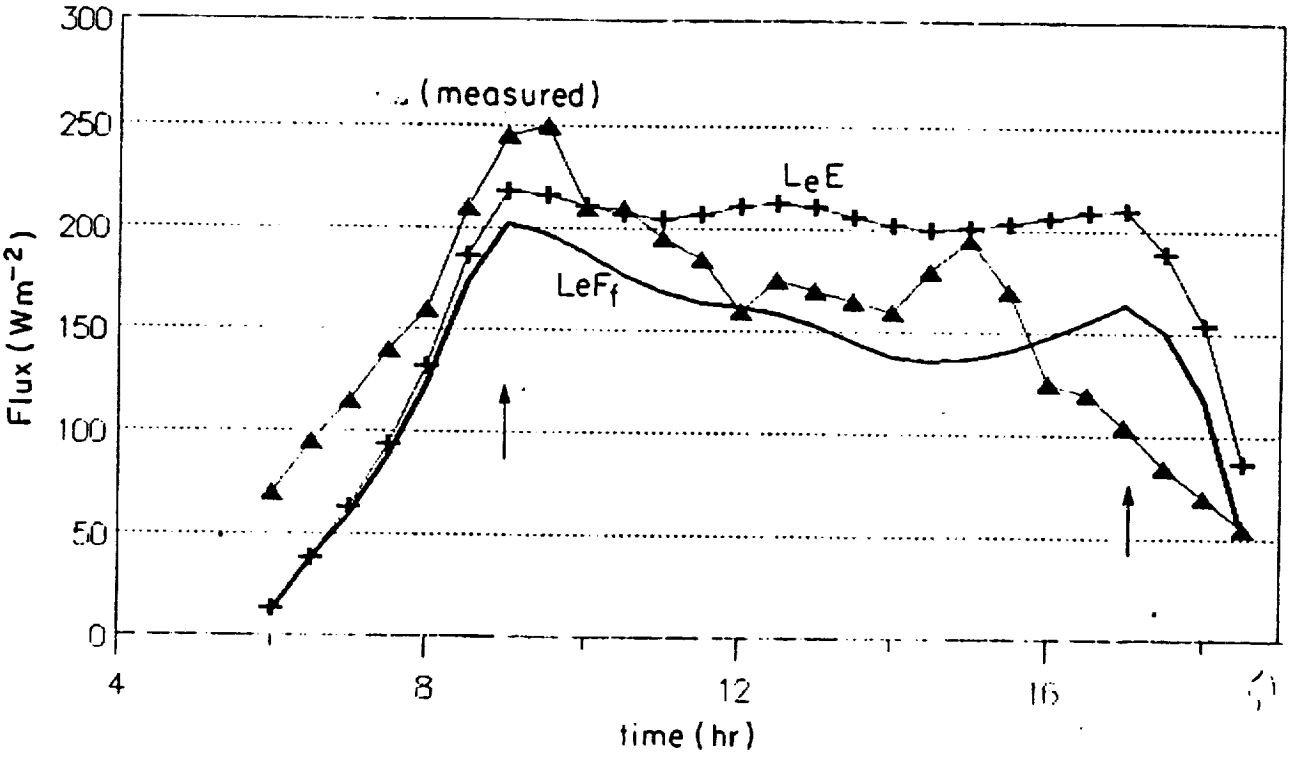

Figure 2. Simulated transpiration ($L_e E_f$; solid line labeled in Wm^{-2}) and evapotranspiration ($L_e E$; crosses) and measured evapotranspiration (MEASURED; triangles) versus time for soybeans on 6 July, 1988, at the Penn State agricultural field site. Vertical arrows denote the duration of the evapotranspiration plateau in the simulations.

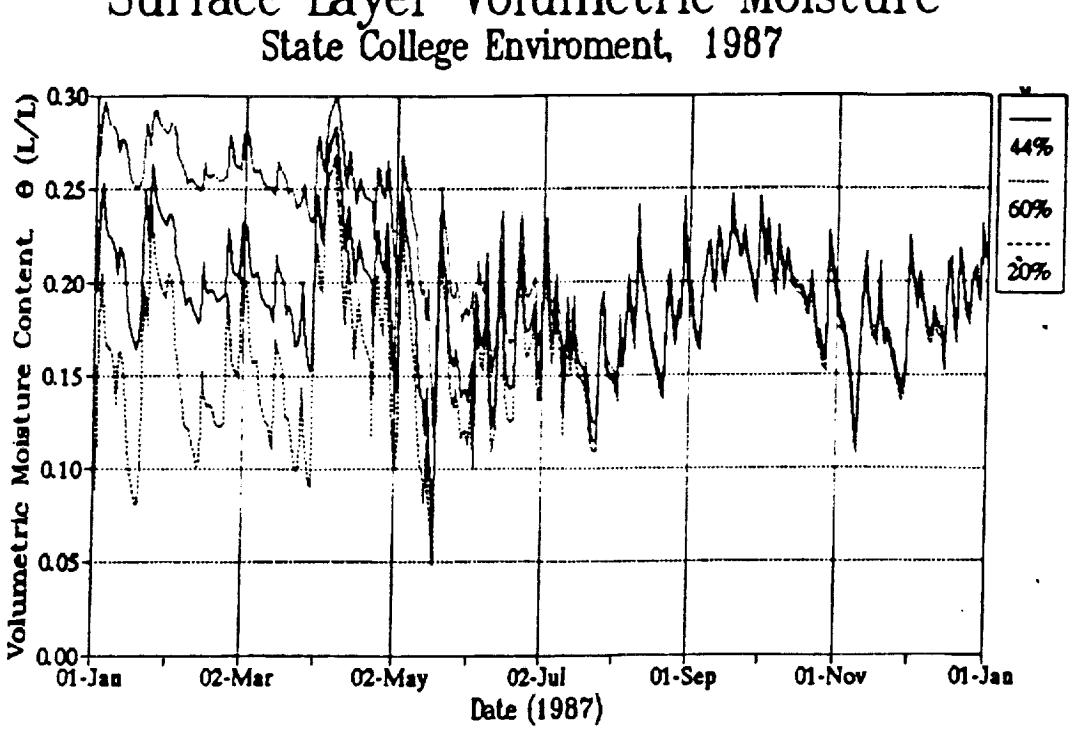

Figure 3. Simulated surface (0 - 10 cm) volumetric water content versus date (1987) using meteorological observations taken at Rock Springs for three differing initial soil water profiles, 20, 44 and 60% of field capacity (0.34 by volume).

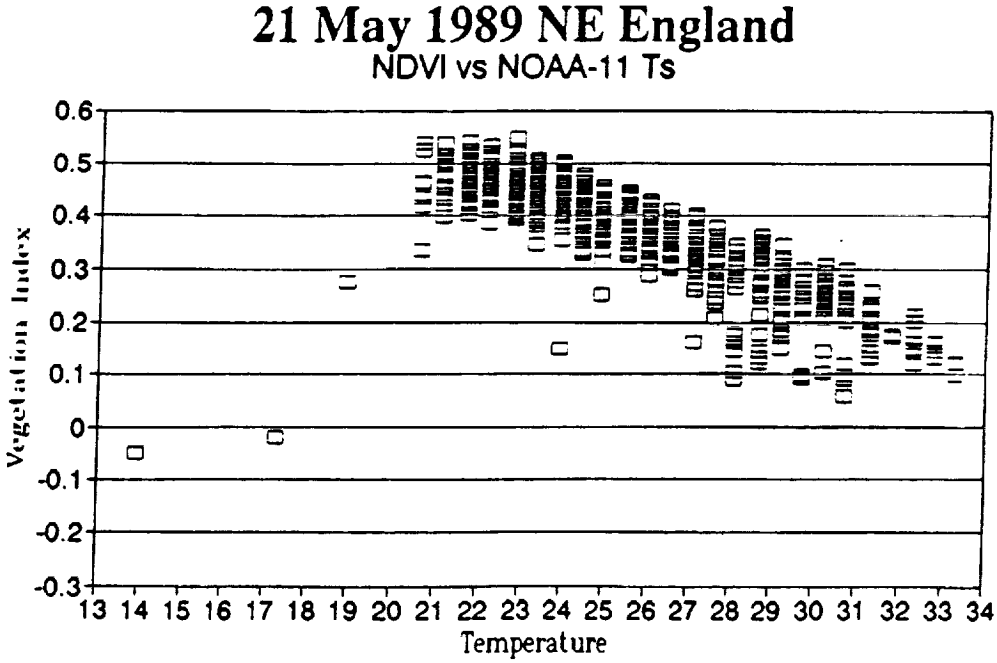

Figure 4. Variation of NDVI versus radiometric surface temperature (^{o}C) for area around Newcastle, England, 21 May, 1989, from AVHRR of NOAA-11 satellite; the footprint for each data point is about 1.1 km.

REFERENCES

Andre, J.C. (and many others), 1988. Evaporation over land-surfaces: First results from HAPEX-MOBILITY special observing period, Annales Geophysical, 6, 477-492.

Belles, J.E., 1990. Calculation of the surface sensible heat flux from the bulk aerodynamic method using a thermal radiometer, Masters Thesis, Dept. of Meteorology, Penn State University, 80 pp.

Buffum, M.J., 1988. A method of estimating daily net evapotranspiration from radiometric temperature measurements, Masters Thesis, Dept. of Meteorology, Penn State University, 105 pp.

Carlson, T.N., 1990. Recent advances in modeling the infrared temperature of vegetation conopies, chapter 21 in Land Surface Evaporation: Measurements and Parameterization, J.P. Andre and T.J. Schmugge, eds., Springer Verlog, chapter 21, 349-358.

Carlson, T.N., J.E. Belles and R.R. Gillies, 1991. Transcent water stress in a vegetation canopy; simulations and measurements, Remote Sensing of Enviornment (in press).

Carlson, T.N. and M.J. Buffum, 1989. On estimating the daily evapotranspiration from remotely sensed temperature measurements, Remote Sensing of the Enviornment, 29, 197-207.

Carlson, T.N. and B. Lynn, 1990. The effects of plant copaertance once boundary layer model, submitted to Ag. and Forest Meteor.

Federer, C.A., 1980. Paper Birch and White Oak Saplings differ in responses to drought, Forest Sci., 26, 313-324.

Jackson, R.D., R.J. Reginato and S.B. Idso, 1977. Wheat canopy temperature: a practical tool for evaluating water requirements, Water Res. Management, 13, 651-656.

Kateiji, N., 1990. Use of simulation methods for determining critical leafwater potential for stomatal closure infield conditions, Ecological Modeling, 50, 133-144.

Lynn, B., 1988. The formulation of a stomatal resistance model within a boundary layer model, Masters Thesis, Dept. of Meteorology, Penn State University, 129 pp.

Lynn, B. and T.N. Carlson, 1990. A model illustrating plant versus external control of transpiration, Agricultural and Forest Meteor., 52, 5-43.

Nizinski, J. and B. Saugier, 1989. A model of transpiration and soil-water balance for a mature oak forest, Agricultural and Forest Meteor., 47, 1-17.

Seguin, B. and B. Itier, 1983. Using midday surface temperature to estimate daily evaporation from satellite thermal IR data, Int. J. Remote Sensing, 4, 371-383.

APPENDIX A

REMOTE SENS. ENVIRON. 29:197–207 (1989)

On Estimating Total Daily Evapotranspiration from Remote Surface Temperature Measurements

Toby N. Carlson
Department of Meteorology, Pennsylvania State University

Martha J. Buffum
Computer Sciences Corp., Falls Church, Virginia

A method for calculating daily evapotranspiration from the daily surface energy budget using remotely sensed surface temperature and several meteorological variables is presented. Values of the coefficients are determined from simulations with a one-dimensional boundary layer model with vegetation cover. Model constants are obtained for vegetation and bare soil at two air temperature and wind speed levels over a range of surface roughness and wind speeds. A different means of estimating the daily evapotranspiration based on the time rate of increase of surface temperature during the morning is also considered. Both the equations using our model-derived constants and field measurements are evaluated, and a discussion of sources of error in the use of the formulation is given.

INTRODUCTION

A desirable goal in remote sensing is to determine the total amount of water evaporated from a surface during 1 day. Use of remotely sensed temperature for inferring surface evapotranspiration is discussed by Bartholic et al. (1972), Jackson et al. (1977), Soer (1980), and Taconet et al. (1986) for regions the size of a single field and by Price (1982), Carlson (1986), Flores and Carlson (1987), and Wetzel and Woodward (1987) for larger-scale areas. These models are generally based on the surface energy budget in combination with governing equations for the fluxes of water, sensible heat, and radiative energy between the surface and atmosphere and in the substrate.

The problem with complex models is that they require a detailed set of initial conditions for the atmosphere, surface, and substrate in order to obtain a solution. As a result, semiempirical methods have been proposed for estimating the total daily evapotranspiration integrated over a 24-h period (LE_{24}) from remotely sensed surface temperature measurements. One such formula, first proposed by Jackson et al. (1977), is

$$LE_{24} = R_{n24} = A + B(T_0 - T_a), \qquad (1)$$

where R_{n24} is the net radiation integrated over a 24-h period (in units of cm), A is a constant, T_0 is the radiometric surface temperature, and T_a is the air temperature. Both T_0 and T_a are measured near solar noon. The slope B and intercept A are determined by linear least squares fit to their data.

Address correspondence to Dr. Toby N. Carlson, Dept. of Meteorol., Pennsylvania State Univ., 503 Walker Bldg., University Park, PA 16802.
Received 26 July 1988; revised 19 May 1989.

0034-4257/89/$3.50

655 Avenue of the Americas, New York, NY 10010

Choice of measurement levels is not always clearly noted in the literature. Seguin and Itier (1983) chose 2 m as a standard height and Jackson et al. (1977) a level of 1.5 m for T_a. Conventional meteorological observations customarily assign the level of surface wind speed measurement at 10 m; in micrometeorological operations, wind speed is often measured closer to the ground.

An advantage of (1) is its simplicity, requiring minimal amounts of ground-based meteorological data. More specifically, only three variables (R_{n24}, T_a, and T_0) need to be measured. Thus, the formula is convenient to use in conjunction with satellite measurements of radiometric surface temperature, such as made by the geostationary earth satellite (GOES) or by the NOAA AVHRR at 2 a.m. and 2 p.m. overpass times (Lagouarde, 1988). Since 24-h integration of sensible heat stored in the substrate is likely to be close to zero, (1) expresses the 24-h integrated surface sensible heat flux into the atmosphere.

The *B*-method, as we will henceforth refer to the use of equations such as (1), arose from analysis of a daily water stress index, which was defined by Jackson et al. (1977) for surface and air temperatures made near 1300 local standard time (LST). Jackson et al. found that a plot of surface–air temperature differences over irrigated wheat versus $R_{n24} - LE_{24}$ yielded a straight line with $B = 0.064$ cm °C^{-1} and $A = 0$. Seguin et al. (1982) collected data over large homogeneous areas in southeastern France and found (1) required $B = 0.025$ and $A = 0.1$.

Seguin and Itier (1983), using the results of Itier and Riou (1982), obtained a modified version of (1), which is

$$R_{n24} - LE_{24} = B(T_0 - T_a)^n, \qquad (2)$$

where n is an exponent. Seguin and Itier found that n was equal to 1.0 for stable or near neutral conditions and 1.5 when the stratification was unstable. They also showed that the value of B depends upon the roughness length z_0 and the wind speed. Consequently, Seguin and Itier (1983) suggested that the imposition of a single value for B and n, even for various climates and types of surfaces, may be unacceptable, although specific values of B may be chosen according to certain broad categories of roughness, static stability, and vegetation type. They concluded that, for "medium rough" surfaces, it was worth assigning only two values of B, one for stable and the other for unstable conditions. They suggested a value of $B = 0.025$ and $n = 1$ in (2) for unstable conditions.

An alternate form of (2) was suggested by Nieuwenhuis et al. (1985). They eliminated R_{n24} and T_a and substituted the potential evapotranspiration and a corresponding reference canopy temperature. Their modified form of (2) depended on a single measurement of temperature with respect to a modeled temperature for a potentially transpiring crop. LE_{24} was calculated as a difference from a modeled daily integrated potential evapotranspiration, which was determined for a completely wet surface using a boundary layer model [the TERGRA model of Soer (1980)]. Their equation is otherwise similar to (2), except that it is expressed in terms of a ratio of actual to potential evapotranspiration. This ratio is similar to the moisture availability parameter defined by Carlson (1986), except that the latter pertains to an instantaneous ratio of evapotranspiration to potential evapotranspiration.

Nieuwenhuis et al. (1985) demonstrate the efficacy of the *B*-method for determining LE_{24} over individual fields; they also showed that the values of the coefficients are sensitive to surface roughness and meteorological conditions. More importantly, Nieuwenhuis et al. (1985) were the first to use a full boundary layer model to generate the coefficient B. Rambal et al. (1985) performed a study similar to ours in which values of B were determined from a boundary layer model with vegetation component for the case of $n = 1.5$. They found that B increases with increasing height and density of tree cover. More recently, Lagouarde and Brunet (1988) investigated the variation of A and B in (1) to changes in surface roughness using a planetary boundary layer model. They show that B varies rapidly with changing surface roughness when the latter is in the range between 0.2 and 10 cm, particularly when the surface–air temperature differences are large.

We have also used a sophisticated planetary boundary layer model to investigate the response of the coefficient B and the exponent n in (2) to changes in surface roughness, wind speed, and vegetation. This model (henceforth referred to as CM) has been described by Carlson (1986) and Taconet et al. (1986). Until now, the primary practical application of the CM has been in remote sensing of the surface energy fluxes; in this con-

text, the model is inverted in conjunction with remote measurements of surface temperature and other parameters to obtain a solution for the surface energy fluxes and soil moisture availability.

A different form of (2) which does not require measurement of an air temperature for calculating the sensible heat flux term is proposed here. Wetzel et al. (1984) show that the soil moisture (and therefore the evapotranspiration) is most sensitive to the *rate* of temperature rise during the morning (e.g., between 8 and 10 local time). As a result the following equation will be examined:

$$R_{n24} - LE_{24} = B'(\Delta T/\Delta t)^{n'} \quad (\text{cm day}^{-1}). \quad (3)$$

Here $(\Delta T/\Delta t)$ is an average rate of temperature rise during the morning (expressed in °C per hour) and B' and n' are constants. It should be emphasized here that (3) represents an intuitive leap from (2). Justification of (3) is based on data generated by the CM, which shows that the rate of surface temperature change with time is highly correlated with the integrated daily sensible heat flux, as expressed by (1) or (2). In omitting reference to T_a, (3) is suggestive of the equation tested by Nieuwenhuis et al. (1985).

The purpose of this paper is to examine the *B*-method with regard to simulations of the parameters in (2) and (3) by the CM. We will show that the parameters B and n in these equations depend on surface roughness, wind speed, reference height, and vegetation. Two sets of simulations were made of B and n (and B' and n'): at 2 and 6.4 m, respectively, for temperature and wind speed and at 50 m for both temperature and wind speed. Choice of the 2 and 6.4 m levels is dictated by the availability of field measurements for testing the *B*-method. Our object is not to add to the bewildering profusion of values for B and n currently available in the literature but to illustrate the sensitivity of B and n to ambient and surface influences and to suggest an alternate form of the *B*-method. Therefore, a part of this paper is devoted to demonstrating the validity of (3).

METHODS

The CM describes the water and energy exchanges between the substrate, the layer of vegetation, an atmospheric surface layer and a mixing layer. Surface layer similarly laws are employed to compute the surface energy fluxes with corrections for changes in static stability. An account is taken of differences between the thermal roughness length for heat and for momentum. Results are determined by a complex nonlinear interaction with evolving static stability and ambient conditions in a multilayered atmosphere and substrate.

Numerous simulations performed with the CM underscore the sensitivity of the *B*-parameter in (2) to changing surface roughness and also show that: 1) the *B*-parameter is also sensitive to wind speed, 2) under some conditions the exponent n differs from a value of 1.0, and 3) the value of B and n depend on the choice of reference levels at which the ambient temperature T_a and wind speed are measured. These simulations suggest that values of B and n can be generated for a wide range of conditions using the CM.

Under minimal advection conditions, T_0 and T_a are closely related. Above the planetary surface layer, however, T_a and wind speed are largely independent of local terrain influences, are relatively homogeneous in space and therefore independent of small-scale horizontal variations in T_0. Therefore, we will discuss the values of B and n at 50 m. Advantages of adopting a level above the surface layer in the use of (2), aside from that of spatial homogeneity, are as follows: First, the laws of similarity used in calculating surface fluxes break down when the measurement level lies with a factor of about 10 times the roughness height above the level of the displacement height. Thus, over rough surfaces, such as some vegetation canopies (notably trees), the 2 m temperatures may be inapplicable to the *B*-method. Second, there are situations in remote sensing where screen-level measurements are not available. Third, 50 m elevation corresponds more closely than screen level to the lowest atmospheric level in weather forecasting and climate models.

Method for Obtaining the Parameters B and n and B' and n'

The reason for using a boundary layer model is to generate a range of meteorological conditions, surface temperature, wind speed, surface roughness length, and vegetation cover from which we can determine the constants in (2) and (3). Since the results are not highly sensitive to the choice of vertical temperature and dewpoint profiles above

the surface layer, the reference set of initial atmospheric conditions for the model was chosen as that used by Taconet et al. (1986) in their simulations for an agricultural (wheat-growing) region in central France (the Beauce) during mid-July (11 July 1983). We regard these initial conditions as representative of a typical sunny day during summer in a temperate climate. It should be pointed out, however, that the choice of a minimum stomatal resistance in the model appropriate to wheat somewhat limits the results for vegetation to similar types of crops.

Net radiation, surface temperature, evapotranspiration, and surface sensible heat flux were calculated as cumulative amounts over 24-h cycles by varying a parameter called the moisture availability from 0.04 to 1.0 in a cycle of seven steps. Since moisture availability strongly modulates the surface temperature, this range of moisture availability allows us to generate a large range of surface temperature. Moisture availability, as defined by Carlson (1986), is simply the ratio of evapotranspiration to potential evapotranspiration at the surface temperature T_0. Moisture availability also constitutes the link between the surface relative humidity and the substrate water content, being set equal to the ratio of actual substrate water content to that at field capacity for the soil (0.34 by volume).

In order to obtain sufficient data to generate values of the model parameters, each moisture availability cycle was run for five surface roughness lengths and wind speeds and three leaf area indices, for a total of 75 moisture cycles (Table 1). For each moisture value, the 1300 LST surface temperature, air temperature (at 2 and 50 m), and wind speed (at 6.4 and 50 m) and the cumulative evapotranspiration and net radiation were computed. The rate of morning increase in temperature, between 0800 and 1300 LST (expressed in °C per hour), was also calculated. We chose to reduce the number of computer simulations by making thermal inertia a weak function of moisture availability. This expedient is justified by our own experience that small changes in thermal inertia do not significantly influence the results, particularly over vegetation.

Table 1. List of Parameters Varied in the Model and Their Values

$z_0(m)$	$h(m)$	$d_0(m)$	*Wind Speed*[a]	*LAI*
0.01	0.077	0.051	0.25 V_r	0
0.065	0.50	0.335	0.5 V_r	2
0.13	1.00	0.67	1.0 V_r	4
0.26	2.00	1.34	1.5 V_r	
0.52	4.00	2.68	2.0 V_r	

[a] V_r-reference wind speed.

Table 1 summarizes the roughness, wind speed, and leaf area index categories used in the simulations. Note that wind speed is simply stated as a fraction of a base (reference) wind speed for the 11 July winds. Thus, $0.25V_r$ means that all the wind speeds in the reference vertical wind speed profile (from the surface to the top of the sounding) were multiplied by 0.25.

Vegetation height (h) and displacement height (d_0) were made a function of surface roughness according to the commonly accepted relationships of Monteith (1975),

$$z_0 = 0.13\ \text{h}, \qquad d_0 = 0.67\ \text{h}.$$

For bare soil, the surface roughness length was also varied over the same range of values, although we recognize that the larger values of roughness would not likely apply to a natural bare soil cover. Air temperatures at 2 m, however, were not calculated for the 0.52 m roughness category, since the implied vegetation height would be above 2 m.

RESULTS

Figure 1 shows the results for seven different values of moisture availability plotted on log–log coordinates. The values of n and B are, respectively, the slope of the line and the ordinate intercept. The "best fit" straight line is defined as that which minimizes the residuals in the linear root-mean-square difference between $R_{n24} - LE_{24}$ (the surface sensible heat flux H_{24}) calculated from the model (the points in Fig. 1) and that determined from the straight line fit through successive pairs of points.

We found that the results varied insignificantly with changing leaf area index in the range 2–4. Consequently, in subsequent discussion, we make no distinction between different leaf area indices, preferring to treat only two different types of surfaces: bare soil and vegetation.

In general, simulated data adhered very closely to the straight line model in log–log coordinates. A characteristic of the best fit lines (such as that in

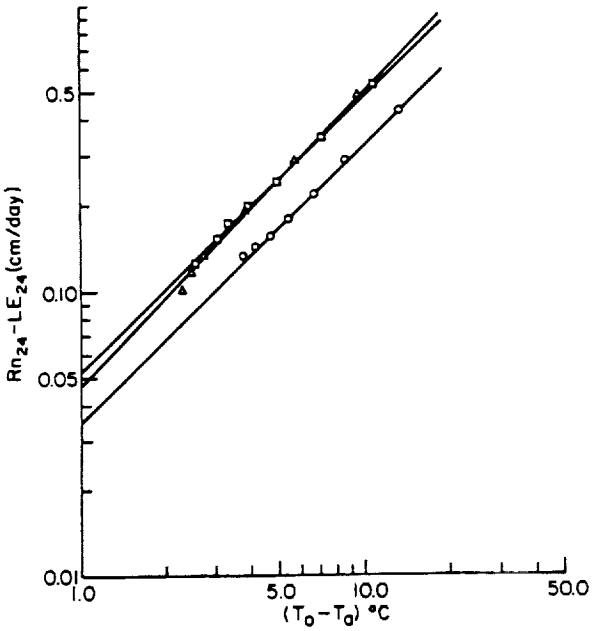

Figure 1. Values of $R_{n24} - L_e E_{24}$ vs surface air temperature differences $(T_0 - T_a)$ generated from a boundary layer model for seven values of moisture availability. The three sets of values, for which the best-fit straight lines are shown, pertain to a surface roughness (z_0) of 0.065 m and a base (reference) wind speed for each of three surface categories: leaf area indices of 2.0 (Δ) and 4.0 (□) and bare soil (○).

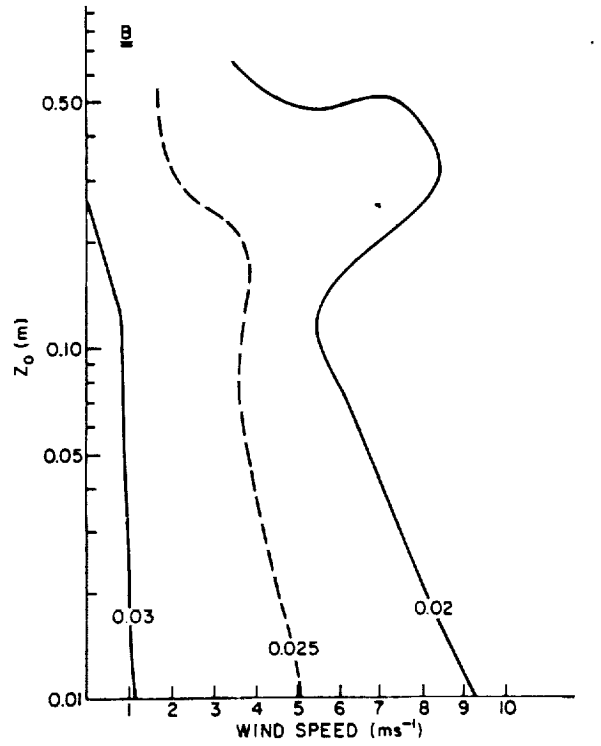

Figure 2a). Distribution of the constant B in Eq. (1) generated by the boundary layer model for the bare soil case. The graph shows the constant as a function of surface roughness (z_0) and wind speed for an air temperature measured at 50 m and a wind speed at 50 m.

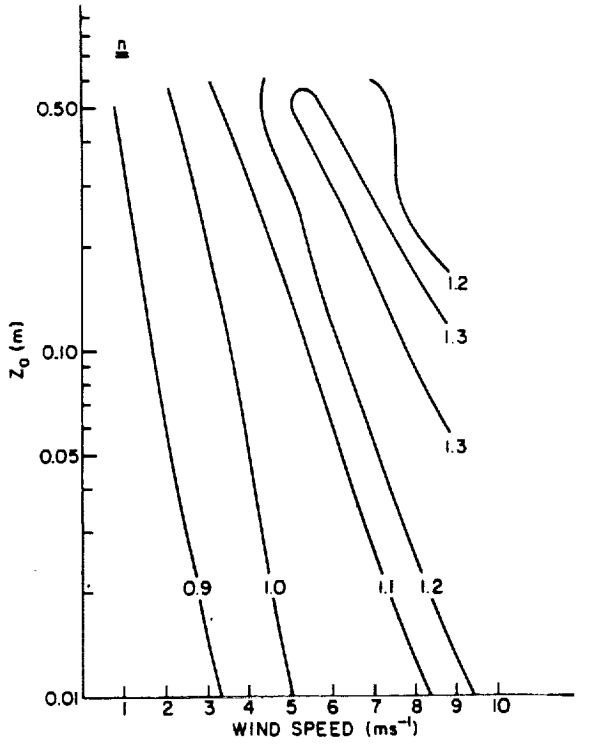

Figure 2b). Distribution of the constant n in Eq. (1) as in Fig. 2a).

Fig. 1), however, is a tendency for the lowest two or three points to deviate systematically from a straight line, although not always in the same sense; usually, however, the deviation was such that the generated values of $R_{n24} - LE_{24}$ fell below the line. The simulated data points using (3) fit a straight line with slightly less fidelity than for (2), but with similar deviations at the lower end. To some extent, this deviation is an artifact of the log–log plot, which exaggerates error on the lower part of the scale. However, while not constituting a serious error, this deviation is felt to be real and will be discussed later in this paper. Nieuwenhuis et al. (1985; Fig. 3) also show a tendency for the data to deviate markedly from a straight line fit (in linear coordinates) for large values of evapotranspiration (low values of $R_{n24} - LE_{24}$).

B and n for Wind Speed and Air Temperature Measured at 50 m

Results are presented in the form of analyses of B and n as a function of $\log z_0$ and the 50 m wind speed for air temperatures measured at 50 m (Figs. 2 and 3). Values of B [Figs. 2a) and 3a)] are close to 0.025. This is similar to values proposed by

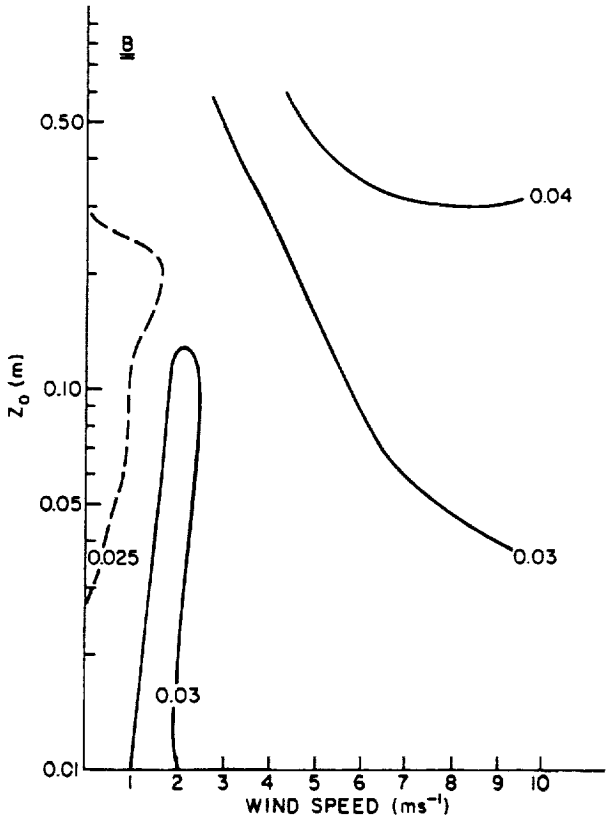

Figure 3a). Same as Fig. 2a) but for vegetation.

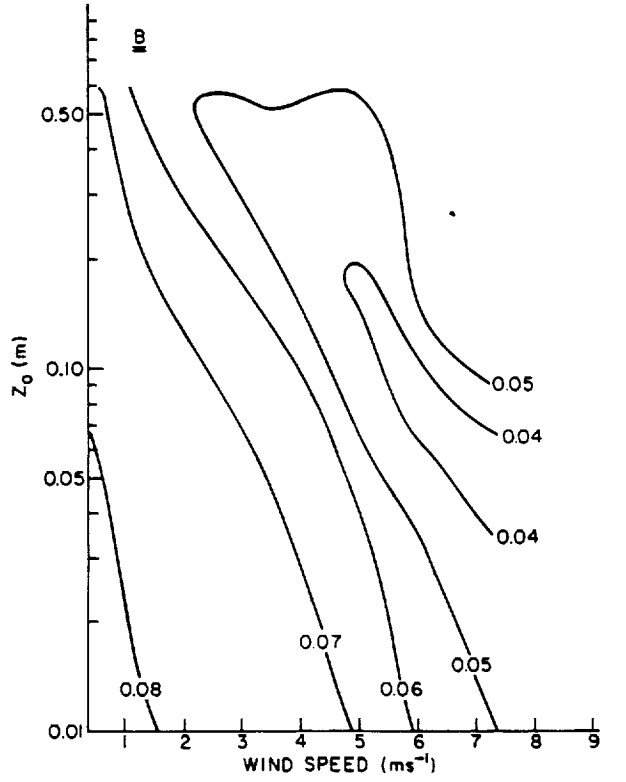

Figure 4a). Same as Fig. 2a) for B' using Eq. (3) [which is based on the rate of increase in morning temperature ($°Ch^{-1}$)] over bare soil; wind speed at 6.4 m.

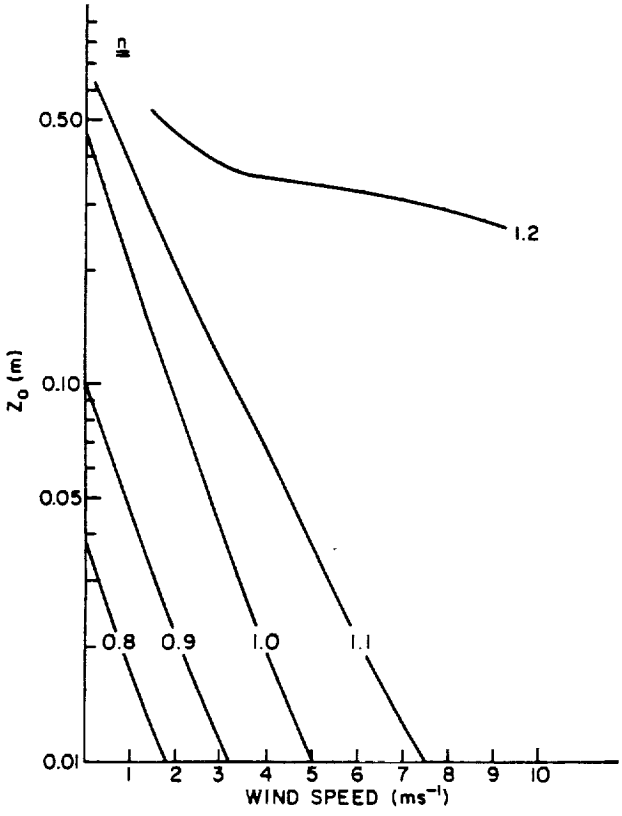

Figure 3b). Same as Fig. 2b) but for vegetation.

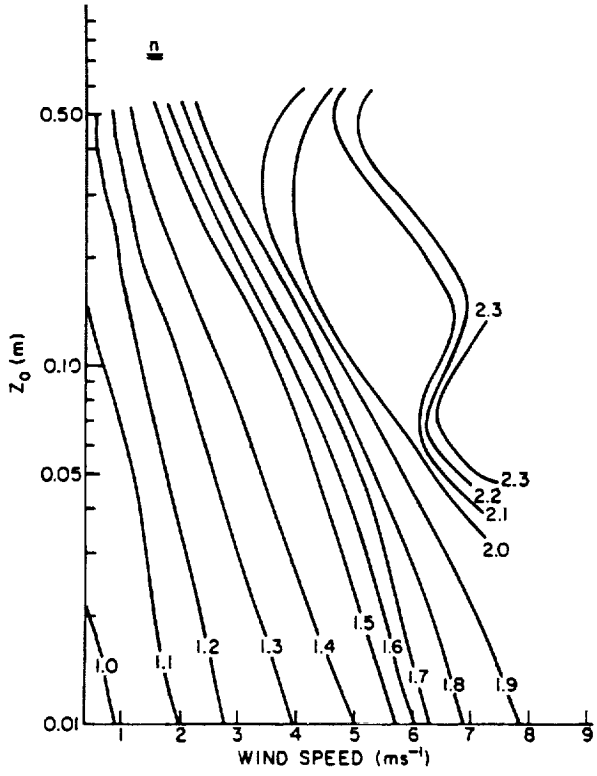

Figure 4b). Same as Fig. 2b) for n' using Eqs. (3) [which is based on the rate of increase in morning temperature ($°Ch^{-1}$)] over bare soil; wind speed at 6.4 m.

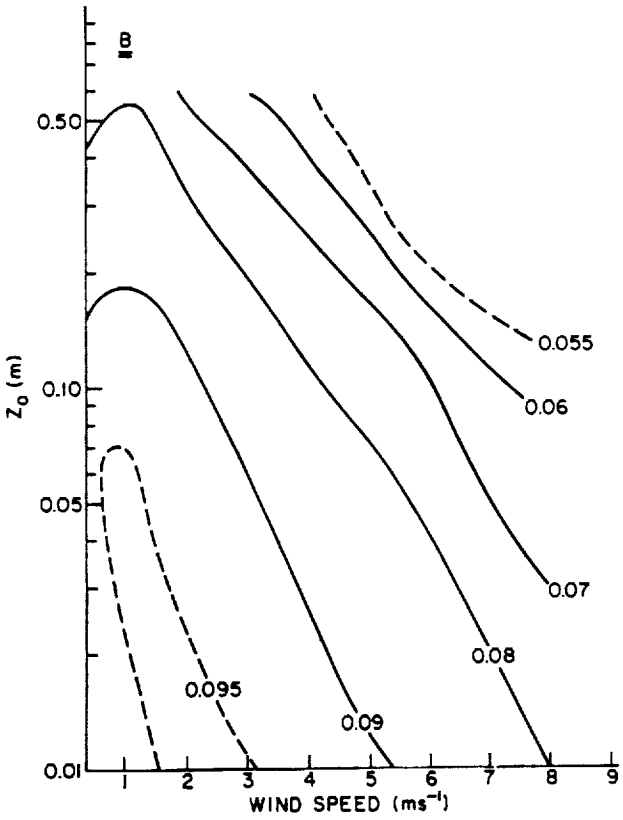

Figure 5a). Same as Fig. 4a) but using the rate of increase in morning temperature over vegetation; wind speed at 6.4 m.

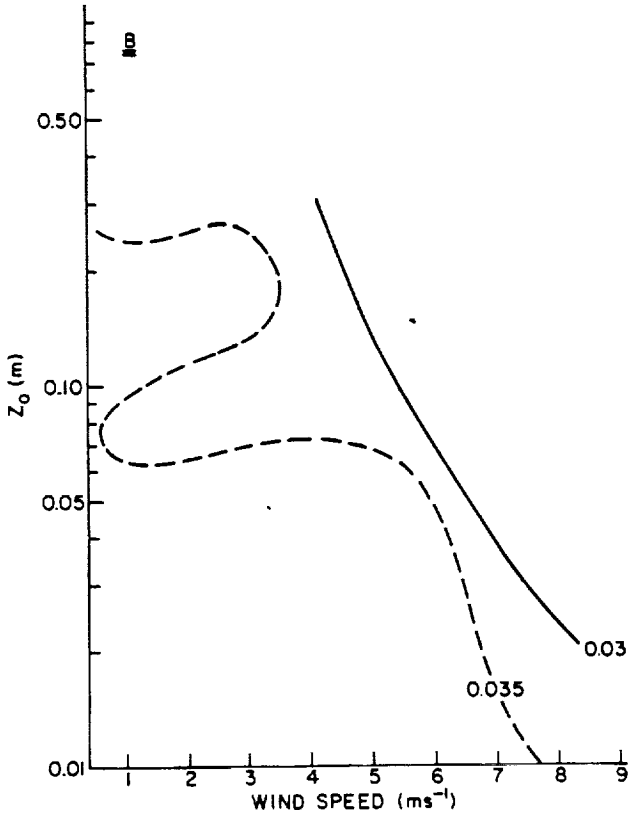

Figure 6a). Same as Fig. 2a) but for bare soil and an air temperature at 2 m; wind speed at 6.4 m.

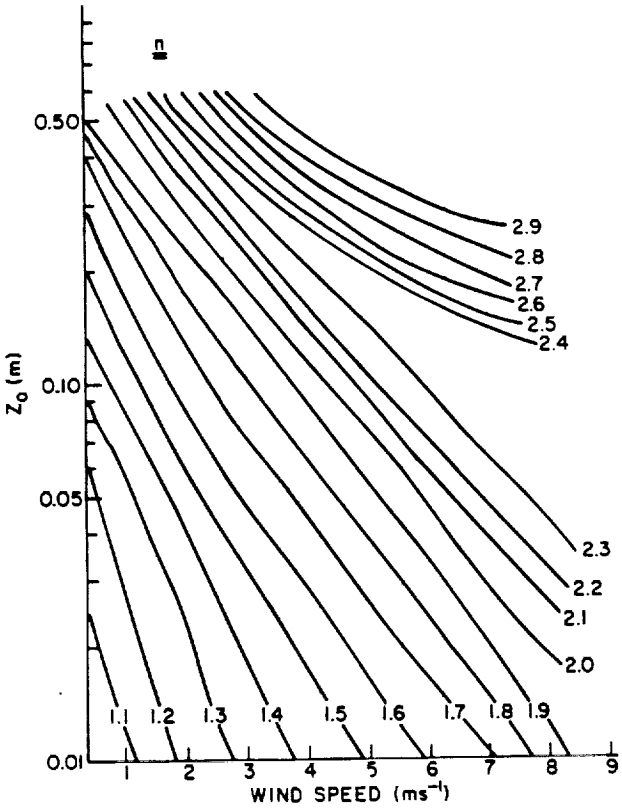

Figure 5b). Same as Fig. 4b) but using the rate of increase in morning temperature over vegetation; wind speed at 6.4 m.

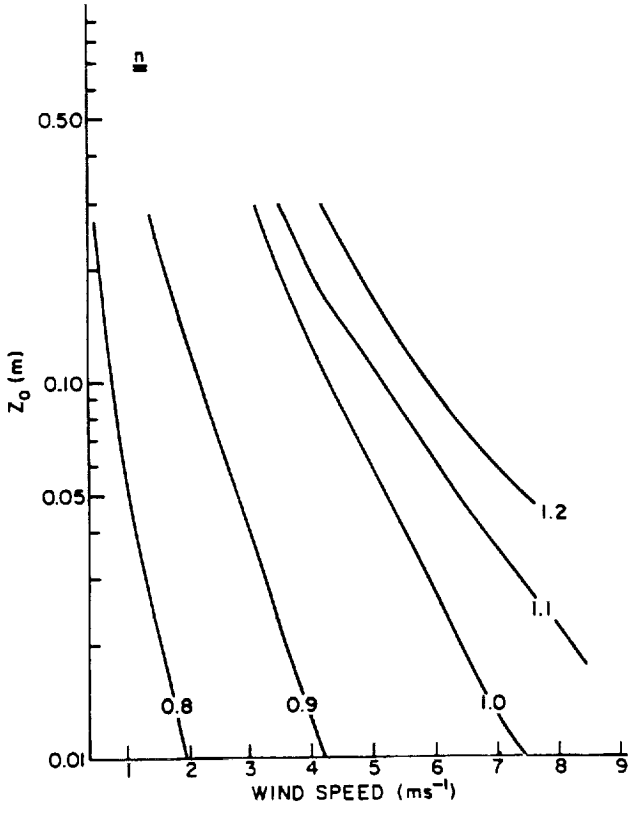

Figure 6b). Same as Fig. 6b) but for bare soil and an air temperature at 2 m; a wind speed at 6.4 m.

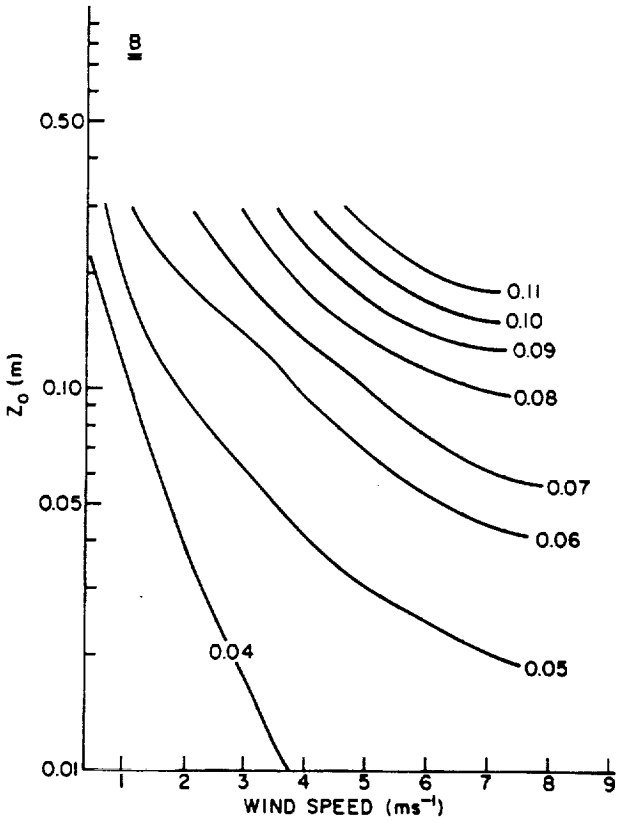

Figure 7a). Same as Fig. 2a) but for vegetation and an air temperature at 2 m; wind speed at 6.4 m.

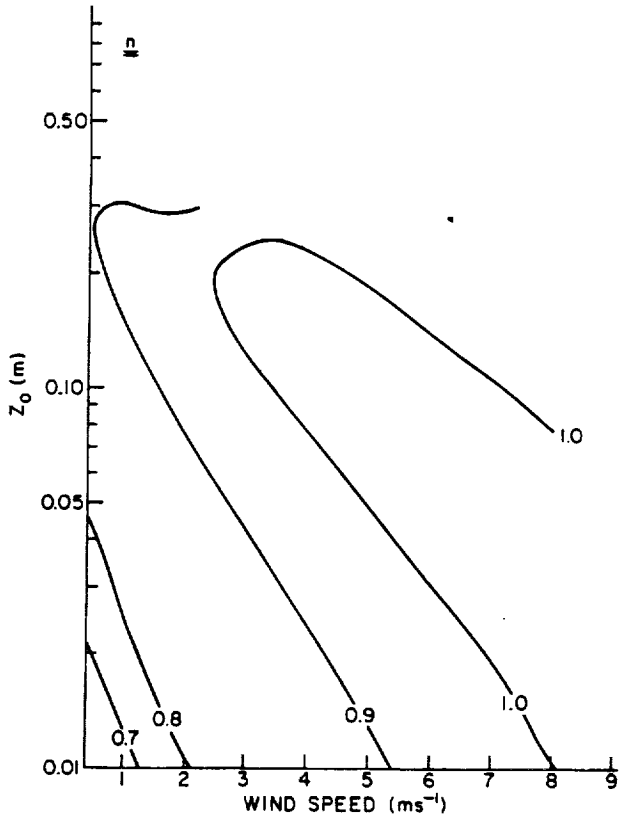

Figure 7b). Same as Fig. 2b) but for vegetation and an air temperature at 2 m; wind speed at 6.4 m.

Seguin and Itier (1983). Although there is some nonlinearity in the distribution of B, this coefficient generally decreases with increasing roughness and wind speed over bare soil [Fig. 2a)] and increases with increasing roughness and wind speed over vegetation [Fig. 3a)]. Differences between bare soil and vegetation are due to the differing methods of calculating sensible heat flux from leaves and bare soil. Within the vegetation layer, sensible heat flux is obtained as a residual between the transpiration and the net radiation absorbed by the vegetation, whereas the bare soil system of equations involves a simultaneous solution between sensible and latent heat fluxes.

The trend in the exponent n with changing wind speed and roughness is similar for bare soil and vegetation [Figs. 2b) and 2c)]. For all practical purposes, however, the value of n is equal to 1.0, which is commonly accepted for the B-method.

B' and n' for Wind Speed Measured at 6.4 m

Figures 4a) and 5a), showing B', are analogous to Figs. 2a) and 3a), but for the temperature tendency variation of the B-method (3) with a wind speed at 6.4 m. The trends in B' with changing surface roughness and wind speed are similar to those in Figs. 2a) and 3a), except that the values differ because the units are different. The exponent n' varies rapidly for both bare soil and vegetation as a function of surface roughness and wind speed [approximately from 1.0 to 2.5; Figs. 4b) and 5b)].

B and n for Wind Speed Measured at 6.4 m and Air Temperature Measured at 2 m

Figures 6 and 7 are analogous to Figs. 2 and 3 but for the 6.4 m winds and 2 m air temperatures. The most significant differences in B between the 50 m and low-level values is that the former are somewhat larger than the latter [compare Figs. 2a) and 6a)]. However, the exponent n decreases from the lower to higher levels [compare Figs. 2b) and 6b)], thereby compensating for the increase in B with height. Because of this compensation, there is little difference in the computed values of $R_{n24} - LE_{24}$ between the 2 and 50 m results for bare soil.

For vegetation however, the differences between the 50 m and lower-level temperature and wind levels are significant. The parameter B is about twice as large as the 50 m values for vegetation [0.04–0.11 versus 0.03; compare Fig. 3a) with Fig. 7a)], although the variation with surface roughness and wind speed is similar at the two levels. The exponent n, while very close to 1.0 for both levels [Figs. 3b) and 7b)], is slightly less than 1.0 for the 50 m results. These 2 m temperature values of B are similar to those proposed by Jackson et al. (1977).

COMPARISON WITH FIELD MEASUREMENTS

We have made an attempt to compare our results with local micrometeorological measurements made at an agricultural site operated by the Department of Meteorology at Pennsylvania State University. The measurements, which were made over wheat both before and after harvesting in July, were obtained as part of a field program, which was in its first full summer of operations during 1986. The site was located in a 15 km wide valley about 1 km north of the foot of a mountain range, whose highest elevations extend about 300–400 m above the valley floor. Air can move in a long fetch from the west parallel to the mountains and reach the sensors in the instrument array after a trajectory of about 200 m over the wheat. For wind directions other than westerly, the fetch is not as uniform, and the air moves a shorter distance over the wheat and may traverse other types of row crops.

Comparisons were made between results of the measured and simulated integrated sensible heat fluxes. Differences between model and measurement were systematic, although measured values of B were about one-third to one-fifth those obtained with the model. We feel that this discrepancy arises from errors in the measured surface sensible heat fluxes, which were too small.

It is easy to demonstrate the deleterious effect of small systematic errors in the individual surface sensible heat fluxes on the 24-h averages. For example, consider an innocuous (but systematic) error of 20 $\mathrm{W\,m^{-2}}$ in surface sensible heat flux on a day when the maximum heat flux is 100 $\mathrm{W\,m^{-2}}$. This error represents an uncertainty of more than a factor of two in the 24-h integrated surface sensible heat flux. Such susceptibility of the integrated sensible heat fluxes to small error may be the reason why no one has yet published a statistical comparison between measurements and modeled fluxes obtained from the B-method using constants derived from a boundary layer model.

SOURCES OF ERROR IN MODELED ESTIMATES OF B, B', n, AND n'

Seguin et al. (1985) refer to a ± 0.1 $\mathrm{cm\,day^{-1}}$ (or about 20%) error in evapotranspiration as being acceptable for the B-method, given the present state of the art. In what follows, the magnitude of the error pertains to the quantity $R_{n24} - LE_{24}$ and an error of less than 0.1 cm is considered to be unimportant. Errors in using (2) and (3) from this paper can arise from two important sources: those due to the model and those due to fitting the model results in a straight line.

Errors in the boundary layer model are difficult to assess. Complex models such as the CM contain many different types of parametrizations. Although this model has been tested under a variety of conditions, it is probably difficult to verify the fluxes to within an uncertainty of about 20% of the maximum value for the day. As we pointed out, this magnitude of error is highly destructive of daily average fluxes.

Errors in determining B and n can occur as the result of a deviation between model and straight line. With regard to Figure 1, the generated data points diverge from a straight line at small surface–air temperature differences. Our results show that virtually all the residuals in this region of the graphs were less than 0.1 cm. Exceptions were at low surface–air temperature differences (less than 4°C) and high wind speeds (greater than 4 $\mathrm{m\,s^{-1}}$), in which errors of up to 50% were found. These errors become larger than 0.1 cm for lower wind speeds and higher surface–air temperature differences as the surface roughness increases. For small roughness lengths (less than 0.1 m), the error in fitting a straight line was less than 0.1 cm over the entire range of wind speeds and surface–air temperature differences that were calculated.

Deviations from the best fit straight line are analyzed in Figure 8, which shows that the lowest

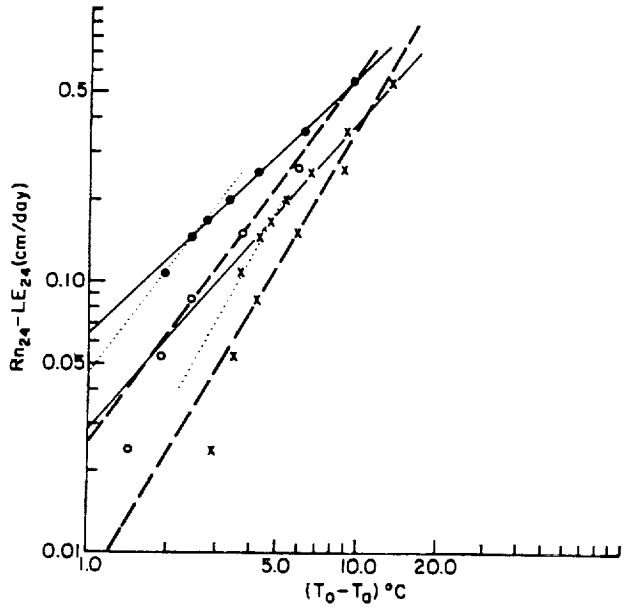

Figure 8. LAI = 4.0; $z_0 = 0.13$; base wind. •—• 2 m midsummer; × — × 50 m midsummer; ∘--∘ 2 m late summer; ×--× 50 m later summer; ... best fit line from 3 to lowest $(T_0 - T_a)$.

three points suggest a straight line with a steeper slope and a lower intercept than the best fit line. When only the net radiation in the model was decreased, commensurate with a change in initial conditions to late summer (September), the best-fit lines resemble those for the lowest three points in the July case. However, the lowest three late-summer points also deviate in the same sense as for the July conditions, suggesting the radiative forcing near the surface is an important factor in the determination of B and n. The same trend was noted for B' and n'. We believe that the weaker radiative forcing and smaller surface–air temperature differences involve weaker static stability near the surface and therefore a change in the calculated surface sensible and latent heat fluxes as dictated by similarity theory.

In order to assess the potential error from choosing an incorrect B or n, we estimated a maximum possible error that would result from choosing a fixed value of B and n (or B' and n') without regard to wind speed and surface roughness. Let us define this maximum error as the maximum variation in $R_{n24} - LE_{24}$ over the entire domain of Figs. 2–7. This domain varies from 1 to 9 $m s^{-1}$ in wind speed and from 0.01 to 0.52 m in surface roughness. Using the values of B and n (or B' and n') at these extrema (the four corner points

Table 2. Representative Values for B, n, B', and n' and Their Maximum Variations in the Domain of z_0 and Windspeed

	Bare Soil		*Vegetation*	
	B	n	B	n
Windspeed at 50 m, T_a at 50 m	0.023	1.0	0.032	1.0
Max variation (cm)	0.06		0.37	
Windspeed at 6.4 m, T_a at 2 m	0.032	1.1	0.032	1.0
Max variation (cm)	0.30		0.63	
	B'	n'	B'	n'
Windspeed at 6.4 m, $\Delta T/\Delta n$	0.062	1.6	0.09	2.1
Max variation (cm)	0.32		1.03	

of Figs. 2–7), we calculated the maximum range in $R_{n24} - LE_{24}$ over the domain of these figures. This maximum range is listed in Table 2 in the row labeled "max variation."

If one were to choose B and n (or B' and n') at the midpoints of these figures (where the surface roughness is about 0.1 m and the wind speed about 5 $m s^{-1}$), instead of at the extrema, the maximum deviation of B and n from this central point would be about one-half that for the maximum range across the entire domain of the figures. The *average* deviation of the integrated evapotranspiration from those in which B and n are chosen in the middle range would be about one-quarter of the maximum possible error listed in Table 2. Dividing the values listed in Table 2 by 4 therefore gives us an estimate of the average error in using (2) and (3), if B and n (or B' and n') were chosen from the center of these graphs. This error is generally less than 0.1 cm in most, but not all, circumstances.

CONCLUSIONS

The present study addresses the variation in the parameters B and n in the B-method. These parameters are sensitive to wind speed and roughness, especially over vegetation. Values of B are similar to those of Jackson et al. (1977) for vegetation and Seguin and Itier (1983) for bare soil. It is interesting to note that Rambal et al. (1985) also find that B increases with increasing vegetation height and density. For $n = 1.5$ Rambal et al. obtained $B = 0.032$ for shrubland and $B = 0.068$

for middense woodland, values which resemble ours for bare soil and vegetation, respectively. For all practical purposes, however, we find that the exponent n was 1.0 for both the bare soil and vegetation cases.

We suggest that the B-method might be more generally applicable to regional-scale remote sensing if the reference level for air temperature and wind speed were taken at 50 m, rather than at 2 m because the temperature and wind speed at the 50 m level are relatively insensitive to local surface inhomogeneities. For this reason we show the distribution of B and n for air temperatures measured both at the customary 2 m elevation (6.4 m for wind speed) and at 50 m. In view of all the errors inherent in the B-method, it may be sufficiently accurate to use regional-scale surface wind and air temperature measurements and to stratify the wind speed, surface roughness, and vegetation type into just two or three categories.

We also propose using the morning rise in radiometric surface temperature [as suggested by Wetzel et al. (1984)] in the B-method, because this does not require knowledge of an air temperature. Although the data for the morning rise in surface temperature fit straight lines in log–log coordinates, the coefficient B' and the exponent n' are highly sensitive to wind speed and surface roughness. Moreover, the latter differed considerably from unity for most combinations of wind speed and surface roughness.

The authors would like to thank Jaser K. El Salem for his assistance in providing the field measurements. The research was supported by a grant from NASA, NAG5-919 as part of the ISLSCP retroactive study program.

REFERENCES

Bartholic, J. F., Namken, L. N., and Weigand, C. L. (1972), Aerial thermal scanner to determine temperatures of soils and crop canopies differing in water stress, *Agron. J.* 64:603–609.

Carlson, T. N. (1986), Regional scale estimates of surface moisture availability and thermal inertia using remote thermal measurements, *Remote Sens. Rev.* 1:197–247.

Flores, A. L., and Carlson, T. N. (1987), Estimation of surface moisture availability from remote temperature measurements, *J. Geophys. Res.* 92:9581–9585.

Itier, B., and Riou, C. (1982), Une nouvelle methode de determination d l'evapotranspiration réelle par thermographie infrarouge, *J. Rech. Atmos.* 16:113–125.

Jackson, R. D., Reginato, R. J., and Idso, S. B. (1977), Wheat canopy temperature: a practical tool for evaluating water requirements, *Water Resource Res.* 13:651–656.

Lagouarde, J.-P. (1988), Use of NOAA-AVHRR data combined with an agometeorological model for evaporation mapping, *Int. J. Remote Sens.*, forthcoming.

Lagouarde, J.-P., and Brunet, Y. (1988), Spatial integration of surface latent heat flux and evaporation mapping, *Adv. Space Res.*, forthcoming.

Monteith, J. L. (1975), *Vegetation and the Atmosphere*, Academic, New York, Vol. I, 278 pp.

Nieuwenhuis, G. J. A., Schmidt, E. H., and Tunnissen, H. A. M. (1985), Estimation of regional evapotranspiration of arable crops from thermal infrared images, *J. Remote Sens.* 6:1319–1334.

Price, J. C. (1982), On the use of satellite data to infer surface fluxes at meteorological scales, *J. Appl. Meteorol.* 21:1111–1122.

Rambal, S., Lacaze, B., Mazurek, H., and Debussche, G. (1985), Comparison of hydrostatically simulated and remotely sensed actual evapotranspiration from some Mediterranean vegetation formations, *Int. J. Remote Sens.* 6:1475–1481.

Seguin, B., and Itier, B. (1983), Using midday surface temperature to estimate daily evaporation from satellite thermal IR data, *Int. J. Remote Sens.* 4:371–383.

Seguin, B., Baelz, S., Monget, J. M., and Petit, V. (1982), Utilisation de la thermographie IR pour l'estimation de l'evaporation regionale II. Resultats obtenus à partir des données de satellite, *Agronomie* 2:113–118.

Seguin, B., Lagouarde, J. P., and Kerr, Y. (1985), Estimation of regional evapotranspiration using midday surface temperature from satellite thermal IR data, *Proceedings of the ISLSCP Conference*, Rome, Italy, pp. 339–344.

Soer, G. J. (1980), Estimation of regional evapotranspiration and soil moisture conditions using remotely sensed crop surface temperatures, *Remote Sens. Environ.* 9:27–45.

Taconet, D., Carlson, T. N., Bernard, R., and Vidal-Madjar, D. (1986), Evaluation of a surface vegetation/model using satellite infrared surface temperatures, *J. Climate Appl. Meteorol.* 25:1752–1767.

Wetzel, P. J., and Woodward, R. H. (1987), Soil moisture estimation using GOES-VISSR infrared data: a case study with a simple statistical method, *J. Climate Appl. Meteorol.* 26:107–117.

Wetzel, P. J., Atlas, P., and Woodward, R. (1984), Determining soil moisture from geosynchronous satellite infrared data: a feasibility study, *J. Climate Appl. Meteorol.* 23:375–391.

APPENDIX B

Agricultural and Forest Meteorology, 52 (1990) 5–43
Elsevier Science Publishers B.V., Amsterdam — Printed in The Netherlands

A stomatal resistance model illustrating plant vs. external control of transpiration

Barry H. Lynn* and Toby N. Carlson
Department of Meteorology, The Pennsylvania State University, University Park, PA 16802 (U.S.A.)

(Received July 3, 1989; revision accepted December 12, 1989)

ABSTRACT

Lynn, B.H. and Carlson, T.N., 1990. A stomatal resistance model illustrating plant vs. external control of transpiration. *Agric. For. Meteorol.*, 52: 5–43.

A stomatal resistance model is proposed that is specifically designed for use within atmospheric boundary layer models. Stomatal resistance is expressed as a product of linear discontinuous functions of leaf water potential and solar flux; vapor pressure deficit is included indirectly by allowing for a gradient of leaf water potential between the surface and the interior of the leaf. An important assumption is that stomatal resistance increases sharply beyond a critical value of leaf water potential and/or critical solar flux. The model is able to simulate a transpiration plateau; this plateau may occur because of high atmospheric demand and/or a limitation in soil water.

INTRODUCTION

Evapotranspiration is highly dependent upon the resistance exerted by the plant on the flow of water from soil to atmosphere. Owing to the complexity of calculating plant resistance, one approach has been to represent the vegetation canopy as a uniform "big leaf". This method employs a combination equation, such as the Penman–Monteith formula (Monteith, 1975), in which the soil/plant (canopy) resistance constitutes a basic unknown. More complex models allow for the calculation of both a soil and vegetation flux, which depend, respectively, on soil and plant (stomatal) resistances (Deardorff, 1978; Soer, 1980; Dickinson, 1984; Halldin et al., 1984/85; Lindroth and Halldin, 1986; Taconet et al., 1986a, b; Sellers and Dorman, 1987; Wetzel and Chang, 1987; Lhomme, 1988; Abramopoulos et al., 1988).

There is a general consensus among plant scientists that stomatal resistance is correlated with a number of factors. These are short-term changes in leaf

*Present address: Goddard Institute for Space Studies, 2880 Broadway, New York, NY 10025, U.S.A.

0168-1923/90/$03.50

water potential, significant drying of the soil (very negative soil water potential), vapor pressure deficit, solar flux, leaf temperature, and ambient carbon dioxide (Turner, 1970, 1974; Van Bavel, 1974; Jarvis, 1976; Tan and Black, 1976; Takami and Uchijima, 1977; Deardorff, 1978; Farquhar, 1978; Federer, 1979; Takami and Yukimura, 1979; Singh and Szeicz, 1980; Fisher et al., 1981; Farquhar and Sharkey, 1982; Kaufmann, 1982; Choudhury, 1983; Zeiger, 1983; Dwyer and Stewart, 1984; Halldin et al., 1984/85; Avissar et al., 1985; Choudhury and Idso, 1985; Körner, 1985; Lindroth, 1985; Simpson et al., 1985; Grantz and Zeiger, 1986; Lindroth and Halldin, 1986; Baldocchi et al., 1987; B. Acock, personal communication, 1989). It has also been proposed that there is an additional dependence of stomatal resistance on soil water potential, caused by the transport of cytokinins from the root in response to soil drying (Gollan et al., 1986; Schulze, 1986; Munns and King, 1988).

In order to express the relationship between these factors and stomatal resistance, it is necessary to combine them in a deterministic manner. There are numerous examples in the literature in which stomatal resistance is expressed as either an additive or multiplicative model. In some cases, deterministic expressions are both additive and multiplicative (Table 1). Almost all models are expressed as a function of solar flux, soil or bulk mesophyllic leaf water potential, and vapor pressure deficit (Table 2).

The purpose of this paper is to formulate a stomatal resistance model that also incorporates an analytical solution for leaf water potential. A unique aspect of this model is that it allows for epidermal control of leaf water potential

TABLE 1

Stomatal resistance functions by type

Model	Type I	Type II	Type III
Avissar et al. (1985)		+	
Baldocchi et al. (1987)		+	
Choudhury (1983)		+	
Choudhury and Idso (1985)		+	
Deardorff (1978)			+
Dwyer and Stewart (1984)	+		
Federer (1979)	+		
Halldin et al. (1984/85)		+	
Jarvis (1976)		+	
Kaufmann (1982)			+
Simpson et al. (1985)			+
Singh and Sziecz (1980)			+
Takami and Yukimura (1979)		+	

Each equation has been assigned a type, i.e. additive (Type I), multiplicative (Type II), while Type III is a hybrid of Type I and Type II.

TABLE 2

Stomatal resistance functions by variable

Modeler	$f(\text{wat})$	$f(S)$	$f(V)$	$f(T)$
Avissar et al. (1985)	ψ_g	S	V_a	T_l
Baldocchi et al. (1987)	ψ_l	PAR	V_a	T_a
Choudhury (1983)	ψ_l	R_{net}	*	*
Choudhury and Idso (1985)	ψ_l	S	*	*
Deardorff (1978)	θ_{vo}/θ_v	S	S	*
Dwyer and Stewart (1984)	θ_v	S	V_a	*
Federer (1979)	ψ_l	S	V_a	T_a
Halldin et al. (1984/85)	-	S	V_a	*
Jarvis (1976)	ψ_l	S	V_a	T_a
Kaufmann (1982)	*	PAR	V_l	*
Simpson et al. (1985)	ψ_{xb}	*	V_a	*
Singh and Sziecz (1976)	*	S	*	*
Takami and Yukumura (1979)	ψ_l	*	*	*

Symbols: (*) indicates not included and (-) is not applicable. Table 2 is a listing of model types and the parameters included in each. $f(\text{wat})$ refers to parameters relating r_s to water content of the soil or leaf. The other headings pertain to the mathematical functions governing r_s for solar flux ($f(S)$), vapor pressure deficit ($f(V)$) and temperature ($f(T)$). R_{net} is the net radiation, S is the incident solar flux, and PAR is the photosynthetically active radiation (proportional to 0.47 S (van Bavel, 1974)). ψ_l is the leaf water potential, ψ_{xb} is the pre-dawn (base) xylem potential, and θ_{vo} and θ_v refer to the surface and root zone soil water content. V and T are the vapor pressure deficit and temperature, respectively. Subscript a refers to the atmosphere while l refers to the leaf or leaf–air difference.

by specifying a gradient of leaf water potential between the surface and the interior of the leaf. This gradient is dependent on the vapor pressure deficit. Leaf water potential is calculated as a function of soil water potential, solar flux, vapor pressure deficit, leaf boundary layer resistance and root–stem resistance, thus incorporating indirectly the effect of these parameters on stomatal resistance.

An assumption in the model is that there exists a critical value of leaf water potential at which stomatal resistance increases sharply with decreasing leaf water potential. A number of researchers have justified this assumption (Turner, 1974; Boyer, 1976; Thomas et al., 1976; Denmead and Millar, 1976a; Katerji, 1979; Pospisilova and Solarova, 1980; Idso, 1983; Dwyer and Stewart, 1984; Schulze et al., 1987). However, in this paper we assume that the critical water potential refers to that of the epidermis as suggested by Sheriff (1984) and Schulze (1986).

In order to allow for the interaction between soil, plant, and atmosphere, we have incorporated the stomatal resistance model within a canopy model (which is an extension of the model by Taconet et al. (1986a) (Fig. 1)), and a one-dimensional boundary layer model of Carlson (1986) and Taconet et

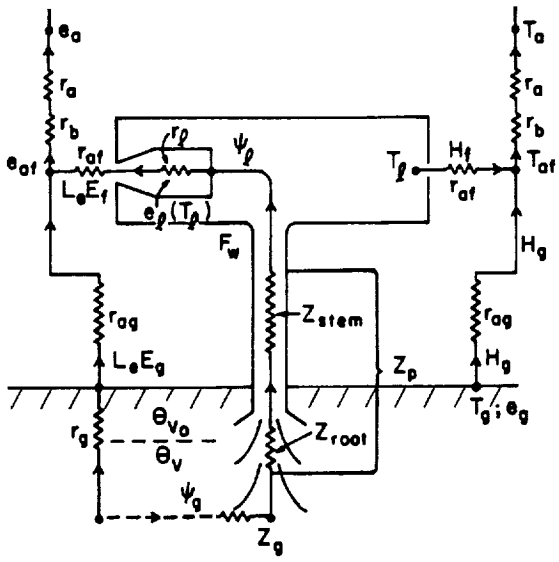

Fig. 1. Structure of the plant-canopy model, showing the exchange of sensible and latent heat fluxes between plant, atmosphere and surface (see text for details).

al. (1986b). In this paper, we discuss the stomatal resistance formulation and the solution to the leaf water potential equation, and discuss its significance. We then show how the model is consistent with some field measurements.

PLANT MODEL

The flow of water from soil to the atmosphere can be described by a flow diagram as seen in Fig. 1. Table 3 contains a listing of all the variables in this figure and the equations below.

Water flow from soil to leaf

The movement of water from the soil to the leaf begins in the soil root zone with soil water content θ_v or soil water potential ψ_g. Following Ohm's law the water flux from soil to leaf is given by

$$F_w = (\psi_g - \psi_l - H)/(Z_p + Z_g) \quad (1)$$

where: the variables are the soil water potential (ψ_g, bar), and the mesophyllic leaf potential (ψ_l, bar); H is the gravitational potential (bar); Z_p is the root–xylem resistance (bar $(W\ m^{-2})^{-1}$); the soil root interface resistance is Z_g (bar $(W\ m^{-2})^{-1}$). Here $H = \rho_w g h$, where: ρ_w is the density of liquid water ($kg\ m^{-3}$); g is the gravitational constant ($m\ s^{-2}$); h is the average height of the leaves above the root zone (m). Equation (1) has gained wide acceptance

with plant scientists (Cowan, 1965 (who cites a seminal paper by van den Honert); Boyer, 1971; Feddes and Rijtema, 1972; Camacho et al., 1974; Denmead and Millar, 1976b; So et al., 1976; Meyer and Green, 1980; Katerji and Hallaire, 1984; Passioura, 1984; Passioura and Munns, 1984; Choudhury and Idso, 1985).

Description of soil water variables

In the boundary layer model, soil water content is initialized with the moisture availability parameters of the surface (M_o) and of the root zone (M). M_o and M are equated to their respective soil water contents by the somewhat arbitrary but empirically justifiable assumption that $M_o = \theta_{vo}/\theta_{vc}$ and $M = \theta_v/\theta_{vc}$. θ_{vo} and θ_v are the soil water contents of the surface layer and root zone, respectively, and θ_{vc} is the value of soil water content at field capacity.

As noted in eqn. (1), the flow of water from soil to leaf is dependent upon soil water potential. Soil water potential ψ_g (bar), for a given soil type, is related to θ_v ($cm^3\ cm^{-3}$) using a parametric equation discussed in Campbell (1974). This equation is:

$$\psi_g = \psi_{sat}(\theta_v/\theta_{vsat})^{-b} \tag{2}$$

where: ψ_{sat} is the value of soil water potential at saturation (bar); θ_{vsat} is the value of soil water content at saturation ($cm^3\ cm^{-3}$); b is a constant.

Z_g expresses the resistance of the flow of liquid water from the soil to the roots, in response to a gradient of water potential that increases as the soil dries (Cowan, 1965). Various ways exist to determine Z_g, e.g. Cowan (1965), Feddes and Rijtema (1972), Denmead and Millar (1976b) and Federer (1979, 1982). The choice for the present model is based on a scheme of Choudhury and Idso (1985) which was originally proposed by Feddes and Rijtema (1972). They let

$$Z_g = (0.0013/(Z_{eff}K_g))K_l \tag{3}$$

where: 0.0013 (m^2) is the ratio of a parameter relating root distance and geometry to the reciprocal of the effective rooting depth; Z_{eff} is the effective rooting depth (m); K_g is the soil hydraulic conductivity ($m\ s^{-1}$), and is given by Campbell (1974) as:

$$K_g = K_{sat}(\theta_v/\theta_{vsat})^{2b+2} \tag{4a}$$

or,

$$K_g = K_{sat}(\psi_{gsat}/\psi_g)^{2+2/b} \tag{4b}$$

where: K_{sat} is the maximum conductivity at field saturation of the soil ($m\ s^{-1}$); θ_{vsat} is the saturation volume water content; b is a constant that is dependent on soil type; ψ_{gsat} is the value of the hydraulic potential at field satu-

TABLE 3

List of variables and coefficients

Variable	Comments	Units
α	leading coefficient, eqn. (7), set equal to r_{min}	$s\ m^{-1}$
b	coefficient in eqns. (2), (3), (4)	
b_1	the slope of the subcritical part of the $f(\psi_e)$ function; $\psi_e > \psi_c$	$s\ m^{-1}\ bar^{-1}$
b_2	the slope of the supercritical part of the $f(\psi_e)$ function; $\psi_e \leq \psi_c$	$s\ m^{-1}\ bar^{-1}$
β	constant describing the difference between mesophyllic and leaf epidermal water potential which is divided by vapor pressure deficit	$bar\ mbar^{-1}$
c_1	the slope of $f(S)$ between S_o and S where $S > S_c$	$s\ m^{-1}\ (W\ m^{-2})^{-1}$
c_2	the slope of $f(S)$ between S_c and S where $S \leq S_c$	$s\ m^{-1}\ (W\ m^{-2})^{-1}$
C_p	the specific heat of dry air at constant pressure	$J\ kg^{-1}\ K^{-1}$
δ_w	$\delta_w = 0$ ($\psi_e > \psi_c$); $\delta_w = 1$ ($\psi_e \leq \psi_c$), and $\psi_e = \psi_c$ in the second term on the righthand side of eqn. (8a)	
δ_s	$\delta_s = 0$ ($S > S_c$); $\delta_s = 1$ ($S \leq S_c$), and $S = S_c$ in the second term on the righthand side of eqn. (8b)	
e_{af}	leaf–air boundary vapor pressure	mbar
$e_1(T_1)$	the saturation vapor pressure at the temperature of the leaf	mbar
F_w	flow of water from soil to leaf	$W\ m^{-2}$
$f(CO_2)$	stomatal resistance factor due to carbon dioxide	
$f(\psi_s)$	stomatal resistance factor due to epidermal leaf water potential	
$f(S)$	stomatal resistance factor due to solar flux	
$f(T_1)$	stomatal resistance factor due to leaf temperature	
g	gravitational constant	$m\ s^{-2}$
γ	$PC_p/0.622L_e$	$mbar\ K^{-1}$
h	the average height of the leaves above the root zone	m
H	gravitational potential	bar
H_f	foliage sensible heat flux	$W\ m^{-2}$
K_g	the soil hydraulic conductivity	$m\ s^{-1}$
K_1	a conversion factor	$bar\ (W\ m^{-2})^{-1}$
L_e	latent heat of vaporization of water	$J\ kg^{-1}$
L_eE_f	foliage latent heat flux	$W\ m^{-2}$
LPSI	Leaf Potential Stress Index	bar
M_o	$M_o = \theta_{vo}/\theta_{vc}$ (surface moisture availability)	
M	$M = \theta_v/\theta_{vc}$ (moisture availability of the root zone)	
P	the atmospheric pressure	mbar
ρ_w	the density of liquid water	$kg\ m^{-3}$
r_a	air resistance in surface layer	$s\ m^{-1}$
r_{af}	the resistance for heat and water vapor flux for the interleaf air spaces	$s\ m^{-1}$
r_{ag}	air resistance between the ground and the interleaf air spaces	$s\ m^{-1}$
r_b	air resistance in transition surface layer	$s\ m^{-1}$
r_{ct}	"critical" resistance	$s\ m^{-1}$
r_{cut}	cuticular resistance	$s\ m^{-1}$
r_l	leaf resistance	$s\ m^{-1}$
r_{min}	minimum stomatal resistance	$s\ m^{-1}$

TABLE 3 (continued)

Variable	Comments	Units
r_s	stomatal resistance	$s\ m^{-1}$
θ_v	soil water content of the root zone	$cm^3\ cm^{-3}$
θ_{vc}	soil water field capacity	$cm^3\ cm^{-3}$
θ_{vo}	surface soil water content	$cm^3\ cm^{-3}$
θ_{vsat}	value of soil water content at saturation	$cm^3\ cm^{-3}$
ψ_c	critical leaf water potential, which is the intersection of the two lines with slopes b_1 and b_2	bar
ψ_e	epidermal leaf water potential	bar
ψ_g	soil water potential	bar
ψ_{gc}	critical soil water potential	bar
ψ_l	mesophyllic leaf water potential	bar
ψ_{sat}	the value of soil water potential at saturation	bar
S_c	the solar radiation threshold, which is at the intersection of lines formed by the slopes c_1 and c_2	$W\ m^{-2}$
S_o	a maximum solar radiation value, loosely defined as the value at which light saturation of the leaves is reached	$W\ m^{-2}$
σ	ρL_e	$kg\ m^{-3}\ J\ kg^{-1}$
T_a	air temperature of the surface layer	K
T_{af}	temperature of the interfoliage air spaces	K
T_g	temperature of the ground surface	K
T_l	temperature of the leaf surface	K
V	the difference between $e_s(T_l)$ and e_{af}	mbar
WPSI	Water Potential Stress Index	bar
Z_{eff}	the effective rooting depth	m
Z_g	the soil root interface resistance	$bar\ (W\ m^{-2})^{-1}$
Z_p	root–xylem resistance	$bar\ (W\ m^{-2})^{-1}$
Z_{root}	root resistance	$bar\ (W\ m^{-2})^{-1}$
Z_{stem}	stem resistance	$bar\ (W\ m^{-2})^{-1}$
Z_t	Z_g+Z_p	$bar\ (W\ m^{-2})^{-1}$

ration. K_1 is a conversion factor which enables Z_g to be expressed in bar $(W\ m^{-2})^{-1}$, given as 0.4×10^{-10}.

ψ_g and Z_g (K_g) vary with soil moisture (θ_v) in a parametric manner as determined by θ_{vsat}, ψ_{gsat}, K_{sat}, and b which are all functions of soil type. ψ_g becomes very negative, and Z_g large (K_g small) when θ_v approaches a critical value. This critical value may sometimes be defined as the "nominal wilting point", or the soil water content at which the leaves have lost or lose turgor in the early morning. The values of these parameters can be found in Cosby et al. (1984). Those for loam were found to agree with measurements made at a local agricultural field site (Rock Springs), provided that θ_{vsat}, which is 0.43 as proposed by Cosby et al. (1984), is replaced by 0.34, which is the field capacity at Rock Springs. Henceforth, this value of field capacity will be used as a basis for calculation throughout this paper.

Root and stem resistance

The internal plant resistance, Z_p, consists of the root and stem resistance, referred to as Z_{root} and Z_{stem}, respectively (see Fig. 1). In principle, Z_p can be determined by dividing the difference between a value of leaf water potential and the pre-dawn leaf water potential by the transpiration rate at the time at which the leaf water potential is made. This calculation is often complicated by a hysteresis effect produced by water storage in the plant (Katerji and Hallaire, 1984).

Unfortunately, very few measurements of Z_p have been published, probably because of the difficulty in measuring leaf water potential and transpiration simultaneously. Some estimates of Z_p can be obtained from, or are listed in Boyer (1971), Denmead and Millar (1976b), Jarvis (1976), Running (1980a); Katerji et al. (1983), and Abdul-Jabbar et al. (1984). Units may be expressed in s, h, or in bar s cm^{-1}; but here, the preferred units are in terms of the drop in potential from root to xylem divided by the flux per unit leaf area (bar $(W\ m^{-2})^{-1}$). The conversion from s to bar $(W\ m^{-2})^{-1}$ is given by the factor $1/(\rho_w L_e \times 10)$, which equals 0.4×10^{-10}. (The value of 10 is the conversion from m to bar (10 m bar^{-1}).) The conversion from bar s cm^{-1} to bar $(W\ m^{-2})^{-1}$ is given by the factor $100/(\rho_w L_e)$, which equals 0.4×10^{-7}. A typical value of Z_p (obtained from Katerji and Hallaire (1984)) is 0.047 bar $(W\ m^{-2})^{-1}$.

It should be noted, however, that the value of Z_p varies by species (Abdul-Jabbar et al., 1984). Z_p also varies during the growing season because it is a function of the number, width, age of the xylem, and the root mass (B. Acock, personal communication, 1989). We suggest that Z_p may vary inversely with crop height as is indicated by the results presented later in the paper. Z_p is an important parameter, because sensitivity tests presented in this paper show that the transpiration rate and the leaf stomatal resistance are indirectly related to the choice of Z_p.

Hailey et al. (1973), Bunce (1978), Jones (1978), Katerji and Hallaire (1984), and Passioura and Munns (1984) caution that the application of Ohm's laws to plants is not always applicable. For instance, Bunce (1978) found that transpiration continued to increase in some species, (e.g. soybeans and cotton), while leaf water potential remained constant. Various theories have been proposed to explain this phenomenon. Bunce suggests that a decrease in root resistance due to root elongation may decrease the value of Z_p. However, Katerji and Hallaire (1984) suggest that large demand causes the plant to release internal sources of moisture for transpiration, an explanation that we favor. This would suggest that the value of Z_p remains relatively unchanged with transpiration. Thus we assume that root–stem resistance remains constant over a range of leaf water potential.

Water flow from the leaf to the atmospheric boundary layer

The flux of water vapor from the leaf to the boundary layer is given as

$$L_e E_f = (\rho C_p/\gamma) V/(r_l + r_{af}) \tag{5}$$

where: V is the difference between the saturation vapor pressure at the temperature of the leaf ($e_s(T_l)$) and the leaf–air boundary vapor pressure (e_{af}) (mbar); γ is equal to $PC_p/0.622L_e$ (P is the atmospheric pressure (mbar), C_p is the specific heat of dry air at constant pressure (J kg^{-1} K^{-1}), and L_e is the latent heat of vaporization of water (J kg^{-1}); the leaf resistance (r_l) (s m^{-1}) is related to the stomatal resistance (r_s) (s m^{-1}) by the formula for parallel resistances

$$1/r_l = 1/r_s + 1/r_{cut} \tag{6}$$

where: r_s is the stomatal resistance; r_{cut} is the cuticular resistance (s m^{-1}); r_{af} is the resistance for heat and water vapor for the interleaf air spaces (s m^{-1}) and is a function of the friction velocity and leaf area index (LAI) (Thom, 1972; Taconet et al., 1986a). The latent flux is linked to the temperature and specific humidity of the boundary layer by atmospheric resistances r_a and r_b (s m^{-1}).

STOMATAL RESISTANCE MODEL

Linear discontinuous model

We adopt a multiplicative model which is based on the product of functions $f(\psi_e), f(S), f(T_l)$, and $f(CO_2)$. These are the inverse fractional conductance due to leaf water potential, solar flux, temperature, and carbon dioxide, respectively. (The effect of vapor pressure deficit (V) is treated separately, and is discussed below; the transport of hormones from the root is not explicitly accounted for.)

Given the assumptions made above, the equation for r_s is written as:

$$r_s = \alpha f(S) f(\psi_e) f(T_l) f(CO_2) \tag{7}$$

where α has the dimensions of resistance and is equated with the minimum stomatal resistance r_{min} (defined as the resistance measured when ψ_e is zero, the leaves are saturated by sunlight, the leaf temperature and carbon dioxide concentration are optimum and the vapor pressure deficit is equal to zero). (The reader need be aware that the definition of minimum stomatal resistance is not universally expressed in this way because a minimum measured value will vary with vapor pressure deficit, solar radiation, leaf (or soil) water potential, and is a function of plant type and plant phenology.) All of the functions may vary from 1.0 to infinity.

Because of the limited availability of data, a simplified representation of the governing factors in eqn. (7) is essential. Accordingly, we propose a "discontinuous linear model" similar to that discussed by Fisher et al. (1981). Unlike Fisher's model, however, the exponential behavior of $f(S)$, $f(\psi_e)$, $f(T_l)$, and $f(CO_2)$ is represented by a pair of straight lines (Fig. 2) whose intersection defines a critical value, S_c, ψ_c, T_c and CO_2. Figure 2 suggests that an appropriate straight line fit to exponential functions can capture the essential discontinuous nature of the functions without great loss of accuracy.

The following is a mathematical description of the factors $f(\psi_e)$ and $f(S)$:

$$f(\psi_e) = (r_{min} + b_1\psi_e + b_2(\psi_c - \psi_e)\delta_\psi)/r_{min} \quad (8a)$$

where: r_{min} is the minimum value of resistance; b_1 is the slope of the subcritical part of the $f(\psi_e)$ function; $\psi_e > \psi_c$; b_2 is the slope of the supercritical part of the $f(\psi_e)$ function; $\psi_e \leqslant \psi_c$; ψ_c is the critical leaf water potential, which is the intersection of the two lines with slopes b_1 and b_2; $\delta_\psi = 0$ $(\psi_e > \psi_c)$; $\delta_\psi = 1$ $(\psi_e \leqslant \psi_c)$, and $\psi_e = \psi_c$ in the second term on the right-hand side of eqn. (8a).

$$f(S) = (r_{min} + c_1(S_o - S) + c_2(S_c - S)\delta_s)/r_{min} \quad (8b)$$

where: c_1 is the slope of $f(S)$ between S_o and S_c; c_2 is the slope of $f(S)$ between S_c and S where $S \leqslant S_c$; S_c is the solar radiation threshold, which is the intersections of lines formed by the slopes c_1 and c_2; S_o is a maximum solar radiation value, loosely defined as the value at which light saturation of the leaves is reached; $\delta_s = 0$ $(S > S_c)$, $\delta_s = 1$ $(S \leqslant S_c)$, and $S = S_c$ in the second term on the right-hand side of eqn. (8b).

It is possible to define the response of the stomata to temperature and car-

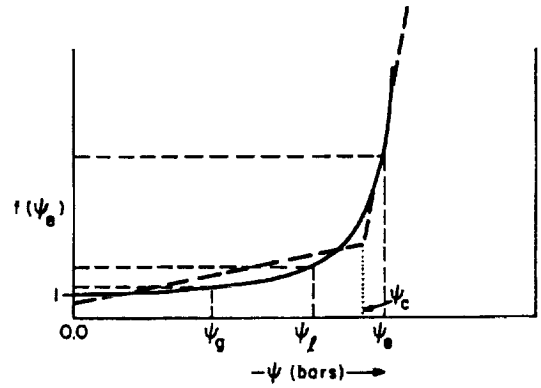

Fig. 2. Schematic illustration of $f(\psi_e)$ function (solid curve) with changing leaf water potential, starting from a base value ψ_g. The vertical dotted line pertains to the critical leaf water potential ψ_c. The sloping dashed lines show the linear approximation to the function by two straight lines intersecting at ψ_c. Also shown are the relative values of $f(\psi_e)$ $f(\psi_l)$, and $f(\psi_g)$ at a given ψ_e, as indicated by the horizontal dashed lines.

bon dioxide as noted above. There is, however, relatively little data on which to base these functions, although the response of the stomata to these factors may be exponential (Jarvis, 1976; Morison, 1987; Baldocchi et al., 1987). Taking into account the findings of the noted authors, we assume that T_l is within an operational range of temperature, and that the ambient carbon dioxide concentration has no effect. Thus $f(T_l)=1.0$ and $f(CO_2)=1.0$. It should be apparent that the use of this linear formulation for the governing factors provides a simple means of representing the effects of each factor.

If $S=S_o$, the multiplicative model reduces to an additive model. If S is less than S_o, then $(S-S_o)$ multiplies the effect of $f(\psi_c)$. This suggests that an underlying assumption of this model is that values of solar flux less than S_o affect the value of leaf water potential.

A survey of the literature suggests that larger values of ψ_c correspond to

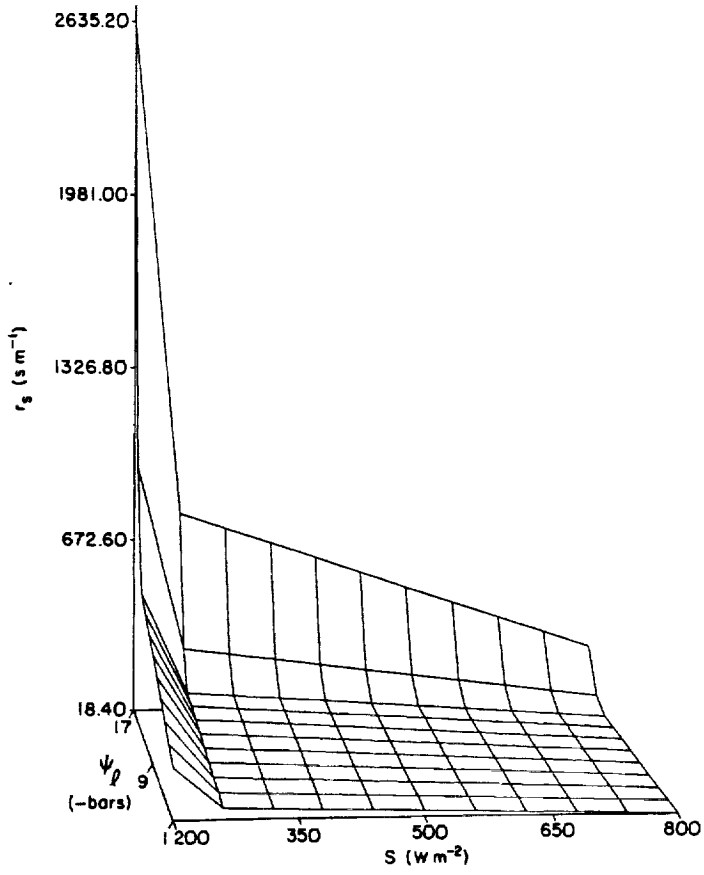

Fig. 3. Stomatal resistance vs. leaf water potential (ψ_c) and solar flux (S) is shown in a three-dimensional plot for $\psi_c=-16$ bar, and $S_c=225$ W m^{-2}.

temperate latitude crops (typically -13 to -16 bar), while the value of forest trees (such as a pine) might be as small as -22 bar (Running, 1976). Tall trees and plants growing in a desert environment might have even lower critical leaf water potentials, and ψ_c may also be a function of soil water type and water stress (Dwyer and Stewart, 1984; B. Acock, personal communication, 1989; J. Norman, personal communication, 1989). The value of S_c typically ranges between 50 and 250 W m^{-2}.

Figure 3 shows how the threshold values dramatically affect resistance. There are relatively small changes in resistance until either the leaf water potential reaches its critical value (ψ_c) or the solar flux becomes less than its critical value (S_c). Beyond the critical thresholds, the rate of change in r_s is most strongly influenced by b_2 and c_2. It is worth noting that either solar intensity or leaf potential can limit transpiration, but owing to the small value of S_c, the leaf water potential is more important than S_c in constraining the transpiration flux.

The effects of vapor pressure deficit

One definition of vapor pressure deficit is the difference between the saturation vapor pressure of the air above the canopy and the actual vapor pressure of the air (similar to the dew point depression). This definition is used because it is relatively easy to measure and corresponds to a parameter in the Penman–Monteith equation (Monteith, 1975). Some researchers, however, such as Camacho et al. (1974), Ackerson and Krieg (1977), and Luxmoore et al. (1981) prefer to work with the leaf–air humidity difference, which is a more fundamental quantity because it represents the actual vapor gradient experienced by the leaf. Since the mathematical relationship between these definitions of vapor pressure deficit is not unique (Choudhury and Monteith, 1986), it is more physically correct to use the definition of V that represents the vapor pressure difference between the leaf surface and that in the interleaf airspaces. We adopt this definition of V.

Most researchers have characterized the response of stomatal resistance to vapor pressure deficit as either linear, exponential, or both, depending upon species. The linear relationships have been proposed by Federer (1979), Choudhury (1983), Halldin et al. (1984/85), Feldhake and Boyer (1985), Simpson et al. (1985) and Lindroth (1985). Exponential formulations have been proposed by Jarvis (1976), Tan and Black (1976), Avissar et al. (1985) and Baldocchi et al. (1987). Camacho et al. (1974), Ackerson and Krieg (1977) and Gollan et al. (1985) have found the stomatal resistance to be both linear and exponential, depending on the crop or range of vapor pressure deficit.

After reviewing the many stomatal resistance formulations summarized in

Table 1, we were unable to understand the basis for a direct effect of vapor pressure deficit on stomatal resistance. It may be possible to explain the response of the stomata to V as a response of the guard cells to epidermal leaf water potential. At the same time, we recognize that transpiration is correlated with vapor pressure deficit and with a gradient of water potential within the leaf. Therefore we postulate two leaf water potentials, one for the mesophyll (ψ_l) and one for the epidermis (ψ_e) (near the guard cells) such that

$$\psi_e = \psi_l - \beta V \tag{9}$$

where β is a constant. Gradients of water potential between the mesophyll and epidermis have been measured (Shackel and Brinckmann, 1985; Shackel, 1987; Frensch and Shulze, 1988).

A virtue of eqn. (9) is that it captures the "feedforward" effect described by Farquhar (1978), Sheriff (1984) and Schulze (1986). The feedforward effect is associated with an increase and then a decrease in transpiration as V increases. This is accompanied by a continued decrease in epidermal leaf water potential, while mesophyllic water potential increases beyond the point of transpiration decrease. Körner (1985) has observed the feedforward response in mountain maple, silver beech, and Scots Pine. Running (1976), and Sellers and Dorman (1987) have also found that the stomata of other coniferous trees show a similar response to vapor pressure deficit. Sheriff (1977), J.A. Bunce (personal communication, 1989), and Baldocchi et al. (1987) have noted that the response of the stomata to vapor pressure deficit varies among crop plants. Others who have investigated the feedforward response are Zieger (1983), Sheriff (1984), El-Sharkaway et al. (1984), Xu et al. (1984), Roessler and Monson (1985), and Grantz and Zeiger (1986).

Solution for leaf potential

Although the representation of natural processes within the soil–plant canopy model is complex, the system of equations presented above allows for a mathematically simple derivation for ψ_e in terms of soil moisture, solar flux, vapor pressure deficit, interleaf air resistance, and plant internal resistance.

Assuming that the plant capacitance or storage capacity, as defined by Jones (1983), is small, then

$$L_e E_f = F_w \tag{10}$$

where F_w is the flux of water from the root zone to the leaves (per unit leaf area). Equation (10), stating that the water flux entering the roots (F_w) is equal to the transpiration rate ($L_e E_f$), assumes a "steady state" (Jarvis, 1976), and results in a quadratic solution for ψ_e, given a linear relationship between r_s and ψ_e.

Before solving for ψ_e, it is necessary to test whether ψ_e is below or above the

threshold value in order to determine the value of δ_ψ. To do so, a critical soil water potential (ψ_{gc}) is defined as the minimum soil water potential that can meet the evaporative demand without ψ_e becoming less than ψ_c. This is derived from eqn. (10) by setting the leaf water potential equal to that of the threshold epidermal leaf water potential, at which point r_s is equal to a critical resistance r_{ct}. Rearranging then yields

$$\psi_{gc} = (\psi_c + \beta V) + (V\sigma Z_t)/\{r_{af} + [r_{cut} r_{ct}/(r_{cut} + r_{ct})]\} + H \quad (11)$$

where $Z_t = Z_p + Z_g$. If the critical soil water potential is less than the value of the soil water potential, the subcritical solution is the correct solution because ψ_e will be greater than ψ_c. If, however, the critical soil water potential is greater than the value of the soil potential, ψ_e is less than ψ_c, requiring the supercritical solution.

After solving for ψ_{gc}, the solution for ψ_e is obtained by solving the following equation, which is obtained by combining eqns. (1), (5), (6), (7), (8a, 8b), and (9) in (10) to yield:

$$A\psi_e^2 + B\psi_e + C = 0 \quad (12a)$$

The coefficients A, B, and C contain all of the independently specified or calculated parameters listed in these equations. This quadratic equation is solved by conventional algebra to yield two roots. The following is selected as the correct root because it is consistent with reasonable values of leaf water potential:

$$\psi_e = (B - (B^2 - 4AC)^{1/2})/2A \quad (12b)$$

(A brief derivation of (eqn. 12) is shown in the Appendix.)

Plant stress

The critical ground water potential ψ_{gc}, derived in eqn. (11), describes the changing relationship between plant water demand and soil water supply, and resembles the plant water supply function defined by Cowan (1965). It is apparent from eqn. (11) that if V is greater than zero, then ψ_{gc} will be greater than ψ_c and that ψ_{gc} increases as V increases; ψ_{gc} also increases as ψ_g decreases through Z_g. This suggests that both V and ψ_g determine the limiting value of soil water potential that may support transpiration without a decrease in ψ_e below ψ_c.

It is possible to define two measures of plant stress, which quantify the dependent water relationships noted above. These are the Water Potential Stress Index (WPSI) and the Leaf Potential Stress Index (LPSI) given as

$$WPSI = \psi_{gc} - \psi_g \quad (13a)$$

and

$$\mathrm{LPSI} = \psi_c - \psi_e \qquad (13b)$$

When WPSI and LPSI are positive, the stomata are closing at a rate equal to the supercritical part of the discontinuous curve. We suggest that these indices are measures of plant stress, and it may be possible to use them to calculate a cumulative effect on plant growth.

THE BOUNDARY LAYER MODEL

The boundary layer model is a time-dependent, initial value model that contains several layers for heat and moisture transport. It consists of two soil layers, a bare soil surface, a layer of vegetation, a surface air layer and a mixing layer. The model starts from a set of initial values and advances at approximately 4-min time steps from near sunrise for a period of nearly 24 h. In coupling the plant component with the full boundary layer model, feedback is allowed between the rates of evapotranspiration and sensible heat flux and the specific humidities and temperatures within and above the canopy. The reader is referred to Carlson (1986), and Taconet et al. (1986b) for details.

SCALING UP FROM A LEAF TO A CANOPY

Similarity theory suggests (Lindroth and Halldin, 1986) that the calculated average leaf resistance (r_l) needs to be divided by the LAI in order to scale from a leaf to a canopy. This is equivalent to multiplying the fluxes of sensible and latent heat by LAI.

In this paper we consider r_l (which contains both the stomatal and cuticular resistances) to be calculated for a single sided upfacing leaf near the sunlight top of the plant canopy; thus r_l is not an average resistance over the depth of the canopy. In order to account for the extinction of S (and thus an increase in ψ_e) within the canopy and the interaction between plants, we also multiply r_l (divide the sensible and latent heat fluxes) by a shelter factor to give a foliage flux (Taconet et al., 1986b), which accounts for these differences in a highly empirical manner. The ratio LAI/P, varies gradually from a value of 1.0 to 2.0 for LAI varying between 2 and infinity. Thus the inclusion of a shelter factor restrains large variations in evapotranspiration and sensible heat fluxes that would occur because of large variations in LAI.

Henceforth all fluxes calculated within the boundary layer model, and referred to in the figures have been scaled by LAI/P and therefore refer to an entire plant canopy, and to a horizontal surface area. It should be noted that this scaling is not strictly correct because it treats r_{cut} in the same way as r_s.

RESULTS AND DISCUSSION

This section consists of three parts. In the first and second parts, we discuss how moisture availability, root–stem resistance, critical leaf water potential, and β (feedforward effect) effect various plant and atmospheric variables. To do so, we use the stomatal resistance model independently and within the boundary layer model. We also discuss an interesting phenomenon, which is the appearance of a plateau in the transpiration. This plateau is associated with a transient increase in stomatal resistance during the midday period. Two indices which are related to the appearance of the plateau are also shown: the Water Potential Stress Index (WPSI), and the Leaf Potential Stress Index (LPSI). The third section, pertaining to measurements made during the HAPEX–MOBILHY experiment, presents experimental evidence suggesting the importance of critical leaf water potential, and root–xylem resistance. (The HAPEX experiments and measurements are discussed by Andre et al. (1988).)

Sensitivity tests of the stomatal resistance model

Tests of the stomatal resistance model were done varying either soil water content, root–xylem resistance, or vapor pressure deficit. In response, leaf and epidermal water potential, stomatal resistance, and transpiration are calculated as functions of the imposed parameters. Solar flux was set $=850$ W m^{-2}, and vapor pressure deficit was set at 30 mbar.

Soil water content

Figure 4 shows the variation of bulk leaf and epidermal water potential, stomatal resistance and transpiration with soil water content. It is important to note that although the stomatal resistance eqn. (7) does not directly contain soil water content, stomatal resistance is still sensitively dependent on soil water content through ψ_g (see Appendix). Bulk leaf and epidermal water potential decrease with decreasing soil water content. Between 0.12 and 0.14, there are sharp decreases in leaf and epidermal water potentials as a result of a large decrease in ψ_g, and a large increase in Z_g (a decrease in K_g). Stomatal resistance increases and transpiration decreases, however, where the epidermal leaf water potential reaches the critical leaf water potential, which occurs at $\theta_v = 0.17$. The value of θ_v at which critical leaf water potential is reached is dependent on the value of V. Higher values of V would cause the leaf water potential to fall below critical leaf water potential at even higher values of soil water content. Interestingly, transpiration appears to be almost independent of soil water content when ψ_e is above ψ_c.

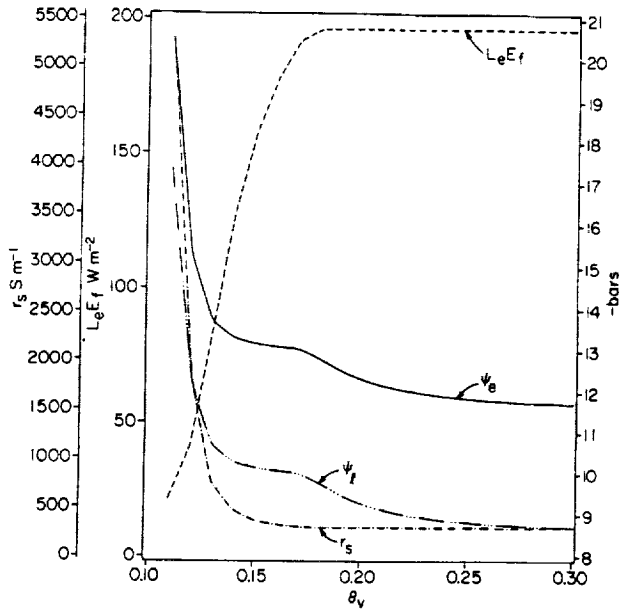

Fig. 4. Soil water content (θ_v) vs. mesophyllic leaf potential (ψ_l), epidermal leaf water potential (ψ_e), stomatal resistance (r_s), and transpiration (L_eE_f). (Parameters and coefficients are the base values given in Table 4.)

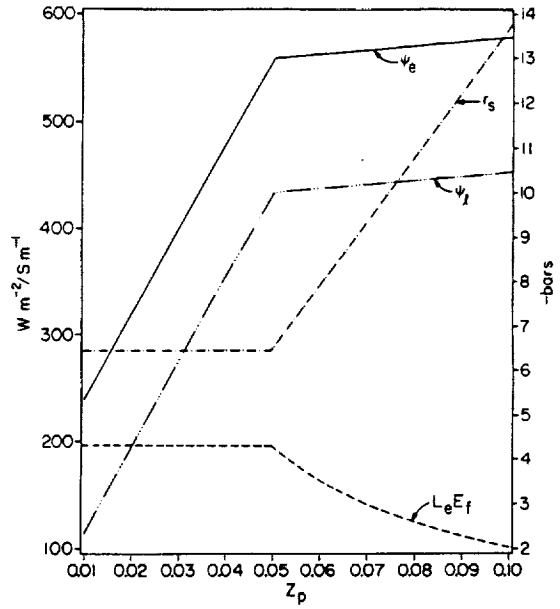

Fig. 5. Root–xylem resistance (Z_p) vs. mesophyllic leaf potential (ψ_l), epidermal leaf water potential (ψ_e), stomatal resistance (r_s), and transpiration (L_eE_f). (Parameters and coefficients are the base values given in Table 4.)

Root–stem resistance

The variation of bulk and epidermal leaf water potential, stomatal resistance and transpiration with root–stem resistance Z_p is shown in Fig. 5. Bulk and epidermal leaf water potential decrease sharply with increasing Z_p until the critical leaf water potential is reached by ψ_e at Z_p equals 0.05. Above $Z_p = 0.05$, r_s increases and transpiration decreases with increasing Z_p. The large increase in stomatal resistance above $Z_p = 0.05$ prevents the water potential of the leaf from decreasing rapidly beyond this value of Z_p.

Vapor pressure deficit

Figure 6 shows the variation of bulk and epidermal leaf water potential, stomatal resistance and transpiration with V. The most interesting result of this test is the corresponding changes in the calculated parameters when ψ_e reaches the critical point at $V = 32$ mbar. As in the two previous figures, stomatal resistance increases sharply with further decrease in ψ_e below ψ_c; transpiration, however, decreases with increasing V beyond ψ_c because ψ_l increases. The divergence of ψ_l and ψ_e beyond the critical leaf water potential is consistent with the feedforward observations of Farquhar (1978) and Sheriff (1984). In this model, the rate of divergence is dependent upon β. It should be noted that the value of V at which ψ_e reaches ψ_c is dependent upon ψ_g (θ_v) and Z_p.

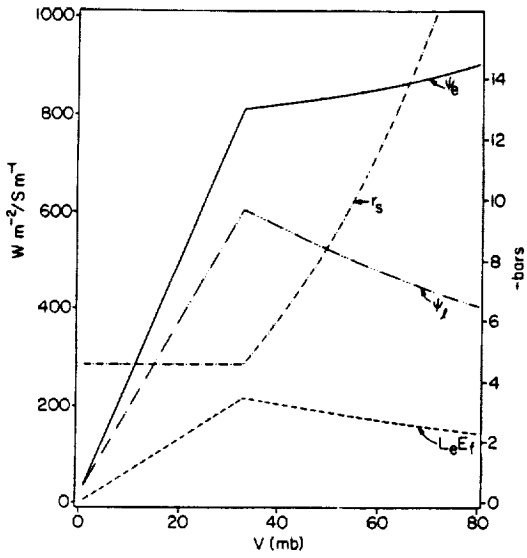

Fig. 6. Vapor pressure deficit (V) vs. mesophyllic leaf potential (ψ_l), epidermal leaf water potential (ψ_e), stomatal resistance (r_s), and transpiration (L_eE_f). (Parameters and coefficients are the base values given in Table 4.)

TABLE 4

Values of the coefficients, ψ_c, Z_p and M

Variable	Base	Test 1	Test 2	Test 3	Units
r_{min}	210	**	**	**	$s\ m^{-1}$
β	0.1	0.0	0.05	0.1	bar $mbar^{-1}$
b_1	−0.0001	**	**	**	$s\ m^{-1}\ bar^{-1}$
b_2	500	**	**	**	$s\ m^{-1}\ bar^{-1}$
c_1	0.5	**	**	**	$s\ m^{-1}\ (W\ m^{-2})^{-1}$
c_2	10	**	**	**	$s\ m^{-1}\ (W\ m^{-2})^{-1}$
ψ_c	−13	−8	−13	−18	bar
S_c	225	**	**	**	$W\ m^{-2}$
Z_p	0.044	0.03	0.05	0.07	bar $(W\ m^{-2})^{-1}$
M	0.65	0.35	0.50	0.65	

Values of the coefficients used in the stomatal resistance (base) and boundary layer inclusive tests are shown in Table 4. Initialization is that of Lubbon, 16 June.

Sensitivity tests with the boundary layer model

The purpose of this section is to discuss what happens when the stomatal resistance model is implanted into the boundary layer model and the combined models are allowed to vary as a function of time for different initial conditions. More precisely, dependence of leaf water potential, stomatal resistance, transpiration, and radiative temperature on moisture availability, root–stem resistance, critical leaf water potential, and β (feedforward) will be shown. The initial conditions are for HAPEX, 16 June 1986; the parameters and coefficients for these simulations are given in Table 4.

Sensitivity to soil water content

Changes in soil moisture availability and therefore in soil moisture affect the plant water flow eqn. (1) through Z_g and ψ_g, whose values change exponentially as θ_v decreases. It is apparent in Fig. 7a that there is little difference in the transpiration rate between $M=0.50$ and 0.65; at these moisture availabilities, ψ_e is greater than ψ_c. With a further decrease in ψ_g, ψ_e reaches ψ_c, leading to the formation of a transient transpiration plateau and then to a collapse of the transpiration as ψ_g reaches ψ_e. It should be noted that the collapse of the transpiration during the entire day is associated with an increase in the radiative temperature of 8K from that for $M=0.50$ (Fig. 7b).

Perhaps a useful means of representing water limitation is through WPSI. WPSI is much greater than zero for $M=0.35$ (Fig. 7c); by comparison, when the supply of soil moisture to the leaves is sufficient to meet the demand, WPSI is less than zero.

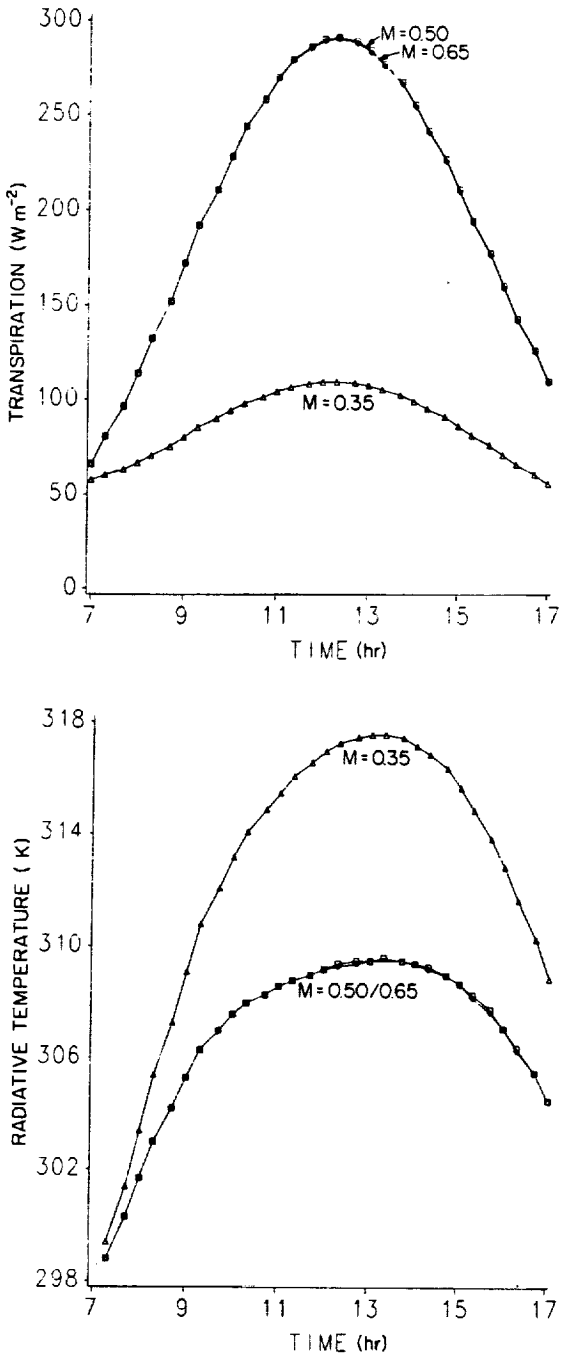

Fig. 7. Sensitivity tests of (a) transpiration (L_eE_f), (b) radiative temperature, and (c) the Water Potential Stress Index (WPSI), varying the moisture availability (M). (Base coefficients are in Table 4.)

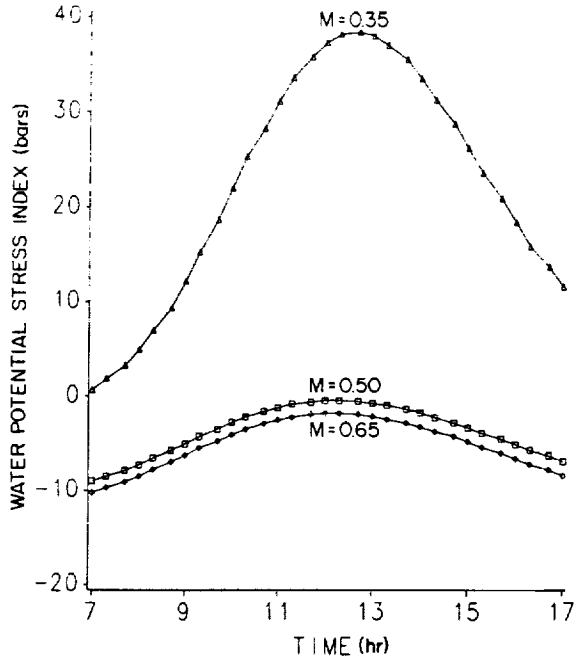

Fig. 7 contd.

Sensitivity to Z_p

As shown in Fig. 5, larger values of the root–stem resistance, Z_p (bar (W $m^{-2})^{-1}$), result in a decrease in ψ_l and ψ_e. Figure 8a shows that even at high moisture availabilities, a relatively high value of Z_p can cause a sharp increase in r_s. This leads to a transpiration plateau which is about 100 W m^{-2} below that for a small value of Z_p (Fig. 8b). In this case, the difference in transpiration corresponds to a canopy radiometric temperature difference of 2K. These results suggest the importance of Z_p in plant models and its effect on boundary layer fluxes and radiometric temperatures.

Sensitivity to ψ_c

Figure 9a, b and c shows how stomatal resistance, transpiration, and canopy radiometric temperature vary with ψ_c. The resistance is largest, and transpiration is smallest for $\psi_c = -8$ bar. In comparison, for $\psi_c = -18$ bar, ψ_e does not reach critical; thus r_s resembles a U-shaped curve and there is no appearance of a transpiration plateau. This variation of r_s with ψ_e also leads to a 3K difference in simulated radiometric canopy temperature.

The LPSI increases as ψ_c increases and is >0 for $\psi_c \leqslant -13$ bar (Fig. 9d). Values of LPSI >0 suggest a "leaf water deficit" and this deficit increases

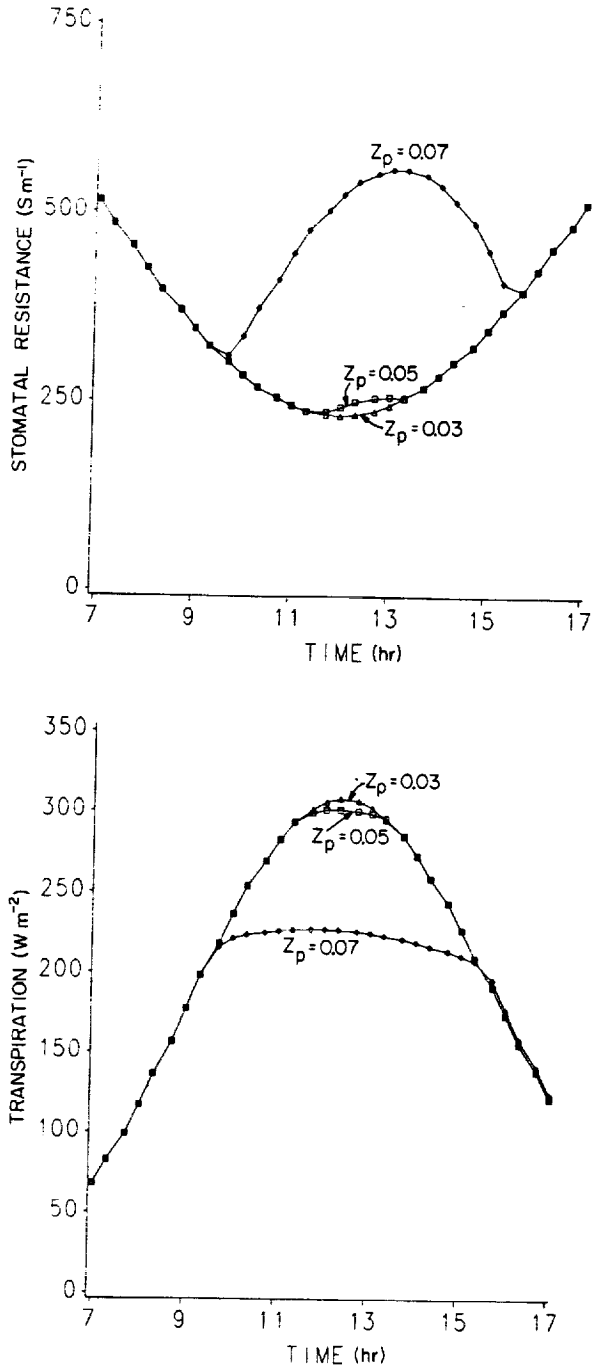

Fig. 8. Sensitivity tests of (a) stomatal resistance (r_s), and (b) transpiration (L_eE_f), varying the root–xylem resistance (Z_p) (bar $(W\ m^{-2})^{-1}$). (Base coefficients are in Table 4.)

with increasing ψ_c. Note, however, that Fig. 9d implies that ψ_e is larger for larger values of ψ_c, suggesting that this deficit is relative to plant species and type. Perhaps, ψ_c may be indicative of a mechanism by which the plant exercises direct control over the transpiration, thus preventing, in the short term, the leaf water potential from falling to a level that can harm the plant.

Sensitivity to β

One other means of plant control of transpiration is through the feedforward effect. Figure 10a shows that transpiration decreases with β, and that there is a bi-modal transpiration curve for $\beta=0.1$ bar mbar^{-1}. This distribution is associated with variations of ψ_e, r_s, and ψ_l (Fig. 10b, c, d) that exemplify results shown in Fig. 6.

HAPEX measurements

The HAPEX-MOBILHY (Hydrologic Atmospheric Pilot Experiment and Modelisation du Bilan Hydrique) program (André et al., 1986, 1988) was conducted over an agricultural region in the south of France during the summer of 1986. Its main purpose was to study the hydrological budget and evaporation fluxes at the scale of a General Circulation Model. A network of rain gauges, flux-measuring devices and conventional meteorological observations, supported by aircraft and additional ground surface measurements were made during an intensive phase which lasted from May until the early part of July 1986.

One of the programs in HAPEX was directed jointly by Penn State and members of the Centre de Recherches en Physique de l'Environment (CRPE) and the Institut National de Recherches Agronomiques (INRA) to study the evolution of the stomatal resistance, leaf water potential and substrate water content during the intensive phase of HAPEX. Briefly, this experiment involved measuring the leaf water potential (using a pressure chamber), the leaf resistance to water vapor flow (using a porometer) and the substrate water content with gypsum blocks, supplemented by gravimetric measurements. These measurements were made at two fields, one near the town of Lubbon and the other near Castelnau. The Lubbon field consisted of corn, planted about the end of May; because of wet weather, the corn at Castelnau was not planted until later in the field experiment. Periodically, LAI and plant heights were also determined.

Surface energy flux measurements were made routinely at about a dozen sites by the Systeme Automatique de Mesure de l'Evapotranspiration Réelle (SAMER), including the Lubbon corn field (André et al., 1988). Additional soil water measurements were made in various fields using neutron probe and gravimetric sampling; these are also discussed by André et al. (1988).

The importance of these HAPEX measurements with regard to this paper

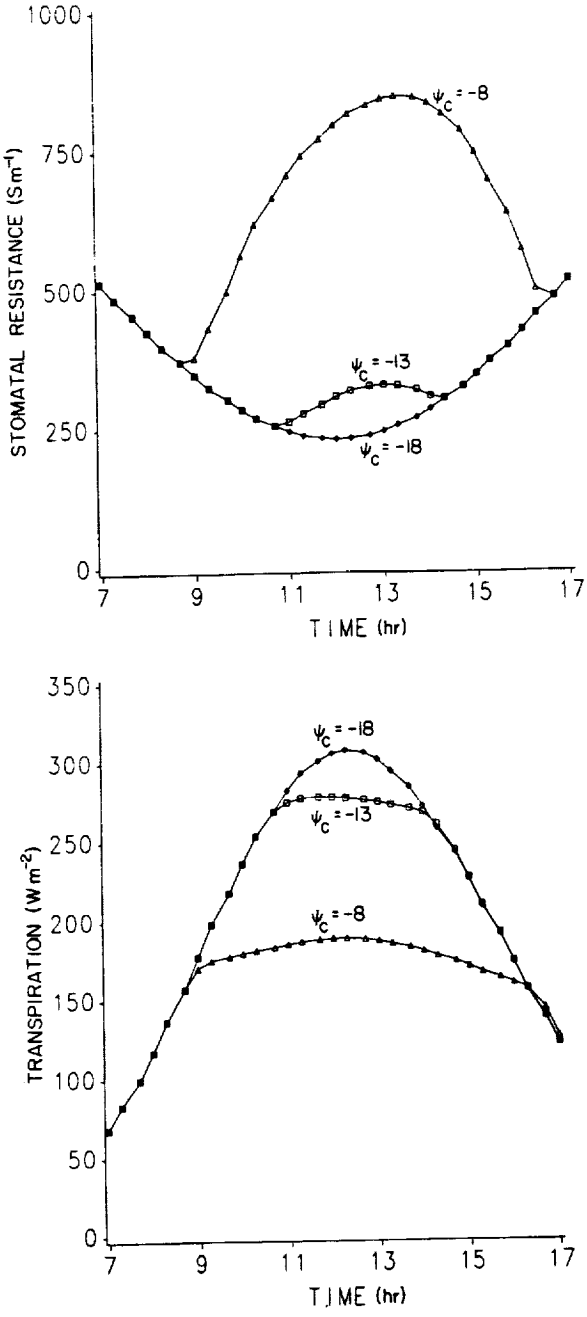

Fig. 9. Sensitivity tests of (a) stomatal resistance (r_s), (b) transpiration (L_eE_f), (c) radiative temperature, and (d) the Leaf Potential Stress Index, varying the critical leaf potential (ψ_c) (bar). (Base coefficients are in Table 4.)

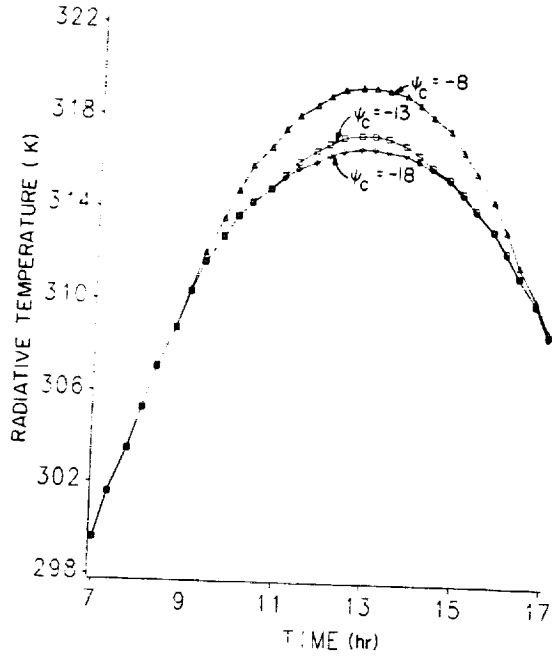

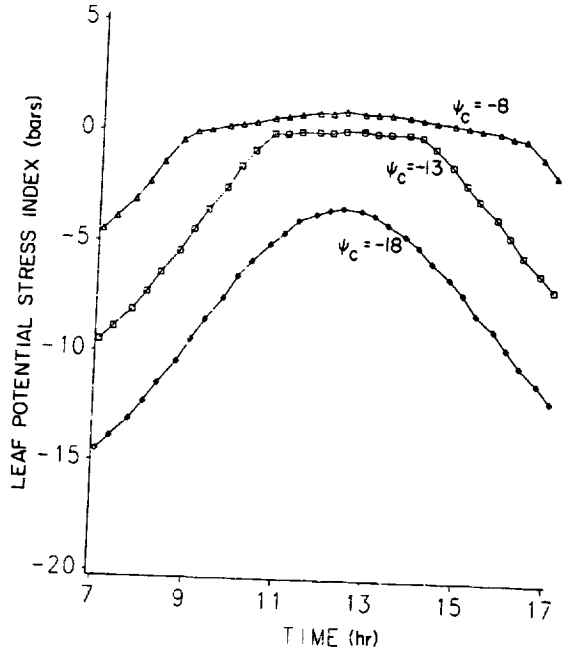

Fig. 9 contd.

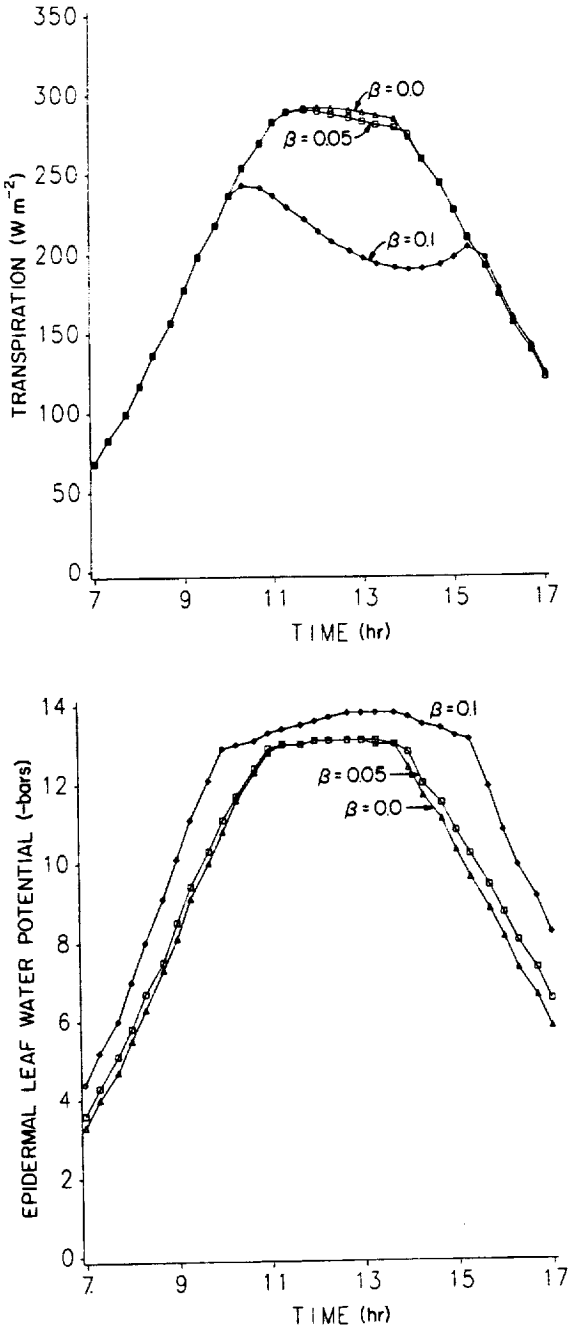

Fig. 10. Sensitivity tests of (a) transpiration (L_eE_t), (b) epidermal leaf water potential (ψ_e), (c) stomatal resistance (r_s), and (d) mesophyllic leaf water potential (ψ_l), varying β (bar mbar^{-1}). (Base coefficients are in Table 4.)

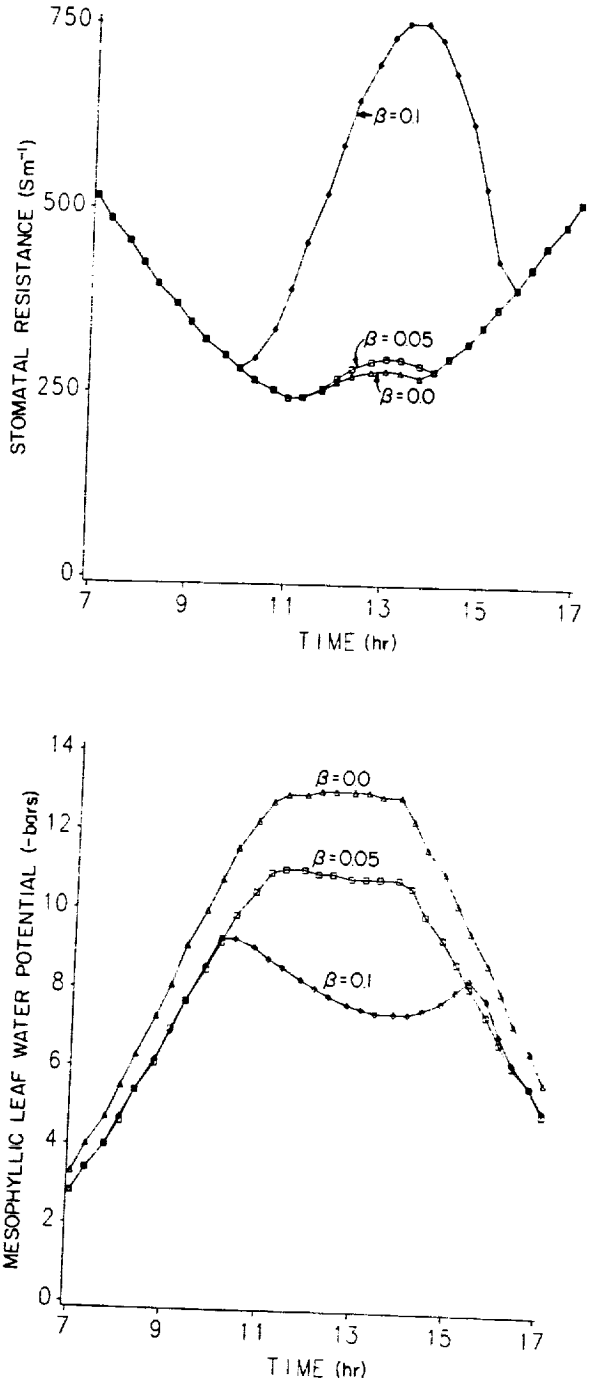
750
500
250
0
STOMATAL RESISTANCE (Sm⁻¹)
β=0.1
β=0.05
β=0.0
7
9
11
13
15
17
TIME (hr)
14
12
10
8
6
4
2
0
MESOPHYLLIC LEAF WATER POTENTIAL (-bars)
β=0.0
β=0.05
β=0.1
7
9
11
13
15
17
TIME (hr)

Fig. 10 contd.

TABLE 5

Parameters for June 16 (Lubbon)

Variable	Lubbon	Units
r_{min}	125	$s\ m^{-1}$
β	0.02	$bar\ mbar^{-1}$
b_1	−0.0001	$s\ m^{-1}\ bar^{-1}$
b_2	500	$s\ m^{-1}\ bar^{-1}$
c_1	0.15	$s\ m^{-1}\ (W\ m^{-2})^{-1}$
c_2	100.0	$s\ m^{-1}\ (W\ m^{-2})^{-1}$
ψ_c	−13.0	bar
S_c	50	$W\ m^{-2}$
Z_p	0.035	$bar\ (W\ m^{-2})^{-1}$

Values of r_{min}, and the coefficients used in running the stomatal resistance model for the HAPEX experiment. Values of critical leaf water potential and internal plant resistance (Z_p) are also given.

is that they show the combined effects of evaporative demand, soil moisture, and root–stem resistance on stomatal resistance, leaf water potential, and transpiration. Furthermore, the data suggests the effect of root–stem resistance on stomatal resistance over a seasonal period.

In simulating these results, values of the coefficients in eqns. (7), (8) and (9) were based loosely on measurements reported in the literature for corn (e.g. Choudhury, 1983) of r_s vs. solar flux and leaf water potential. The value of Z_p was chosen on the basis of work performed by Abdul-Jabbar et al. (1984); see Table 5.

Stomatal resistance

Stomatal resistances (more properly, leaf resistances) were measured with a porometer during a period of about one month in HAPEX. Several leaves were sampled from different plants several times a day. Measurements were made on both adaxial and abaxial sides of the leaf and in three areas on each side, the tip, middle and stem region. Measurements were then linearly averaged over the several leaves for each of the leaf domains and then each leaf domain was combined into a single one-sided value of leaf resistance. The latter operation involved using different weights for the different leaf sectors, rather than taking a straight average of inverse resistances. (Mean values of r_s are similar to straight inverse averages.)

All the stomatal (leaf) resistance data for the summer field program are shown in these two figures, one being for unstressed leaves (Fig. 11a) and the other for visibly stressed leaves (Fig. 11b), as determined subjectively in the field at the time of measurement. Note that the former exhibits a U-shaped distribution in the hourly averages, with a minimum at about 14:00 LST, while

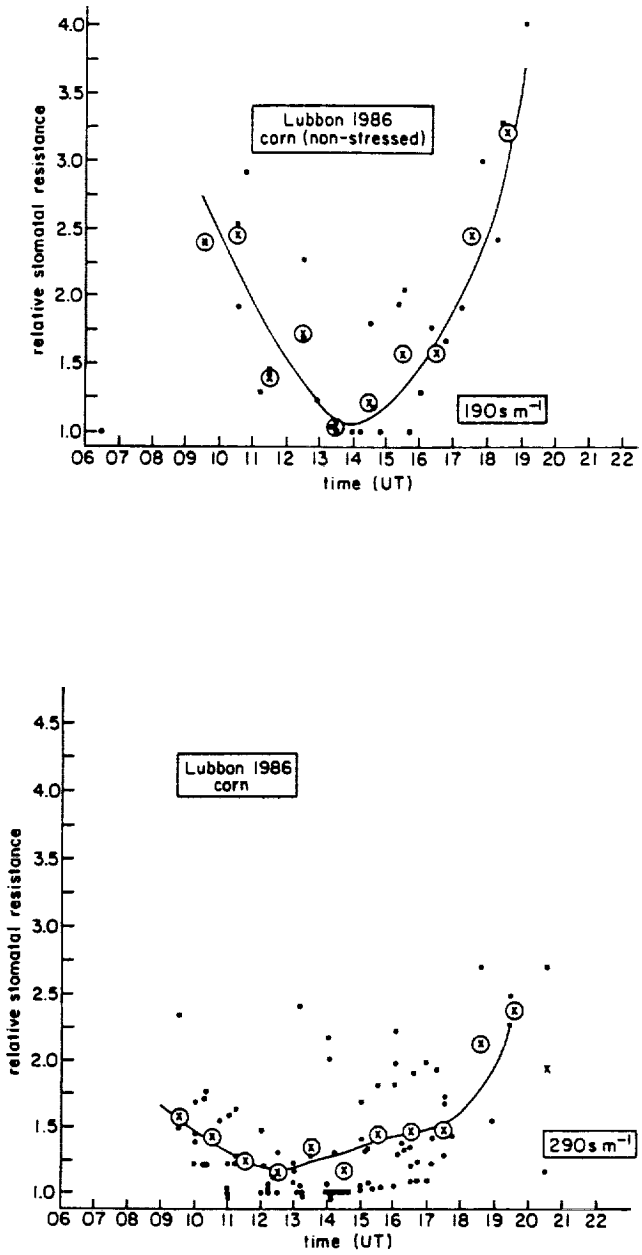

Fig. 11. Normalized measured (relative) stomatal (leaf) resistances (small filled circles) for (a) unstressed and (b) stressed corn leaves composited for the entire month of June 1986 (Field N6) at Lubbon, France. Circled crosses refer to hourly averages. Normalization refers to division by the minimum leaf resistance for the day. The average minimum stomatal resistance for June is indicated in the box.

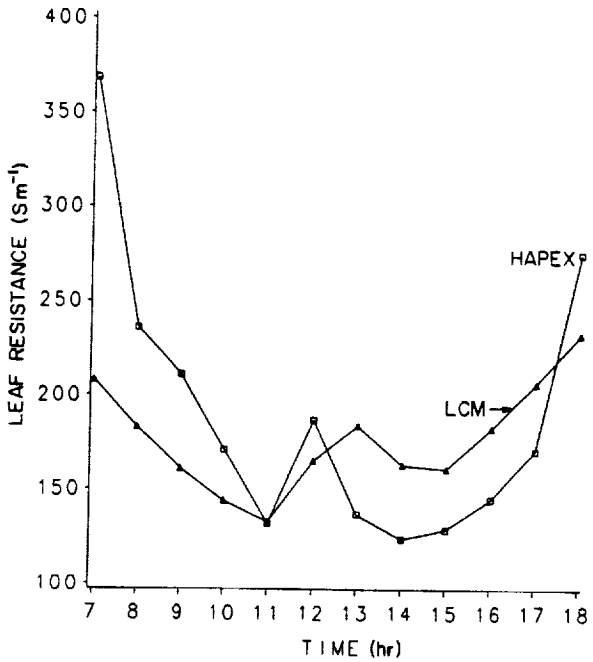

Fig. 12. Simulated leaf resistance vs. time plotted against the measured leaf resistance (HAPEX) on 16 June 1986, Lubbon. Measured resistances have been scaled by the shelter factor and LAI.

the measurements for stressed leaves show a flat distribution, with a minimum at about 12:30 LST, and generally larger values of leaf resistance throughout the middle of the day than for non-stressed leaves. The difference between Figs. 11a and b may be due to transient water stress.

We also compared the measured values of stomatal resistances for 16 June in HAPEX. Figure 12 shows the measured resistances which have been scaled by LAI and the shelter factor P, vs. the simulated values, which are calculated for the leaves at the top of the canopy. The model appears capable of generating a rich complexity of behavior, which is also found in actual measurements. For example, both simulated and measured resistances suggest a midday increase in leaf resistance, followed by a slight decrease. It is possible that the midday increase in the stomatal resistance is a manifestation of the leaf water potential reaching its critical value.

The leaf water potential and transpiration plateau

Much of the apparent increase in r_s during the period of maximum solar flux occurs in conjunction with changes in leaf water potential. This is apparent in Fig. 13, which shows the variation of ψ_l with time. Note that there is a period from about 12:00 to 18:00 LST when the differences between the leaf water potential and the predawn (base) value of the leaf water potential were

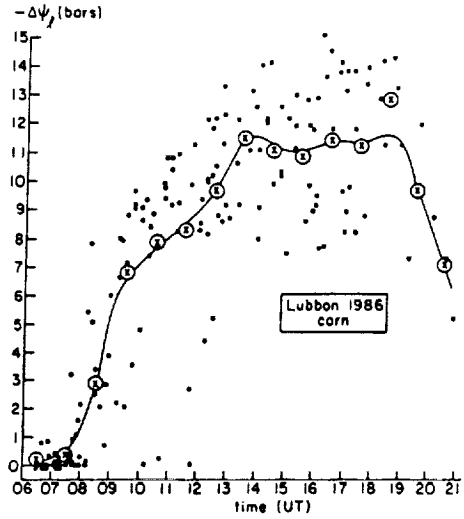

Fig. 13. Measured difference in leaf water potential from the pre-dawn (base) potential value ($\Delta\psi_l$) plotted vs. time. Dots represent individual HAPEX measurements composited for the month of June 1986. Circled crosses represent hourly averages.

almost constant with time in the hourly averages of the composite data. This behavior suggests that the leaf water potential was reaching its critical potential during the afternoon, leading to a commensurate increase in r_s. Since the base potential was typically between -1 and -2 bar, the leaf water potential distribution suggests a value of about -13 bar for the critical leaf potential. Although we have defined ψ_c in terms of a surface (epidermal) potential, the difference between the measured leaf (mesophyllic) and the epidermal leaf potential would not be large in these measurements, since the vapor pressure deficit effect in corn is thought to be small (B. Acock, personal communication, 1989). Typically, corn seems to have a critical leaf water potential of about -15 bar (B.J. Choudhury, personal communication, 1989).

The appearance of a plateau in ψ_l is also associated with a plateau in the transpiration (assumed to be proportional to the evapotranspiration). As seen in Fig. 14, both distributions of evapotranspiration measured by SAMER in adjacent fields were virtually identical before 08:00 h and after 16:00 h. In between, each field exhibited various degrees of the transpiration plateau. The dry field exhibits a wide plateau at about 300 W m^{-2} because both soil moisture is low and evaporative demand (V) is high. A slight plateau may also be present in the wet field because of high evaporative demand; thus this plateau is of shorter duration and the magnitude of the flux is larger than in the unirrigated field.

The appearance of a leaf water potential and transpiration plateau is consistent with simulations shown in Figs. 8 and 9. If r_s increases sharply at a

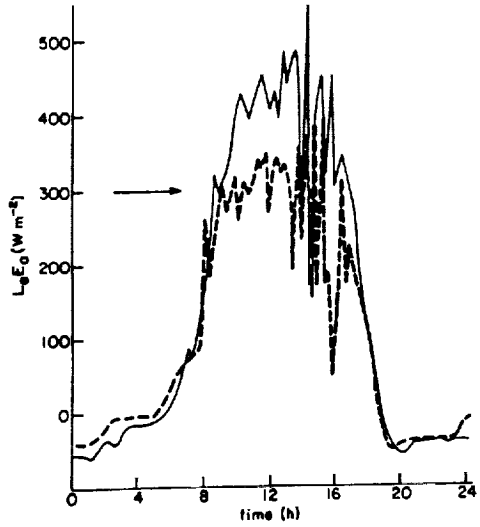

Fig. 14. Measured evapotranspiration (W m^{-2}) during the HAPEX experiment, Castelnau, France. Dashed line is for a non-irrigated field of corn while the solid line is for an adjacent irrigated field of corn. Horizontal arrow indicates an evapotranspiration plateau near 300 W m^{-2} for the unirrigated field, suggesting that $\psi_e < \psi_c$ during this period.

critical value of leaf water potential, then a plateau in both the leaf water potential and transpiration must occur. If a transpiration plateau consistently occurs at a particular value of leaf water potential, then there must be a critical value of leaf water potential owing to the constraints of the system (eqn. (10)). If one accepts that there is a critical value of leaf water potential, then there is no critical value of soil water potential (excluding a "nominal wilting" value of soil water potential) or vapor pressure deficit at which r_s increases sharply and transpiration levels off, because there is no monotonic relationship between leaf water potential and vapor pressure deficit or soil water potential.

Variation of Z_p

We have plotted all the data for the minimum daily stomatal resistances (the values between 11:00 and 13:00 LST) and their hourly averages in a composite (Fig. 15). Regardless of how the choice of weighting functions for determining the mean r_l was made, there was an unmistakable trend downward with time in the leaf resistance during the period, from about 265 to 160 s m^{-1}.

The smoothed decrease in the minimum daily leaf resistance shown in Fig. 15 is intriguing because there was no correlation between the substrate water content and leaf resistance. Indeed, the water content in the root zone remained relatively high (about 0.18 cm^3 cm^{-3}) during June 1986. During this

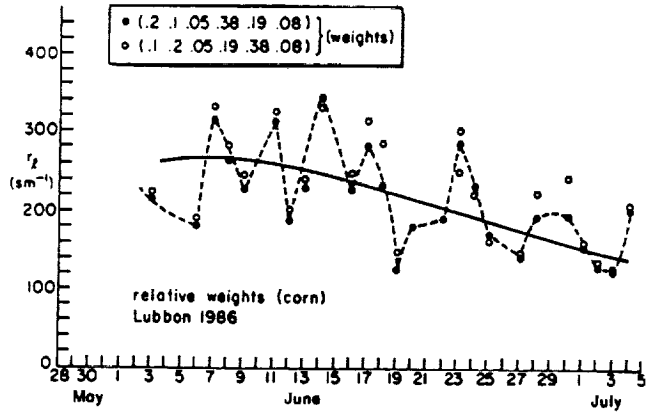

Fig. 15. Average daily minimum stomatal (leaf) resistances (s m^{-1}) for corn leaves at approximately 1300 UT in a field at Lubbon, France, during June 1986, as a function of date. Solid and open circles refer to alternate averages over leaf using the weighting factors shown above (values refer, from left to right, to the top, middle and bottom of the upfacing side of the leaf). The solid line is a subjectively determined fit through the data.

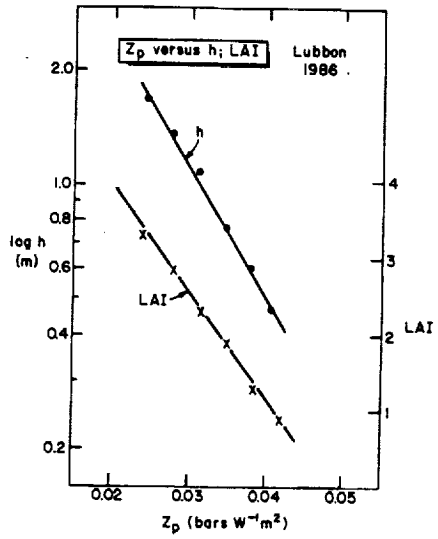

Fig. 16. Simulated values of Z_p (bar (W m^{-2})$^{-1}$) vs. LAI and logarithm of the height of the corn (m), based on fitting the modeled stomatal resistance to the smoothed curve for measured resistances in Fig. 15.

month, however, the plants grew from small shoots to over a meter in height and the LAI exceeded 3.0 in the corn by the end of the month. We suggest that the decline in r_l with increasing LAI and crop height is related to the growth of prop roots, associated with an increase in the water transport effi-

ciency from soil to leaf. Such an increase in efficiency would correspond to a decrease in Z_p.

This hypothesis was examined using the boundary layer model in the following way. First, the smoothed trend of r_s in Fig. 15 was plotted as a function of the LAI and crop height. Next, a value of Z_p was chosen such that the simulation yielded the same daily minimum stomatal resistance measured on 16 June at Lubbon. Using the same initial conditions, Z_p was varied over a succession of simulations such that the minimum stomatal resistance generated by the model followed the smoothed trend in minimum stomatal resistances depicted in Fig. 15. The result, shown in Fig. 16, is that Z_p varied inversely with both LAI and the logarithm of the crop height. This suggests the possibility that minimum daily stomatal resistance depends on the value of Z_p.

CONCLUSION

The sharp increase in stomatal resistance associated with a decrease in epidermal leaf water potential beyond the critical leaf water potential can lead to the appearance of a transpiration plateau, or a bi-modal transpiration curve. Transpiration (and radiometric canopy temperature) is tied not just to the supply of moisture in the root zone and atmospheric demand, but to constraints imposed by plant physiology which affects water flux through the plant.

Suggestions for future research

It is necessary to further examine the relationship between stomatal resistance, transpiration, and leaf water potential. There is also a need to clarify the vapor pressure deficit effect and to examine the role of the epidermal leaf potential, and its relationship to the mesophyllic leaf potential. Other factors, such as the effect of CO_2 and temperature on r_s need to be further investigated, and a larger data base generated for all parameters.

Equation (10) was derived under the assumption of steady state. Jones (1978, 1983), Waring and Running (1978), Running (1980b) and Tyree (1988) suggest that the capacitance or storage capacity of the plant may be important. The effects of capacitance can be included in this model.

Finally, the model is based upon a vertically averaged canopy with the implication of horizontal homogeneity. We question whether a vertical average properly captures the complex vertical variation of stomatal resistance within the canopy. More attention needs to be focused on the methods of making vertical and horizontal averages.

ACKNOWLEDGEMENTS

The authors would like to thank the sponsors of this research, the National Aeronautics and Space Administration under grant NAG 5-919, the United States Geological Survey under grant #14-08-0001-G1490, and the United States Department of Agriculture/Agriculture Research Service under grant #58-32U4-8-27. We are also grateful to Dennis Baldocchi, Basil Acock, James Bunce, Baskhar Choudhury, John Norman and Kenneth Shackel for invaluable information and advice provided during the course of various discussions.

APPENDIX: DERIVATION OF THE STEADY STATE EQUATION FOR ψ_e

Using eqn. (10) as the representation of steady state (Jarvis, 1976), we substitute eqn. (9) into eqn. (1) and eqns. (6), (7) and (8) into eqn. (5) to derive the following:

$$A\psi_e^2 + B\psi_e + C = 0 \tag{a1}$$

Since eqn. (8) is discontinuous, there are two parts to the solution to (a1). If $\psi_g \geq \psi_{gc}$ then the roots to this equation are

$$A = -f(S)f(T)f(CO_2)b_1(r_{cut} + r_{af}) \tag{a2}$$

$$B = f(S)f(T)f(CO_2)(r_{cut} + r_{af})$$
$$[-r_{min} + b_1\{\psi_g - \beta V - H - Z_t\sigma V/(r_{cut} + r_{af})\}] \tag{a3}$$
$$-r_{cut}r_{af}$$

$$C = f(S)f(T)f(CO_2)(r_{cut} + r_{af})$$
$$(r_{min})\{\psi_g - \beta V - H - Z_t\sigma V/(r_{cut} + r_{af})\} \tag{a3}$$
$$+r_{cut}r_{af}(\psi_g - \beta V - H) - r_{cut}Z_t\sigma V$$

if $\psi_g \leq \psi_{gc}$ then

$$A = f(S)f(T)f(CO_2)b_2(r_{cut} + r_{af}) \tag{a4}$$

$$B = f(S)f(T)f(CO_2)(r_{cut} + r_{af})$$
$$[-(r_{min} + b_1\psi_c + b_2\psi_c)$$
$$-b_2\{\psi_g - \beta V - H - Z_t\sigma V/(r_{cut} + r_{af})\}] \tag{a5}$$
$$-r_{cut}r_{af}$$

$$C = f(S)f(T)f(CO_2)(r_{cut} + r_{af})$$
$$(r_{min} + b_1\psi_c + b_2\psi_c) \qquad (a6)$$
$$\{\psi_g - \beta V - H - Z_t \sigma V/(r_{cut} + r_{af})\}$$
$$+ r_{cut} r_{af}(\psi_g - \beta V - H) - r_{cut} Z_t \sigma V$$

where σ is the density of vapor (air) times the latent heat of evaporation. (This solution is available on computer diskette from the authors.)

REFERENCES

Abdul-Jabbar, A.S., Lugg, D.G., Sammis, T.W. and Gay, L.W., 1984. A field study of plant resistance to water flow in alfalfa. Agron. J., 76: 765–769.

Abramopoulos, F., Rosenzweig, C. and Choudhury, B., 1988. Improved ground hydrology calculations for global climate models (GCMs): soil water movement and evaporation. J. Clim., 1: 921–941.

Ackerson, R.C. and Krieg, D.R., 1977. Stomatal and nonstomatal regulation of water use in cotton, corn, and sorghum. Plant Physiol., 60: 850–853.

André, J.C., Goutorbe, J.P. and Perrier, A., 1986. HAPEX-MOBILHY: A hydrological atmospheric experiment for the study of water budget and evaporation flux at the climatic scale. Bull. Am. Meteorol. Soc., 67: 138–144.

André, J.C. et al., 1988. Evaporation over land-surfaces: First results from HAPEX-MOBILHY special observing period. Ann. Geophys., 6: 477–492.

Avissar, R., Avissar, P., Mahrer, Y. and Bravdo, B.A., 1985. A model to simulate response of plant stomata to environmental conditions. Agric. For. Meteorol., 34: 21–29.

Baldocchi, D.D., Hicks, B.B. and Camara, P., 1987. A canopy stomatal resistance model for gaseous deposition to vegetated surfaces. Atmos. Environ., 21: 91–101.

Boyer, J.S., 1971 .Resistances to water transport in soybean, bean, and sunflower. Crop. Sci., 11: 403–407.

Boyer, J.S., 1976. Water deficits and photosynthesis. In: T. Kozlowski (Editor), Water Deficits and Plant Growth IV. Academic Press, New York, NY, pp. 153–190.

Bunce, J.A., 1978. Effects of shoot environment on apparent root resistance to water flow in whole soybean and cotton plants. J. Exp. Biol., 29: 595–601.

Camacho-B, S.E., Hall, A.E. and Kaufmann, M.R., 1974. Efficiency and regulation of water transport in some woody and herbaceous species. Plant Physiol., 54: 169–172.

Campbell, G.S., 1974. A simple method for determining unsaturated conductivity from moisture retention data. Soil Sci., 117: 311–314.

Carlson, T.N., 1986. Regional-scale estimates of surface moisture availability and thermal inertial using remote thermal measurements. Remote Sensing Rev., 1: 197–247.

Choudhury, B., 1983. Simulating the effects of weather variables and soil water potential on a corn canopy temperature. Agric. Meteorol., 29: 169–182.

Choudhury, B.J. and Idso, S.B., 1985. An empirical model for stomatal resistance of field-grown wheat. Agric. For. Meteorol., 36: 65–82.

Choudhury, B.J. and Monteith, J.L., 1986. Implications of stomatal response to saturation deficit for the heat balance of vegetation. Agric. For. Meteorol., 36: 215–225.

Cosby, B.J., Hornberger, G.M., Clapp, R.B. and Ginn, T.R., 1984. A statistical exploration of the relationships of soil moisture characteristics to the physical properties of soils. Water Resour. Res., 20: 682–690.

Cowan, I.R., 1965. Transport of water in the soil–plant–atmospheric system. J. Appl. Ecol., 2: 221–239.
Deardorff, J.W., 1978. Efficient prediction of ground surface temperature and moisture with inclusion of a layer of vegetation. J. Geophys. Res., 83: 1889–1903.
Denmead, O.T. and Millar, B.D., 1976a. Water transport in wheat plants in the field. Agron. J., 68: 297–303.
Denmead, O.T. and Millar, B.D., 1976b. Field studies of the conductance of wheat leaves and transpiration. Agron. J., 68: 305–311.
Dickinson, R.E., 1984. Modeling evapotranspiration for three-dimensional global climate models. Geophys. Monogr., 29: 58–72.
Dwyer, L.M. and Stewart, D.W., 1984. Indicators of plant stress in corn (*Zea mays* L.). Can. J. Plant. Sci., 64: 537–546.
El-Sharkaway, M.A., Cock, J.H. and Held K, A.A., 1984. Water use efficiency of cassava. II. Differing sensitivity of stomata to air humidity in cassava and other warm-climate species. Crop Sci., 24: 503–507.
Farquhar, G.D., 1978. Feedforward response of stomata to humidity. Aust. J. Plant Physiol., 5: 787–800.
Farquhar, G.D. and Sharkey, T.D., 1982. Stomatal conductance and photosynthesis. Ann. Rev. Plant Physiol., 33: 317–345.
Feddes, R.A. and Rijtema, P.E., 1972. Water withdrawal by plant roots. J. Hydrol., 17: 33–59.
Federer, C.A., 1979. A soil–plant–atmosphere model for transpiration and availability of soil water. Water Resour. Res., 15: 555–562.
Federer, C.A., 1982. Transpirational supply and demand: plant, soil, and atmospheric effects evaluated by simulation. Water Resour. Res., 18: 355–362.
Feldhake, C.M. and Boyer, D.G., 1985. Resistance to water loss from warm and cool-season forage canopies in a growth chamber. Agric. For. Meteorol., 34: 269–275.
Fisher, M.J., Charles-Edwards, D.A. and Ludlow, M.M., 1981. An analysis of the effects of repeated short-term soil water deficits on stomatal conductance to carbon dioxide and leaf photosynthesis by the legume *Macroptilium atropurpureum* cv. Siratro. Aust. J. Plant Physiol., 8: 347–357.
Frensch, J. and Schulze, E.-D., 1988. The effect of humidity and light on cellular water relations and diffusion conductance of leaves of *Tradescantia virginiana* L. Planta, 173: 554–562.
Gollan, T., Turner, N.C. and Schulze, E.D., 1985. The response of stomata and leaf gas exchange to vapour pressure deficits and soil water content III. In the sclerophyllous woody species *Nerium oleander*. Oecologia, 65: 356–362.
Gollan, T., Passioura, J.B. and Munns, R., 1986. Soil water status affects the stomatal conductance of fully turgid wheat and sunflower leaves. Aust. J. Plant Physiol., 13: 459–464.
Grantz, D.A. and Zeiger, E., 1986. Stomatal responses to light and leaf–air water vapor pressure difference show similar kinetics in sugarcane and soybean. Plant Physiol., 81: 865–868.
Hailey, J.L., Hiler, E.A., Jordan, W.R. and van Bavel, C.H.M., 1973. Resistance to water flow in *Vigna sinensis* L. Crop Sci., 13: 264–267.
Halldin, S., Saugier, B. and Pontailler, J.Y., 1984/85. Evapotranspiration of a deciduous forest: simulation using routine meteorological data. J. Hydrol., 75: 2–19.
Idso, S.B., 1983. Stomatal regulation of evaporation from well-watered plant canopies: a new synthesis. Agric. Meteorol., 29: 213–217.
Jones, H.G., 1978. Modelling diurnal trends of leaf water potential in transpiring wheat. J. Appl. Ecol., 15: 613–626.
Jones, H.G., 1983. Plants and Microclimate. Cambridge University Press, New York, NY, 323 pp.
Jarvis, P.G., 1976. The interpretation of the variations in leaf water potential and stomatal

conductance found in canopies in the field. Philos. Trans. R. Soc. Lond. Ser. B, 273: 593–610.
Katerji, N.B., 1979. Etude comparative de la resistance du couvert vegetal au transfert de lat vapeur d'eau le potential hydrique des feuilles chez le Blé. Oecol. Plant., 14: 55–60.
Katerji, N. and Hallaire, M., 1984. Les grandeurs de reference utilisables dans l'etude de l'alimentation en eau des cultures. Agronomie, 4: 999–1008.
Katerji, N., Hallaire, M., Perrier, A. and Durand, R., 1983. Transfert hydrique dans le vegetal. Acta Oecologica, 4: 11–26.
Kaufmann, M., 1982. Leaf conductance as a function of photosynthetic flux density and absolute humidity difference from leaf to air. Plant Physiol., 69: 1018–1022.
Körner, Ch., 1985. Humidity responses in forest trees: precautions in thermal scanning surveys. Arch. Meteorol. Geophys. Bioklimatol. Ser. B., 36: 83–98.
Lhomme, J.P., 1988. Extension of Penman's formulae to multi-layer models. Boundary-Layer Meteorol., 42: 281–291.
Lindroth, A., 1985. Canopy conductance of coniferous forests related to climate. Water Resour. Res., 21: 297–304.
Lindroth, A. and Halldin, S., 1986. Numerical analysis of pine forest evaporation and surface resistance. Agric. For. Meteorol., 38: 59–79.
Luxmoore, J.K., Stolzy, J.L. and Holdeman, J.T., 1981. Sensitivity of a soil–plant–atmospheric model to changes in air temperature, dew point temperature, and solar radiation. Agric. Meteorol., 23: 115–129.
Meyer, W.S. and Green, G.C., 1980. Water use by wheat and plant indicators of available soil water. Agron. J., 72: 253–257.
Monteith, J.L., 1975. Principles of Environmental Physics. Edward Arnold, London, 241 pp.
Morison, J.I.L., 1987. Intercellular CO_2 concentration and stomatal response to CO_2. In: E. Zeiger, G.D. Farquhar and I.R. Cowan (Editors), Stomatal Function. Stanford University Press, Stanford, CA, pp. 229–251.
Munns, R. and King, R.W., 1988. Abscisic acid is not the only stomatal inhibitor in the transpiration stream of wheat plants. Plant Physiol., 88: 703–708.
Passioura, J.B., 1984. Hydraulic resistance of plants. I. Constant or variable? Aust. J. Plant Physiol., 11: 333–339.
Passioura, J.B. and Munns, R., 1984. Hydraulic resistance of plants. II. Effects of rooting medium, and time of day, in barley and lupin. Aust. J. Plant Physiol., 11: 341–350.
Pospisilova, J. and Solarova, J., 1980. Environmental and biological control of diffusive conductances of adaxial and abaxial leaf epidermes. Photosynthetica, 14: 90–127.
Roessler, P.G. and Monson, R.K., 1985. Midday depression in net photosynthesis and stomatal conductance in *Yucca glauca*. Oecologia, 67: 380–387.
Running, S.W., 1976. Environmental control of leaf water conductances in conifers. Can. J. For. Res., 6: 104–112.
Running, S.W., 1980a. Field estimates of root and xylem resistance in *Pinus contorta* using root excision. J. Exp. Bot., 31: 555–569.
Running, S.W., 1980b. Relating plant capacitance to the water relations of *Pinus contorta*. For. Ecol. Manage., 2: 237–252.
Schulze, E.D., 1986. Carbon dioxide and water vapor exchange in response to drought in the atmosphere and in the soil. Ann. Rev. Plant Physiol., 37: 247–274.
Schulze, E.D., Robichaux, R.H., Grace, J., Rundel, P.W. and Ehleringer, J.R., 1987. Plant water balance. Bioscience, 37: 30–37.
Sellers, P.J. and Dorman, J.L., 1987. Testing the simple biosphere model (SiB) using point micrometeorological and biophysical data. J. Clim. Appl. Meteorol., 26: 622–651.
Shackel, K., 1987. Direct measurement of turgor and osmotic potential in individual epidermal cells. Plant Physiol., 83: 719–722.

Shackel, K. and Brinckmann, E., 1985. 'In situ' measurement of epidermal cell turgor, leaf water potential, and gas exchange in "*Tradescantia virginia*" L. Plant Physiol., 78: 66–70.

Sheriff, D.W., 1977. The effect of humidity on water uptake by, and viscous flow resistance of, excised leaves of a number of species: physiological and anatomical observations. J. Exp. Bot., 28: 1399–1407.

Sheriff, D.W., 1984. Epidermal transpiration and stomatal responses to humidity: some hypotheses explored. Plant. Cell Environ., 7: 669–677.

Simpson, J.R., Fritshen, L.J. and Walker, R.B., 1985. Estimating stomatal diffusion resistance for Douglas-Fir, Lodgepole Pine and White Oak under light saturated conditions. Agric. For. Meteorol., 33: 299–313.

Singh, B. and Szeicz, G., 1980. Predicting the canopy resistance of a mixed hardwood forest. Agric. Meteorol., 21: 49–58.

So, H.B., Aylmore, L.A.G. and Quirk, J.P., 1976. The resistance of intact maize roots to water flow. Soil Sci. Soc. Am. J., 40: 222–225.

Soer, G.J.R., 1980. Estimation of regional evapotranspiration and soil moisture conditions using remotely sensed crop surface temperatures. Remote Sensing Environ., 9: 27–45.

Taconet, O., Bernard, R. and Madiar, D.V., 1986a. Evapotranspiration over an agricultural region using a surface flux/temperature model based on NOAA-AVHRR data. J. Clim. Appl. Meteor., 25: 284–307.

Taconet, O., Carlson, R., Bernard, R. and Vidal-Madiar, D., 1986b. Evaluation of a surface/vegetation parameterization using satellite measurements of surface temperature. J. Clim. Appl. Meteor., 25: 1752–1767.

Takami, S. and Uchijima, Z., 1977. A model for the greenhouse environment as affected by the mass and energy exchange of a crop. J. Agric. Meteorol., 33: 117–127.

Takami, S. and Yukimura, T., 1979. Varietal difference in leaf status and water use of sorghum as affected by the stomatal sensitivity. Mem. Coll. Agric., 113: 1–24.

Tan, C.S. and Black, T.A., 1976. Factors affecting the canopy resistance of a Douglas-fir forest. Boundary-Layer Meteorol., 10: 475–488.

Thom, A.S., 1972. Momentum, mass and heat exchange of vegetation. Q.J.R. Meteorol. Soc., 98: 124–134.

Thomas, J.C., Brown, K.W. and Jordan, W.R., 1976. Stomatal response to leaf water potential as affected by preconditioning water stress in the field. Agron. J., 68: 706–708.

Turner, N., 1970. Response of adaxial and abaxial stomata to light. New Phytol., 69: 647–653.

Turner, N.C., 1974. Stomatal behavior and water status of maize, sorghum, and tobacco under field conditions. Plant Physiol., 53: 360–365.

Tyree, M.T., 1988. A dynamical model for water flow in a single tree: evidence that models must account for hydraulic architecture. Tree Physiol., 4: 195–217.

Van Bavel, C.H.M., 1974. Soil water potential and plant behavior: a case modeling study with sunflowers. Ecol. Plant., 9: 89–109.

Waring, R.H. and Running, S.W., 1978. Sapwood water storage: its contribution to transpiration and effect upon water conductance through the stems of old-growth Douglas Fir. Plant, Cell, Environ., 1: 131–140.

Wetzel, P.J. and Chang, J.-T., 1987. Concerning the relationship between evapotranspiration and soil moisture. Clim. Appl. Meteorol., 26: 18–27.

Xu, D., Li, D., Shen, Y.K. and Liang, G., 1984. On midday depression of photosynthesis of wheat leaf under field conditions. Acta Phytophysiol. Sin., 10: 269–276.

Zeiger, E., 1983. The biology of stomatal guard cells. Annu. Rev. Plant Physiol., 34: 441–475.

APPENDIX C

Agricultural and Forest Meteorology, 52 (1990) 45–69
Elsevier Science Publishers B.V., Amsterdam — Printed in The Netherlands

Remote estimation of soil moisture availability and fractional vegetation cover for agricultural fields

Toby N. Carlson[1], Eileen M. Perry[2] and Thomas J. Schmugge[3]
[1]*Department of Meteorology, The Pennsylvania State University, University Park, PA 16802 (U.S.A.)*
[2]*USDA/ARS, Tucson, AZ 85719 (U.S.A.)*
[3]*Hydrology Laboratory, USDA/ARS, Beltsville, MD 20705 (U.S.A.)*

(Received July 3, 1989; revision accepted December 12, 1989)

ABSTRACT

Carlson, T.N., Perry, E.M. and Schmugge, T.J., 1990. Remote estimation of soil moisture availability and fractional vegetation cover for agricultural fields. *Agric. For. Meteorol.*, 52: 45–69.

The purpose of this paper is to present a method for using remote measurements to estimate vegetation fraction, surface energy fluxes and the root zone and soil surface water contents for partial vegetation canopies. The primary tools are a boundary layer model with vegetation and substrate components and two image products: the variation of surface radiometric temperature vs. normalized difference vegetation index (NDVI), and the standard deviation of radiometric surface temperature vs. radiometric surface temperature. The method is based on determining: (1) asymptotic values of two radiometric surface temperatures for sunlit bare soil and for dense sunlit vegetation; and (2) a relationship between NDVI and surface temperature, which we call the axis of variation. The method is illustrated using aircraft and surface measurements made at Lubbon during the French HAPEX field experiment (1986).

INTRODUCTION

Models for estimating the surface turbulent energy fluxes and the soil moisture generally depend on a sensitivity of the surface radiometric temperature to soil water content. Over bare soil, variations in radiometric surface temperature tend to be highly correlated with variations in surface water content (Jackson et al., 1977; Schmugge, 1978; Jackson, 1982). Various models have been constructed to exploit the relationship between surface temperature and soil moisture. When used in conjunction with remote measurements of surface temperature, such as determined from a satellite, these models yield estimates of the surface moisture availability, the surface energy fluxes and the thermal inertia (Carlson and Boland, 1978; Carlson et al., 1981; Price, 1982;

0168-1923/90/$03.50

Hatfield et al., 1984; Raffy and Becker, 1985; Taconet et al., 1986; Wetzel and Woodward, 1987; Lagouarde and Choisnel, 1990). Some of these models also take into account a layer of vegetation (Taconet et al., 1986; Wetzel and Woodward, 1987; Lagouarde and Choisnel, 1990).

The relationship between soil moisture and surface temperature is vastly more complex over vegetation than over bare soil. Over vegetation there is a considerable amount of temperature variability owing to the structure of the vegetation canopy and particularly to the amount of bare soil viewed by the radiometer and exposed to the direct solar beam. Leaves tend to be cooler than the exposed bare soil because the intercellular airspaces are nearly saturated with water vapor, which is drawn from a relatively deep soil layer, the root zone. Bare soil temperatures reflect the soil moisture only over the top one or two centimeters (Idso et al., 1975).

Emitted surface radiance constitutes a blend of radiances emitted from either shaded or unshaded bare soil and vegetation. Thus, radiometric surface temperature variations over vegetated surfaces may be the result of variations in the amount of bare soil visible to the radiometer. The situation is complicated further by the problems introduced by canopy architecture, which includes the variation in solar elevation angle and viewing angle of the radiometer.

A significant step in the direction of modeling sparse or patchy vegetation cover was taken by Shuttleworth and Wallace (1985) who adapted the Penman–Monteith equation (Monteith, 1975) to account for energy partitioning between crop and soil. In order to circumvent the inconsistency of using a one-dimensional model to represent horizontally inhomogeneous surfaces, Shuttleworth and Wallace introduced the idea of two asymptotic temperature limits, one for bare soil and the other for vegetation. Their model was expressed as separate bare soil and vegetation components with identical ambient conditions above the crop. Latent heat fluxes from each of the components were combined using weighting factors, which were expressed in terms of combinations of soil and plant resistances determined from a knowledge of crop height and leaf area index (LAI).

Shuttleworth and Wallace recognized that the intractable complexity of a vegetation canopy required that they make simplifications that allow them to avoid confronting the aspects of the three-dimensional canopy. While not dismissing the effects of vegetation structure on the interception of solar radiation, they proposed that much of the fine-scale detail of the three-dimensional canopy would tend to cancel over time, leaving the first-order effects to be represented by a one-dimensional model.

Stated differently, the fluxes over bare soil are relatively independent of the adjacent vegetation (and vice versa), but are linked via common substrate and atmospheric properties. In such a geometry, LAI has two values, one for the ensemble of vegetation clumps and one for the ensemble of vegetation

clumps and contiguous bare patches. The one-dimensional model operates separately in each regime; bare soil and vegetation. Total fluxes for the combined bare soil and vegetation are related through an additional parameter, the fractional vegetation cover.

We propose a similar approach to that of Shuttleworth and Wallace, in which a boundary layer model is used in conjunction with remote measurements of surface temperature and normalized difference vegetation index (NDVI) to calculate fractional vegetation cover, LAI, substrate water content in two layers, and surface energy fluxes. The method is illustrated using remote measurements made during the French HAPEX/MOBILHY field experiment.

THE BOUNDARY LAYER MODEL

Like Shuttleworth and Wallace, we will ignore the intractable aspects of the three-dimensional canopy, and imagine a simple structure in which clumps of vegetation (which may consist of a single plant) are interspersed with bare soil patches (Fig. 1). Within the vegetation clumps, no direct solar radiation reaches the ground and no bare soil is visible to the radiometer. Uniformly distributed sparse vegetation and small dense clumps of vegetation are separated, perhaps randomly, by bare soil. The fractional part of the surface covered by the vegetation clumps is f_v and that covered by bare soil is $(1-f_v)$. No distinction is made between sunlit and shaded vegetation or between sunlit and shaded soil visible to the radiometer, although shaded bare soil may be much cooler than unshaded bare soil. Vegetation fraction also depends on the viewing angle of the radiometer; it will effectively increase with decreas-

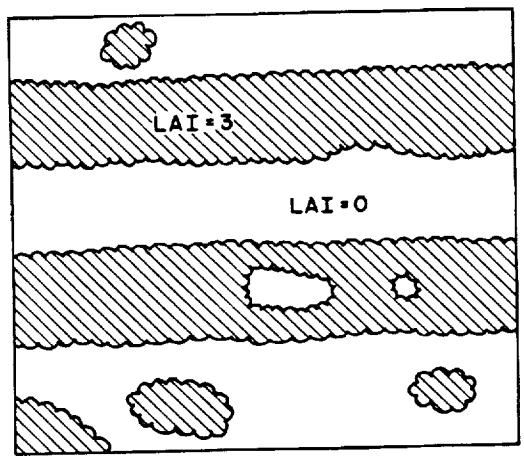

Fig. 1. Schematic view of a partial vegetation cover with leaf area index (LAI) equal to 3.0 in contiguous vegetation patches (hatching). Area represents that of a single pixel or combination of pixels.

ing elevation angle of the radiometer. This variation of f_v with viewing angle is not considered.

Since the details of the boundary layer model are not as important as the technique of applying such a model to the estimation of fractional vegetation cover and soil moisture, we will present only the basic elements of the architecture and equations; the reader is referred to Carlson et al. (1981) and Taconet et al. (1986) for a discussion of the bare soil and vegetation components, respectively. Results presented in this paper should be reproducible with any comparable model, e.g. that of Wetzel and Woodward (1987). Henceforth, the boundary layer model will be referred to as the CM. An overview of the plant and substrate structure in the CM is presented in Fig. 2.

The CM contains a single layer of vegetation, and interleaf air layer, two soil layers, a surface and a mixing layer. Fractional vegetation cover (f_v) is specified for a mixture of bare soil and vegetation. In the vegetation component, vegetation density is expressed in terms of LAI. Bare soil and vegetation regimes are calculated separately, but allowed to interact through exchanges of momentum, heat and water vapor with a common surface air layer above the canopy and a common substrate below.

Downward solar flux (S) and downward long-wave radiation ($R_l\downarrow$) are identical over both bare soil and vegetation regimes. Surface fluxes of sensible and latent heat and upward fluxes of long-wave radiation for bare soil and vegetation ($R_{lb}\uparrow$ and $R_{lv}\uparrow$) are determined separately for each regime. Radiometric temperature of the canopy (T_c) is computed from a weighted average of bare soil and vegetation components of upward long-wave radiation fluxes.

The flow of water vapor and sensible heat is expressed as follows. In the vegetation, latent heat flux (LE_f) passes from the inside of the leaf at leaf temperature (T_l) and specific humidity ($q_l(T_l)$) to the interleaf air spaces,

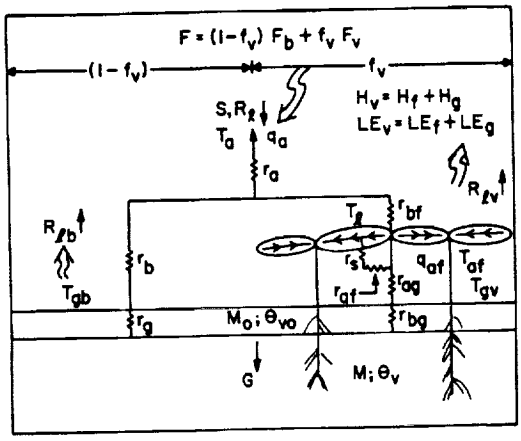

Fig. 2. Overview of plant canopy model. Fractional vegetation cover is f_v and the weighting for fluxes (F) is given by the formula at the top. The remaining symbols are defined in text.

which have a specific humidity (q_{af}), through the stomatal and the leaf boundary layer resistances (r_s; r_{af}). Stomatal resistance is calculated from a knowledge of substrate water content, incident solar flux and LAI. Sensible heat flux (H_f) passes from the leaf (at temperature (T_l)) to the interleaf air spaces, which are at temperature (T_{af}), through the leaf boundary layer resistance (r_{af}).

At the soil surface below the plants, latent heat flux (LE_g) passes from the ground surface beneath the canopy, which is at temperature (T_{gv}), to the interleaf air space through surface resistance (r_{bg}) and interleaf air space resistance (r_{ag}). Sensible heat flux (H_g) passes from the ground across resistors (r_{ag}) between the ground temperature and the interleaf air space temperature (T_{af}). These parallel fluxes (LE_f; LE_g; H_f; H_g) sum to the total vegetation fluxes of latent and sensible heat (LE_v; H_v) at the top of the vegetation canopy and pass through the canopy boundary layer resistance (r_{bf}) and the surface layer resistance (r_a).

Similarly, the calculation of fluxes over bare soil patches is simpler, but expressed in the same notation as over vegetation. Latent heat flux passes from the substrate through a soil resistance (r_g), a boundary layer resistance (r_b) and a surface layer resistance (r_a). Sensible heat flux passes from the ground surface at temperature T_{gb} directly to the atmospheric surface layer through the resistors (r_b) and (r_a). The reader is referred to Taconet et al. (1986) for further details concerning the model.

For a mixture of solid vegetation and bare soil patches, fluxes of sensible and latent heat and the upward flux of long-wave radiation above the plant canopy and the substrate heat flux (G) are taken as weighted averages of the bare soil and vegetation components, according to the vegetation fraction (f_v) using the weighting equation shown in Fig. 2. Temperature and specific humidity at the top of the surface layer (T_a; q_a) and the temperature and water content in the soil are identical for both bare soil and vegetation fractions. Air resistances for both vegetation and bare soil fractions depend on the wind speed and temperature above the canopy and therefore, indirectly, on conditions in both the vegetation and bare soil components. Radiometric temperature of the canopy (T_c) is determined from the weighted upwelling long-wave radiation flux.

An important parameter in the model is the moisture availability, which is defined for the soil surface layer with volumetric water content θ_{vo} as

$$M_o = \theta_{vo}/\theta_{sat} = (r_a + r_b)/(r_g + r_a + r_b)$$
$$= (r_a + r_{bf})/(r_{bg} + r_a + r_{bf}) \quad (1)$$

and for the root zone water content as

$$M = \theta_v/\theta_{sat} \quad (2)$$

where θ_{sat} is the volumetric water content of the soil at field capacity (θ_v). Moisture availability, the primary moisture parameter, is also defined for the surface air layer as the ratio of evaporation to potential evaporation. It should be noted that M_o, is identical for both bare soil and vegetation dominants. Since r_b and r_{bf} are calculated, eqn. (1) imposes small differences in the values of r_g and r_{bg}, which are not directly employed. Further, there is some contention in the idea that M_o can be directly equated to soil water content, although it is generally agreed that the former depends closely on the latter.

MEASUREMENTS

The HAPEX field experiment

The HAPEX-MOBILITY (Hydrologic Atmospheric Pilot Experiment and Modelisation du Bilan Hydrique) program was conducted over a 100 km by 100 km square, located within an agricultural region over southwestern France during the summer of 1986 (Andre' et al., 1988). Its main purpose was to study the hydrological budget and evaporation fluxes at the scale of a General Circulation Model. At network of rain gauges, flux-measuring devices and conventional meteorological observations, supported by aircraft and additional ground surface measurements were made during an intensive phase which lasted from May until mid-July 1986.

One of the programs in HAPEX was directed jointly by Penn State (PSU), the Centre de Recherches en Physique de l'Environment (CRPE) and the Institut National de Recherches Agronomique (INRA) to study the evolution of various plant parameters (stomatal resistance, leaf water potential, LAI, crop height) and their relationship to substrate water content and radiometric surface temperature during the intensive phase of HAPEX. PSU ground measurements were made in two fields of corn, one near the town of Lubbon (in Field N6) in the north of the test area and the other near the town of Castelnau in the south. The former was situated in a field of corn with sandy soil, within a large clearing surrounded by a forest (Les Landes); the latter was located in a corn field on a ridge. Soil water content was measured once or twice daily using gypsum blocks. These devices were calibrated at both sites by gravimetric methods, both in situ and in separate pots of soil. Additional soil water measurements were made periodically by PSU, INRA and NASA groups at this and other sites using gravimetric sampling or neutron probe. Unfortunately, because of late planting due to wet weather, the corn at Castelnau did not emerge until mid-June. Consequently, the focus of this paper is on the Lubbon measurements.

The aircraft program consisted of a series of 16 flights with a NASA C-130 aircraft over the target area during the intensive phase of HAPEX. Two multispectral scanners covering the wavelength region from the visible to the ther-

mal infrared and 21-cm microwave radiometer were mounted aboard this aircraft. Fifteen flights were made at 300 m and 1500 m; additional high altitude (6000 m) flights were made for the purpose of comparison with satellite measurements. One of the scanners was the Thermal Infrared Multi-Spectral Scanner (TIMS) and the other one the NS001 scanner which was functioning at solar wavelengths only (Schmugge and Janssen, 1988). Overflights at Lubbon were made at approximately 11:30 h local time (LST). The focus of this paper is on 4 days during the HAPEX experiment, 6, 16 and 27 June and 2 July. These were the only days in which flights were made during clear or nearly clear sky conditions.

Radiometric temperatures

Temperature measurements were obtained in an across-track scanning mode in the form of digital (DN) counts interpolated between cold and hot reference sources. Absolute accuracy of the blackbody references are estimated to be about 0.5 K, resolution accuracy about 0.35 K and calibration accuracy about 0.8 K. Corrections for water vapor and carbon dioxide attenuation as functions of viewing angles were made using a model of Price (1982), which calculates the temperature correction for water vapor and carbon dioxide attenuation for different viewing angles given a temperature and moisture sounding. Since all the flight data discussed in this paper refer to the 1500 m altitude passes, the total water vapor correction was only a few degrees K. Overall, the accuracy of the radiometer including atmospheric correction is felt to be about 1.0–1.5 K. Pixel size for the 1500 m flights was approximately 4 m in diameter at nadir; no corrections for pixel size as a function of viewing angle were made.

NDVI

The NS001 Thematic Mapper simulator (TMS) was used to measure shortwave spectral radiances from the C-130. Although having a similar resolution to that of the TIMS and an across-track scanning pattern, the instantaneous field of view and surface co-location was slightly different from the TIMS radiometer owing to different scan angles and swath widths. NDVI measurements were made using the formula:

$$\mathrm{NDVI} = (R_4 - R_3)/(R_4 + R_3) \tag{3}$$

where R_3 is the radiance from Channel 3 (wavelength band 0.633–0.697 μm and R_4 is that for Channel 4 (wavelength 0.767–0.910 μm). No corrections were made for solar elevation and radiometer viewing angles. Viewing angles, however, were all less than 30°. According to Paltridge and Mitchell (1989),

corrections to a nadir NDVI for NOAA satellites are less than 10% for viewing angles less than 30°.

Soil moisture

Eight gypsum block locations were installed at each of the two PSU field sites, Lubbon and Castelnau. Average and standard deviations of volumetric soil water contents (θ_v) were determined for each site at approximately 5, 10, 20 and 40 cm depth. In general, the standard deviation of θ_v was about ± 0.04. Although this is not an insignificant variation, it is very similar to the mean standard deviation obtained by Bell et al. (1980) for that of natural soils.

ANALYSES

General approach

Fractional vegetation cover and LAI are determined by matching simulated radiometric surface temperatures, vegetation fraction and LAI with measured values of NDVI and radiometric surface temperatures. Asymptotic limits for sunlit leaves and sunlit bare soil are determined by inspection of the distribution of NDVI vs. radiometric surface temperature. Asymptotic leaf and soil temperatures are used to solve for, respectively, the root zone and soil surface water contents and fractional vegetation cover using the CM. Spurious effects of mutual leaf shading and small-scale variations in soil moisture are largely ignored, although they can be assessed qualitatively from inspection of image products. We make no distinction between different types of crops (corn, soybeans) in either the modeling or the interpretation of the images.

Method

The significance of NDVI

The NDVI constitutes a very useful tool in the study of vegetation cover. Normalization of the radiance differences between spectral intervals on either side of the near-infrared reflectance discontinuity tends to reduce effects of changing sun or viewing angle. Importantly, the NDVI is known to be correlated with the green leaf area, such as the one-sided LAI (Tucker, 1979; Holben et al., 1980; Curran, 1983; Asrar et al., 1984; Best and Harlan, 1985; Gallo et al., 1985; Sellers, 1985; Hansen and Soegaard, 1987; Peterson et al., 1987; Nemani and Running, 1989a). Tucker (1979) and later Best and Harlan (1985) show that the optimum sensitivity to biomass and LAI can be found in the ratio of near infrared (0.70–0.80 μm) to red (0.63–0.69 μm) radiances, bands which are similar to those referred to above. When these ratios

are compared with actual field measurements the error in LAI is typically about ± 1.0 for a given site.

NDVI increases almost linearly with increasing LAI and then enters an asymptotic regime in which NDVI increases very slowly with increasing LAI. Curran (1983) points out that the latter asymptotic region pertains to a surface almost completely covered by leaves. Although there is some variation, an upper asymptote of NDVI vs. vegetation density or LAI usually occurs near 0.5–0.8 for dense vegetation. This upper limit, however, is rather variable and depends on vegetation type, age, and leaf water content (Paltridge and Barber, 1988). For bare soil NDVI tends to vary between -0.1 and 0.2.

Curran also shows that the asymptotic region for LAI begins at values of 3–4 for short crops such as wheat, corn, sorghum and various grasses. Asymptotic regimes for LAI were found by Tucker (1979), Holben et al. (1980) for soybeans (above 2), Asrar et al. (1984) for wheat (above 2.5), Best and Harlan (1985) for oats (above 2), Gallo et al. (1985) for corn (above 3) and Sellers (1985) for various idealized canopies (above values from 1 to 3, depending on leaf angle). Nemani and Running (1989a) show that the change in LAI is nearly linear with NDVI until the former exceeds values of 3–4, above which NDVI rapidly approaches an asymptotic limit. In some conifers, however, the asymptotic region is at large values of LAI, such as in the study of Peterson et al. (1987), who found that the asymptotic domain was in excess of LAI = 6. Such large values of LAI are found on trees with large numbers of clumped needles.

Both Curran (1983) and Asrar et al. (1984) discuss contributions to the reflected radiance from leaves and from the underlying soil surface. They suggest that the asymptotic regime for LAI is one in which the reflectance from soil beneath the vegetation becomes very small. Alternatively stated, the asymptotic part of the LAI vs. NDVI curve occurs when the vegetation cover is close to 100%. Above an LAI of 3.0, little increase occurs in the fraction of bare soil visible to the radiometer. A modeling assumption used to obtain the vegetation fraction (f_v) is that solid vegetation cover ($f_v = 1.0$) begins at LAI = 3.0. LAI can increase above 3.0 but f_v remains at 1.0. Exact choice of the value of LAI for which $f_v = 1.0$ is not critical insofar as the sensitivity of the results is concerned. We found by trial and error that LAI = 3 for the threshold of solid vegetation yielded optimum agreement with HAPEX measurements. Another value might be more appropriate for other types of vegetation, such as trees.

The vertical variation of soil moisture at Lubbon

Figure 3 is a composite of measurements showing the vertical profile of soil water content for 16 June at Lubbon. Despite considerable scatter, it is clear that the deeper substrate (below about 10 cm) is relatively moist ($\theta_v = 0.2$), while the surface is very dry ($\theta_v = 0.02 - 0.06$). It should be noted that all of

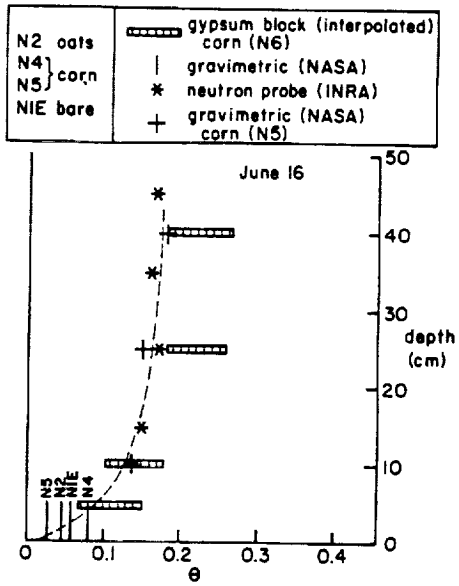

Fig. 3. Vertical profile of volumetric soil water content (θ_v) vs. depth in cm measured by different devices on 16 June 1986 at Lubbon.

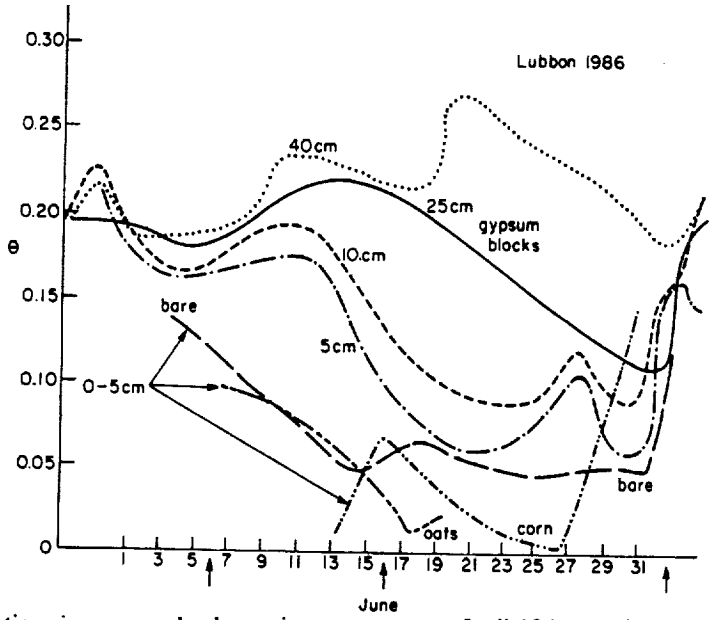

Fig. 4. Variations in measured volumetric water content of soil (θ_v) at various substrate levels during June 1986 at Lubbon. The 5, 10, 25 and 40 cm curves represent measurements made with gypsum blocks in the N6 corn field. The 0–5 cm curves are from gravimetric samples in the oat (N2), corn (N6) and bare (N1) fields at Lubbon.

the gravimetric measurements show a marked soil surface dryness after the early part of June until after 23 June (Fig. 4). By contrast, the deeper substrate remained fairly moist, but with some decrease in the 5 and 10 cm values of θ_v between 10 and 19 of June. Some irrigation was carried out on and after 23 June owing to lack of precipitation during the first three weeks of the month. Despite the irrigation and some minor rainfall episodes during the last few days of June, the large vertical soil water content gradient was present as late as 27 June. By early July, surface soil water contents had increased toward those at deeper levels.

Thermal imagery

Figure 5 is a thermal image made from digital scan data from the C-130 aircraft over the Lubbon region. Here, temperature is represented by a gray scale shading, dark representing cooler temperatures and light warmer temperatures. Field N6, consisting of corn about 0.8 m high with an LAI of 1.8, was the location of the Penn State measurement operation. The average temperature of this field was about 47°C. In contrast, Field N2 contained oats with a temperature of about 28°C, while Field N4 with newly planted corn and Field N1, which was bare, exhibit radiometric surface temperatures well in excess of 50°C. This image clearly shows the large differences in radiometric surface temperatures between the exposed sunlit bare soil areas and the

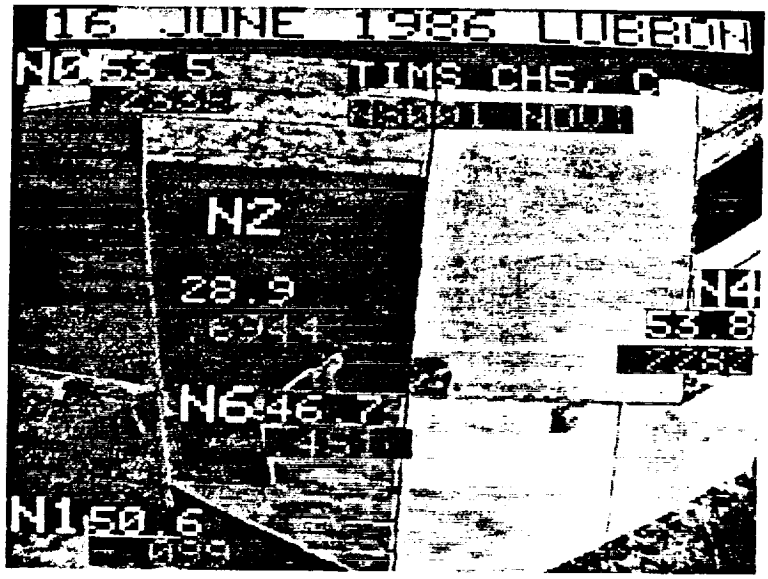

Fig. 5. TIMS thermal infrared image made from NASA C-130 flying at 1500 m on 16 June 1986 near Lubbon. Dark is cool and light is warm. Field numbers are indicated and field averages of temperature (°C) and NDVI are listed.

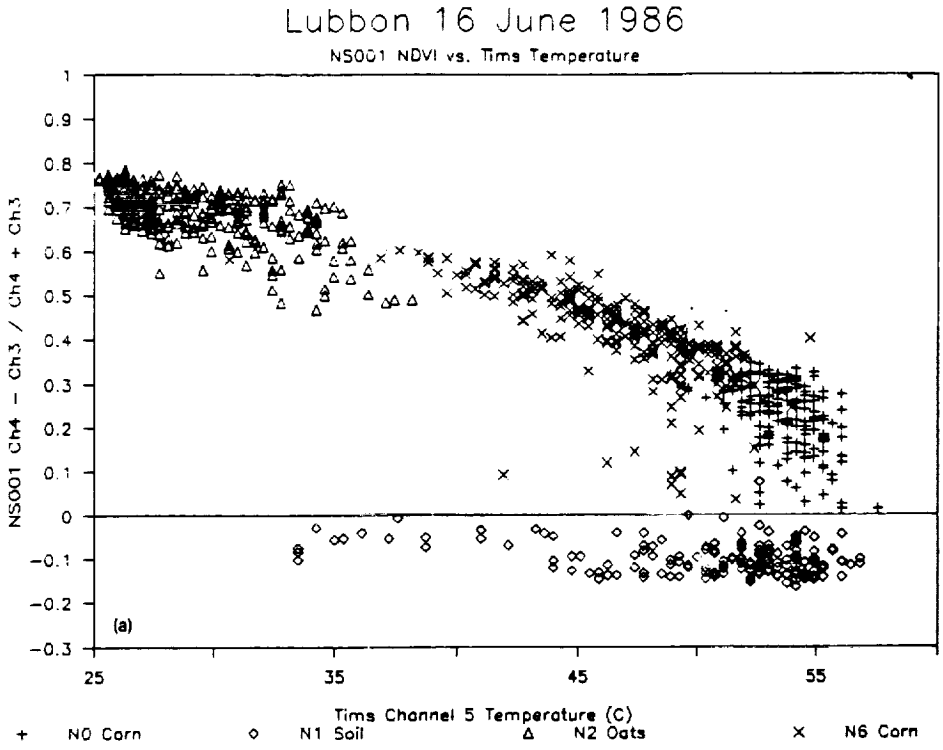

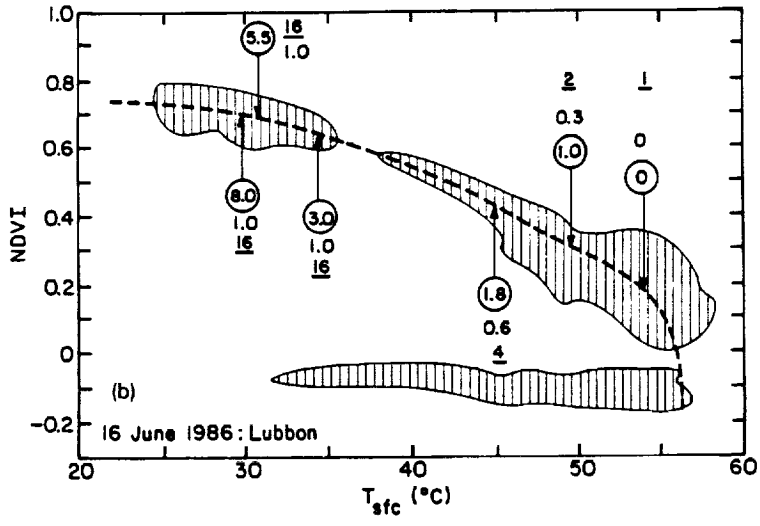

vegetation, which is uniformly dark. It indirectly reflects the large vertical variation in soil dryness between the surface and substrate shown in Figs. 3–4.

Large temperature differences between vegetation and bare soil occurred on all 4 days in which temperature images were made. While less bare soil is visible on 27 June (figure not shown) than on 16 June (Fig. 5), the distribution of warm bare soil and cool vegetation temperatures are similar. By contrast, however, images for 6 June and 2 July (not shown) respectively exhibit small and large fractions of vegetation.

Combining NDVI and thermal measurements

Spatial variations in surface radiometric temperature, such as shown in Fig. 5, are related to variations in the vertical variation of soil water content modulated by fractional vegetation cover. The relationship between radiometric surface temperature and vegetation amount is illustrated in Figs. 6–9. Symbols plotted on the figures pertain to individual resampled pixels. The best example is that of 16 June, which is shown in Fig. 6. Data fall into two general clusters. One cluster contains positive values of NDVI in an envelope that slopes from the upper left-hand to lower right-hand sides of the NDVI/T_c distribution (Fig. 6a). The other cluster comprises points scattering horizontally and having negative values of NDVI. The sloping region extends from cool temperatures and high NDVI over the oat field (Field N2) to very high temperatures and low values of NDVI over newly planted corn fields (Field N0).

The figures exhibit a remarkable range of surface temperatures, with very warm values over bare or nearly bare soil. In the sloping distribution, pixels with high NDVI (in excess of 0.6) and low temperatures represent the asymptotic region in which the temperature approaches that for a sunlit leaf; (shaded leaves would be somewhat cooler but with approximately the same NDVI). At this end of the distribution, the upwelling long-wave radiation from the soil is almost totally attenuated. Large NDVI values for the oats probably correspond to an LAI well in excess of 3.0 and a vegetation fraction of 1.0. At the other end of the distribution, the very warm temperatures correspond to virtually bare soil with LAI almost equal to 0 and a zero vegetation fraction.

Fig. 6a. Distribution of NDVI vs. radiometric surface temperature (°C, corrected for atmospheric attenuation) for individual pixels over the scene in Fig. 5. The type of vegetation planted in each field is indicated by a symbol defined below the figure.

Fig. 6b. Same as Fig. 6a but in schematic form to show how the axis of variation (dashed line) was constructed from the data in Fig. 6a. Circled numbers are the values of LAI determined with the aid of the boundary layer model by matching observed and simulated temperatures given the surface and root-zone moisture contents. Decimal number represents the fractional vegetation cover, circled numbers the derived LAI, and the underlined number the value of surface roughness (cm) used in the model for that simulation.

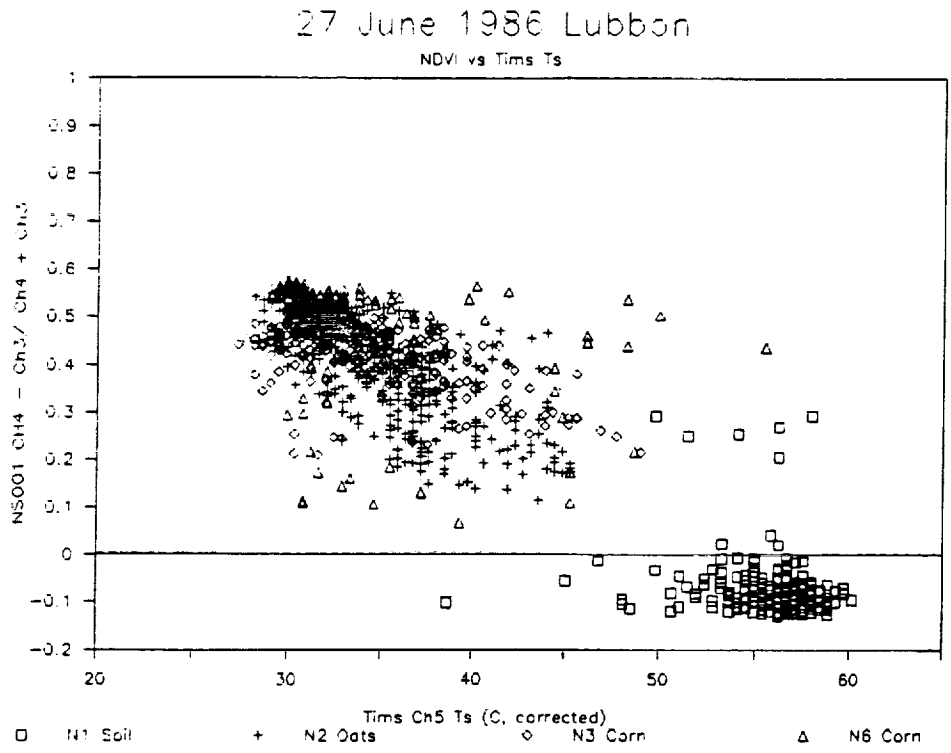

Fig. 7. Same as Fig. 6a but for 27 June.

Two other features in Figs. 6–9 are worth noting: one is a horizontal scatter of surface temperature, a cluster of pixels with a constant NDVI (e.g. the horizontal width of the envelope of data points in Fig. 6a). This cluster is probably associated with spatial variations in soil moisture and to variable effects of the canopy architecture, e.g. mutual shading of leaves. The second feature is the apparent decrease in the maximum NDVI with time between 6 June and 2 July. This trend may be due to changes in vegetation color with age.

Goward et al. (1985) and Nemani and Running (1989b) have proposed that NDVI/T_c diagrams can be used to infer vegetation amount or canopy resistance. The axis of the sloping distribution of points in Figs. 6–9 defines the variation of vegetation fraction with surface radiometric temperature. Providing that there is not a great deal of noise and the distribution of points exhibits a definable slope over a wide range of NDVI, one can define an "axis of variation" through the center of the sloping distribution of points, which, in this case, connects the mean values of T_c and NDVI for each field. This axis describes a spectrum of temperatures and NDVI values with visible bare soil fractions varying from almost zero to virtually 100% cover. For the sake

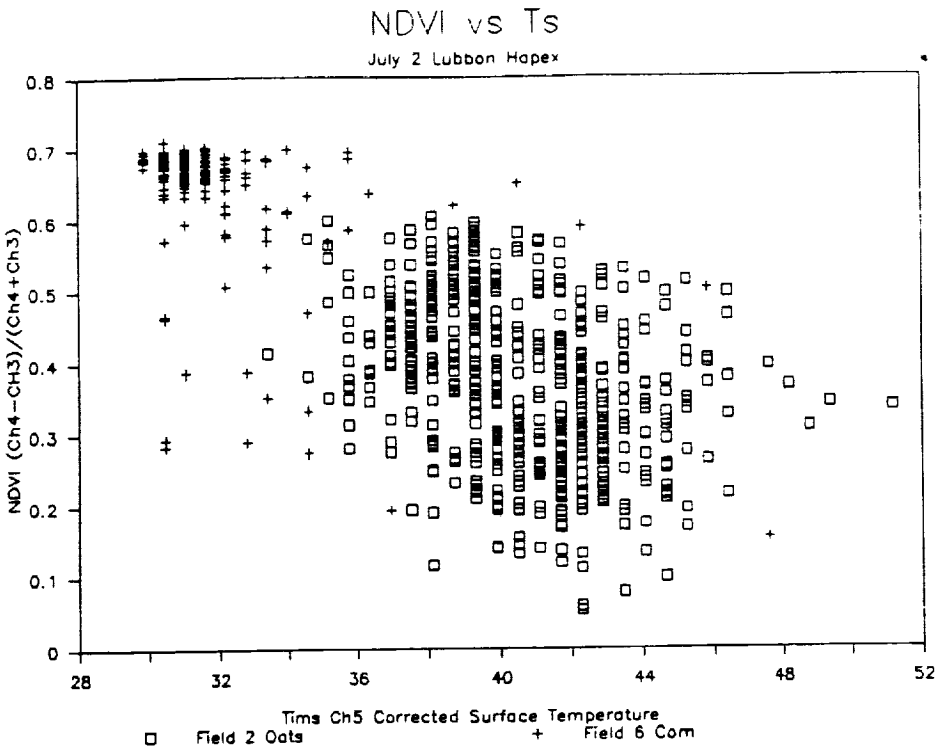

Fig. 8. Same as Fig. 6a but for 2 July.

of illustration, the axis of variation for Fig. 6a is shown by itself in Fig. 6b, but superimposed on a schematic background of pixel represented by hatching.

The NDVI/T_c distribution was less coherent on 27 June (Fig. 7) than on 16 June, although the variation in surface temperature was as large. A gap exists in the axis of variation at high surface temperatures and low values of NDVI owing to the relatively few bare soil patches between the plants. The separate cluster of bare soil temperatures, representing bare fields, is still present.

Field N6 was relatively cool and verdant on 2 July. Considerable scatter in the NDVI/T distribution (Fig. 8) may have been caused by the effects of irrigation, which was administered unevenly, and to ripening or senescence of the oats. Consequently, no axis of variation could be drawn with much confidence.

Most of the fields on 6 June were bare. The NDVI/T_c distribution (Fig. 9) for that date shows a horizontal variation of radiometric surface temperature along the zero NDVI axis, with one isolated cluster of pixels at NDVI=0.6 and 10°C. No axis of variation could be drawn with any confidence.

An oddity of Fig. 6 is the presence of a separate horizontally distributed

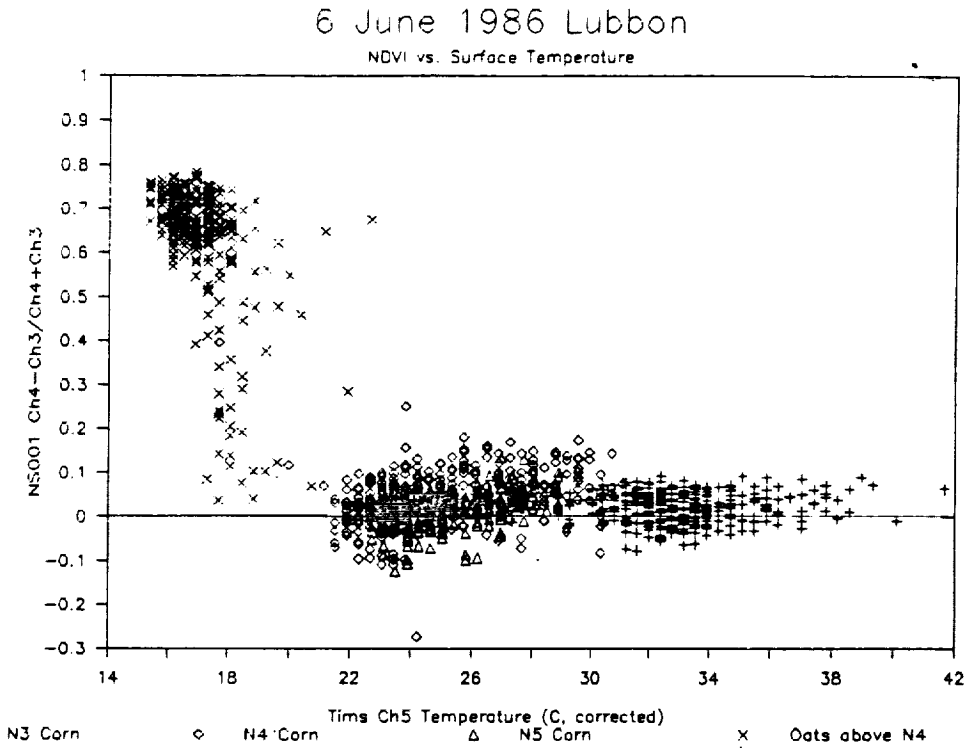

Fig. 9. Same as Fig. 6a but for 6 June.

cluster of pixels near or below the zero NDVI axis. This cluster represents pixels from unplanted or newly planted fields without vegetation, as distinct from bare soil patches between plants in fields that contain maturing vegetation. The reason for this difference is that freshly plowed bare fields would exhibit clods of relatively wetter earth interspersed with fragments of very dry surface soil, whereas bare soil between the plants would be dryer and littered with dead plant debris.

Interpretation of the imagery using a boundary layer model

Based on the assumptions described above, fractional vegetation as a function of NDVI or surface temperature was derived with the aid of the boundary layer model according to the following procedure.

First, asymptotic temperature extrema were determined for sunlit bare soil and sunlit leaf temperatures with the aid of the NDVI/T_c distribution (Figs. 6–9) and the "arch diagram". The arch diagram was originally developed by Coakley and Bretherton (1982) to analyze cloud cover in partially filled fields of view and later used by Albrecht et al. (1988) to separate sea surface temperatures from those at the top of marine stratus clouds. Figures 10–12 show

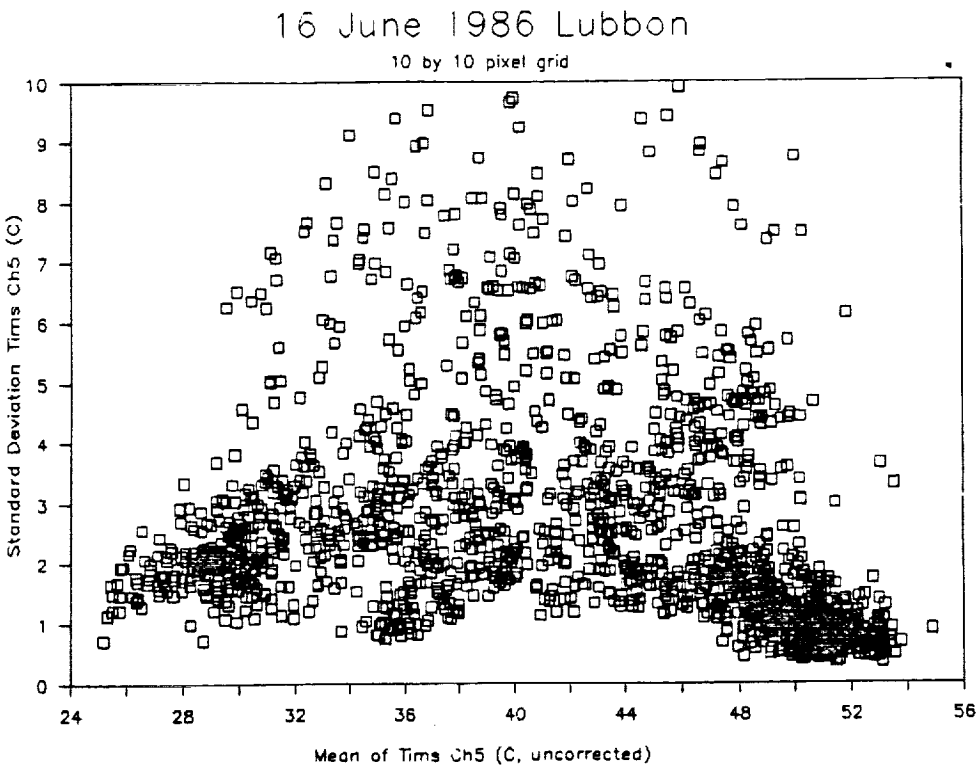

Fig. 10. The arch diagram: standard deviation of radiometric surface temperature vs. uncorrected radiometric surface temperature (°C) for 16 June at Lubbon (the image in Fig. 5). Each data point represents a sub-area consisting of about 10×10 original pixels.

the arch diagrams for 16 and 27 June and 2 July. The arch diagram consists of the standard deviation of temperature (in 10×10 pixel subsets) of the image vs. radiometric surface temperature averaged over that subset. No correction was made for viewing angle or for atmospheric attenuation. The two "feet" of the arch, characterized by dense clusters of relatively low standard deviations, suggest areas of uniform vegetation and bare soil temperatures, which correspond to the temperature extrema along the axis of variation in the NDVI/T_c distribution (e.g. Fig. 6b).

The second step was to use the boundary layer model to calculate substrate water content using the asymptotic temperatures. Thus the water contents (θ_{vo}; θ_v), pertain, respectively, to sunlit bare soil ($f_v=0$; LAI=0; $T_c=55°C$) and sunlit vegetation ($f_v=1.0$; $T_c=28°C$). Solutions are obtained by forcing agreement between simulated and measured surface temperatures at flight time (11:30 LST) (Table 1) for bare soil and solid vegetation.

The third step was to use these derived substrate water contents to calculate f_v as a function of surface radiometric temperature. In these simulations, LAI

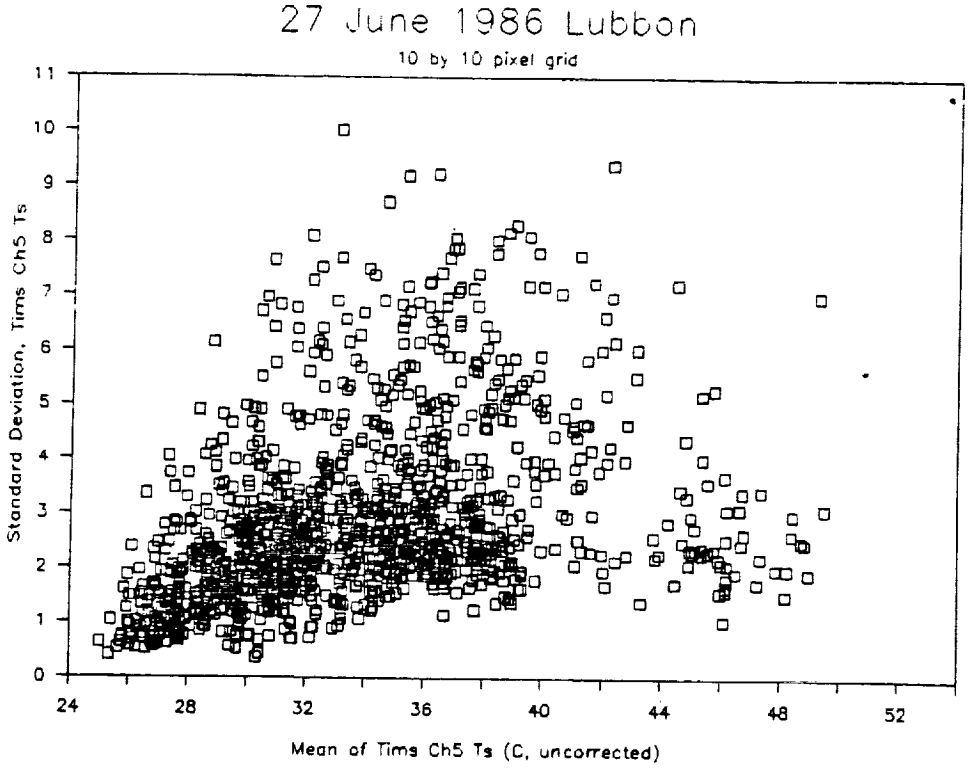

Fig. 11. Same as Fig. 10 but for 27 June.

is fixed at 3.0 for the vegetation fraction and 0 for the bare soil fraction (Fig. 1). We force the simulated and measured radiometric surface temperatures to agree along the axis of variation for different values of f_v in the model. Results are not sensitive to the choice of the solid vegetation value for LAI since the model is used only to convert a given temperature range to a fraction (f_v) between 0 and 1.0. Given f_v vs. T_c, one obtains the distribution of NDVI vs. f_v from the NDVI/T_c diagram. Figure 6b shows the values of LAI, f_v and surface roughness used to simulate temperatures along the axis of variation on 16 June. For example, given LAI = 1.8 (Field N6) the radiometric surface temperature is about 46°C, the NDVI is about 0.4 and $f_v = 0.6$.

A final step was to perform a simulation to generate a range of surface radiometric temperatures as LAI varies above 3.0 with $f_v = 1.0$. This operation simply allows us to determine LAI as a function of radiometric temperature for the solid cover, but has no bearing in determining f_v. Similar calculations were made for 27 June.

At this point, it is possible to specify vegetation fraction (f_v between 0 and 1.0) and the average value of LAI for each resampled pixel, given its measured values of radiometric surface temperature and NDVI. From this information one calculates the fluxes of sensible and latent heat for each pixel.

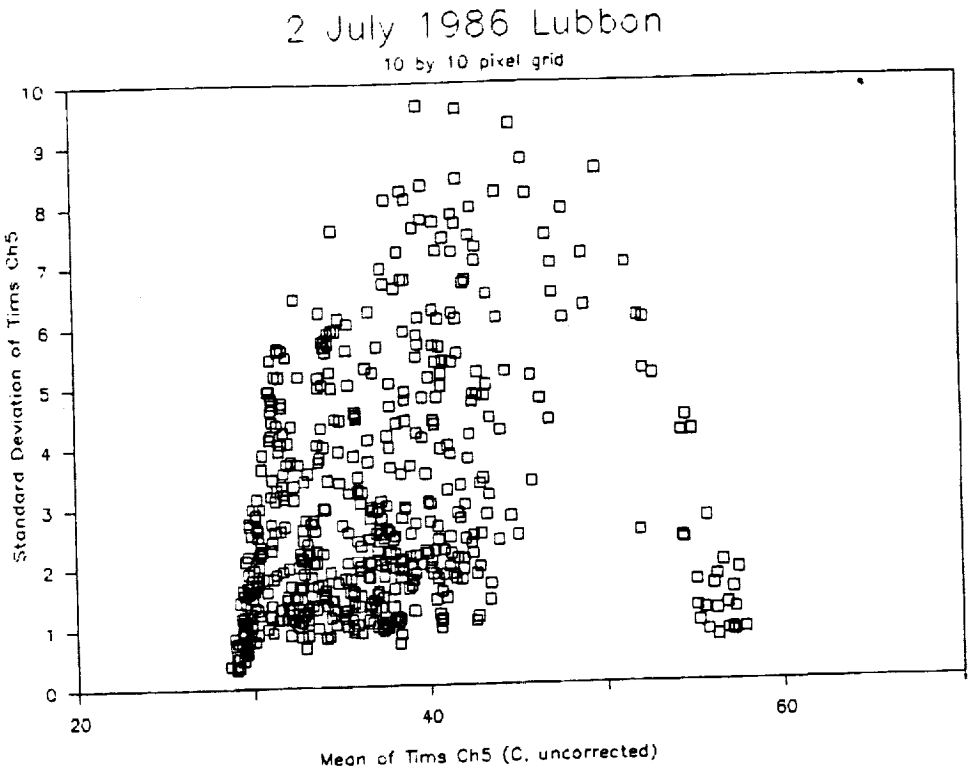

Fig. 12. Same as Fig. 10 but for 2 July.

TABLE 1

Average values of measured and derived quantities for Field N HAPEX (Lubbon), 1986

	LAI(m)[a]	LAI	f_v	T_c(m) (°C)	T_{bare} (°C)	T_{veg} (°C)	NDVI(m)	θ_{vo}	θ_v
6 June[b]	0.6	–	–	–	–	–	–	–	–
16 June	1.8	1.8	0.6	46	55	30	0.45	0.01	0.22
27 June	3.2	3	1.0	33	(48)[c]	33	0.48	0.01	0.22
2 July	3.7	5	1.0	32	(58)	32	0.64	0.01	0.17

[a]m = measured; [b]No aircraft measurements made over Field N6; [c]Values in parentheses are uncertain.

DISCUSSION

Results of simulations

Not surprisingly, the high temperature asymptote corresponds to a low soil

surface water content ($M_o = 0.02$; $\theta_v = 0.006$). We were unable to simulate the highest temperatures without specifying a very low thermal inertia, appropriate to the sandy soil of Lubbon. Simulations for wet soil show little variation in temperature as a function of M between $M = 0.6$ and $M = 1.0$ (θ_v between 0.21 and 0.34). Thus, it was more difficult to simulate precisely the root zone water content at the cool end of the axis of variation, since surface temperature is insensitive to substrate water content in wet conditions. Accordingly, we chose to let $M = 0.65$ and $\theta_v = 0.22$ for both 16 and 27 June, values corresponding to those measured in the root zone (Figs. 3–4).

Simulations were made for the bare soil cluster (NDVI less than zero). These showed that the surface moisture availability (M_o) varied from about 0 to 0.6 between the warm and cool temperatures.

Asymptotic temperatures on 27 June were approximately the same as on 16 June, although it was more difficult to derive a bare soil asymptote on 27 June because of greater scatter and a gap in the measured NDVI/T_c distribution. The arch diagram (Fig. 11) for 27 June suggests a small amount of dry, bare soil with temperatures approaching 60°C, but the NDVI/T_c distribution does not lend confidence in determining the warm end of the axis of variation. (Recent evidence published by the French indicates that the measured temperatures from TIMS are too warm, perhaps by as much as several °C for the high temperatures. This error is due to deterioration in the block body target in the radiometer. See: M. Stoll, Temperature de Surface restituee a partir du radiometre aeroporte T.I.M.S. Rapport de stage effective au CNRM, Toulouse, 29 June 1989 promotion I.M. 87/89, 56 pp.) Simulations for 27 June yield similar results to those of 16 June, which is not surprising in view of the fact that the NDVI/T_c distributions appear to be similar. However, we cannot explain why the axis of variation was at lower values of NDVI on 27 than on 16 June (Fig. 7).

Simulations for 6 June show that the surface moisture availability (M_o) varied from about 1.0 on the cool side to about 0.1 ($\theta_v = 0.03$) on the warm side of this cluster of bare soil temperatures. Surface temperatures were not as warm as during late June, although a few pixels were extremely hot. The isolated cluster of cool pixels in Fig. 9, which represent the oats canopy, could not be simulated without reducing the solar flux intensity below that for clear skies. This suggests that these pixels may have been partly shaded by leaves or by cloud.

Although no axis of variation was obtainable for 2 July because of the enormous amount of scatter, the NDVI/T_c distribution does suggest that the warmest soil temperatures were about 45°C, the equivalent in the model of a surface moisture availability (M_o) of about 0.1. These values reflect the somewhat higher surface soil moisture contents found on this day (as compared with 16 June); the arch diagram indicates that there were still some very high surface temperatures corresponding to almost zero surface moisture availability in some bare patches.

Table 1 summarizes some results for Field N6. Presented are values of LAI (measured), LAI (derived), f_v (derived), NDVI (measured) and the pure sunlit leaf and sunlit bare soil temperatures (LAI = 3.0 and 0) and for the appropriate field average of LAI which allows measured and simulated surface temperature to agree. Also shown are simulated root zone water contents. The last two days constitute 100% canopy cover for Field N6 (LAI exceeding 3.0), whereas 16 June is an example of partial vegetation cover in a single field.

Comparison with measurements

Some independent confirmation of the results can be made by comparing the measured values of LAI and NDVI with the simulated values of NDVI and LAI as a function of simulated vegetation fraction (f_v). LAI was measured at the PSU site in Field N6 on four occasions during the same period. Figure 13 shows the distribution of measured NDVI vs. measured LAI and the derived NDVI (from the axes of variation) as simulated by the model. The comparison is obviously very good for 16 June but agreement with measurements is not as close for 27 June because of greater scatter in the data (Fig. 7). Had we chosen a somewhat smaller LAI threshold for solid vegetation than 3.0, agreement between measured and modelled LAI would have been closer to the measured LAI on 27 June.

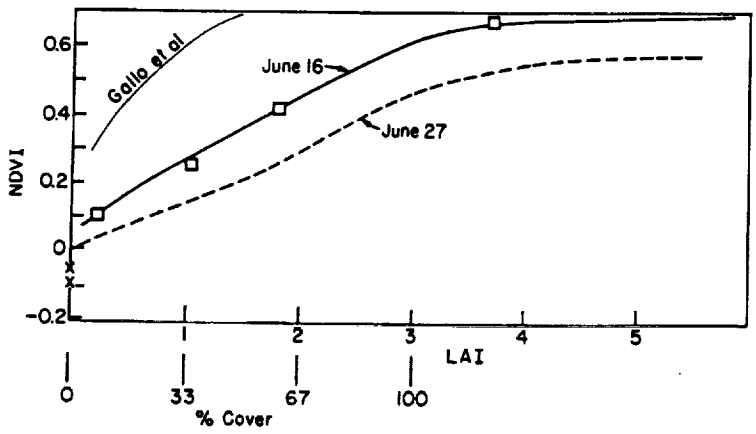

Fig. 13. NDVI vs. percent cover and LAI for model simulations for 16 June and 27 June at Lubbon. Squares represent simultaneous aircraft measurements of NDVI and ground measurements of NDVI made on 4 days over the Lubbon field (N6) during June; crosses represent measured NDVI and LAI for almost bare soil. Heavy solid line represents simulated LAI and fraction vegetation cover vs. NDVI, consistent with axis of variation for measurements. The thin solid line obeys a formula proposed by Gallo et al. (1985) for NDVI vs. LAI over corn.

Problems in applying the method

The difficulty in determining the axis of variation, especially on 6 June and 2 July underscores the central problem in this method. To some extent, poorer agreement with measurements on 27 June, as compared with 16 June, is due to the wide horizontal scatter of points and the lack of values on the warm side of the axis of variation. Clearly, the distribution of points on 16 June is ideal, because the variance of temperature at constant NDVI is quite small.

The derived fractional vegetation cover depends on the architecture of vegetation, the geometry of bare soil distribution, the type of soil and vegetation and the solar and radiometer viewing angles; f_v will tend to increase with increasing solar or viewing angles. The present results, however, suggest that various crops can be combined to produce a meaningful axis of variation. However, extending the method to a mixture of trees and crops may prove untenable.

A difficulty in applying the method would be encountered with regard to satellite measurements because of their relatively low resolution. Instruments such as the AVHRR (1 km resolution) may be incapable of producing a wide range of NDVI and surface temperature over a target area. Thus, it may be necessary to extrapolate the axis of variation and to composite satellite measurements over successive images. Nemani and Running (1989b) have recently presented some encouraging results showing that the AVHRR is capable of determining an axis of variation over forests. Their figures show that the slope of the axis of variation varies according to the amount of surface moisture.

SUMMARY

This study suggests a method to derive a spatial distribution of fractional vegetation cover and soil moisture in the surface and root zone over patchy or sparse vegetation. The method makes use of two types of image products: the distribution of NDVI vs. radiometric surface temperature (the NDVI/T_c) and the "arch" diagram, which shows the distribution of radiometric surface temperature in subgroups of pixels vs. the standard deviation of the radiometric surface temperature in those subgroups. These two diagrams aid in identifying asymptotic limits of the sunlit leaf and the sunlit bare soil temperature. It also allows one qualitatively to assess the degree of noise produced by small-scale variations in soil moisture and leaf shading.

The boundary layer model is used to estimate soil surface and root zone water contents, given the asymptotic vegetation and bare soil temperatures. A crucial aspect of the method is to define the relationship between NDVI and surface radiometric temperature, which we call axis of variation. From this, we obtain average soil moisture values for surface and root zone, and a

vegetation fraction, surface turbulent heat fluxes and LAI as functions of NDVI for each pixel.

Some subjectivity is inherent in the method. An axis of variation may not always be easy to define, for example when small-scale variations in soil moisture are large (perhaps owing to irrigation), where the amount of bare soil is negligible or where the soil surface temperature and leaf temperatures are similar, as in the case of wet soil. Large horizontal variations in soil moisture increase the scatter. Nevertheless, even when the axis of distribution is obscured because of noise, the NDVI/T_c and arch diagrams yield useful qualitative information on the distribution of vegetation cover, small-scale variations in soil moisture and vertical gradient of soil water content. A reliable axis of variation could be determined by compositing measurements obtained from a sequence of images.

The method needs to be tested on many types of soils and vegetation. Application to analysis of AVHRR satellite data may prove useful over different types and mixes of vegetation, although it is still too early to determine if lower-resolution satellite radiometers can define a usable axis of variation.

ACKNOWLEDGEMENTS

The authors would like to thank the sponsors of this research, the National Aeronautics and Space Administration under grant NAG 5-919, the United States Geological Survey under grant no. 14-08-0001-G1490, and the United States Department of Agriculture/Agriculture Research Service under grant no. 58-32U4-8-27.

REFERENCES

Andre', J.C., et al., 1988. Evaporation over land surfaces: First results from HAPEX-MOBILHY special observing period. Ann. Geophys., 6: 477–492.

Asrar, G., Fuchs, M., Kanemasu, E.T. and Hatfield, J.L., 1984. Estimating absorbed photosynthetic radiation and leaf area index from spectral reflectance in wheat. Agron. J., 76: 300–306.

Albrecht, B.A., Randall, D.A. and Nicholls, S., 1988. Observations of marine stratocumulus clouds during FIRE. Bull. Am. Meteorol. Soc., 69: 618–626.

Bell, K.R., Blanchard, B.J., Schmugge, T.J. and Witzak, M.W., 1980. Analysis of surface moisture variations within large field sites. Water Resour. Bull., 16: 796–810.

Best, E.G. and Harlan, J.C., 1985. Spectral estimation of green leaf area index of oats. Remote Sensing Environ., 17: 27–36.

Carlson, T.N. and Boland, F.E., 1978. Analysis of urban–rural canopy using a surface heat flux/temperature model. J. Appl. Meteorol., 17: 998–1013.

Carlson, T.N., Dodd, J.K., Benjamin, S.G. and Cooper, J.N., 1981. Remote estimation of surface energy balance, moisture availability and thermal inertia. J. Appl. Meteorol., 20: 67–87.

Coakley, J.A. and Bretherton, F.P., 1982. Cloud cover from high resolution scanner data: Detecting and allowing for partially filled fields of view. J. Geophys. Res., 87: 4917–4932.

Curran, P.J., 1983. Multispectral remote sensing for the estimation of green leaf area index. Philos. Trans. R. Soc. London, Ser. A., 309: 257–270.

Gallo, T.F., Daughtry, C.S.T. and Bauer, M.E., 1985. Spectral estimation of absorbed photosynthetically active radiation in corn canopies. Remote Sensing Environ., 17: 221–232.

Goward, S.N., Cruickshanks, G.D. and Hope, A.S., 1985. Observed relation between thermal emission and reflected radiance of a complex vegetated landscape. Remote Sensing Environ., 18: 137–146.

Hansen, B. and Soegaard, H., 1987. Monitoring vegetation index and biomass production in southern Greenland based on NOAA-AVHRR data. 21st International Symposium on Remote Sensing of Environment, Ann Arbor, MI, 26–30 October 1987. 10 pp.

Hatfield, J.L., Reginato, R.J. and Idso, S.B., 1984. Evaluation of canopy temperature-evapotranspiration models over various crops. Agric. For. Meteorol., 32: 41–53.

Holben, B.N., Tucker, C.J. and Fan, C-J., 1980. Spectral assessment of soybean leaf area and leaf biomass. Photogramm. Eng., 46: 651–656.

Idso, S.B., Schmugge, T.J., Jackson, R.D. and Reginato, R.J., 1975. The utility of surface temperature measurements for remote sensing of soil water studies. J. Geophys. Res., 80: 3044–3049.

Jackson, R.D., 1982. Canopy temperature and crop water stress. In: D. Hillel (Editor), Advances in Irrigation. Academic Press, Vol. 1, pp. 43–85.

Jackson, R.D., Reginato, R.J. and Idso, S.B., 1977. Wheat canopy temperature: A practical tool for evaluating water requirements. Water Res. Manage., 13: 651–656.

Lagouarde, J.P. and Choisnel, E., 1990. A new agrometeorological model for evaporation and surface temperature. Agric. For. Meteorol, submitted.

Monteith, J.L., 1975. Vegetation and the Atmosphere, Vol. I, Academic Press, New York, NY, 278 pp.

Nemani, R.R. and Running, S.W., 1989a. Testing a theoretical climate–soil–leaf area hydrological equilibrium of forests using satellite data and ecosystem simulation. Agric. For. Meteorol., 44: 245–260.

Nemani, R.R. and Running, S.W., 1989b. Estimation of regional surface resistance to evapotranspiration from NDVI and Thermal-IR AVHRR data. J. Appl. Meteorol., 28: 276–284.

Paltridge, G. and Barber, J., 1988. Monitoring grassland dryness and fire potential in Australia with NOAA/AVHRR data. Remote Sensing Environ., 28: 384–393.

Paltridge, G. and Mitchell, R.M., 1989. Atmospheric and viewing angle correction of vegetation indices and grassland soil moisture content derived from NOAA/AVHRR data. Remote Sensing Environ., in press.

Peterson, D.L., Spanner, M.A., Running, S.W. and Teuber, K.B., 1987. Relationship of thematic mapper simulator data to leaf area index of temperate coniferous forests. Remote Sensing Environ., 22: 323–341.

Price, J.C., 1982. On the use of satellite data to infer surface fluxes at meteorological scales. J. Appl. Meteorol., 21: 1111–1122.

Raffy, M. and Becker, F., 1985. An inverse problem for remote sensing in the thermal infrared bands and its solution. J. Geophys. Res., D3(90): 5809–5819.

Schmugge, T., 1978. Remote sensing of surface soil moisture. J. Appl. Meteorol., 17: 1549–1557.

Schmugge, T.J. and Janssen, L., 1988. Aircraft remote sensing in HAPEX. Procedures of the 4th International Colloqium on Spectral Signatures in Objects of Remote Sensing. Aussois, France, 18–22 June 1988, (ESA SP-287), pp. 463–467.

Sellers, P.J., 1985. Canopy reflectance, photosynthesis and transpiration. Int. J. Remote Sensing, 6: 1335–1372.

Shuttleworth, W.J. and Wallace, J.S., 1985. Evaporation from sparse crops – an energy combination theory. Q. J. R. Meteorol. Soc., 111: 839–855.

Taconet, O., Carlson, T.N., Bervard, R. and Vidal-Madjar, D., 1986. Evaluation of a surface/vegetation parameterization using satellite measurements of surface temperature. J. Climate Appl. Meteorol., 25: 1752–1767.

Tucker, C.J., 1979. Red and photographic infrared linear combinations for monitoring vegetation. Remote Sensing Environ., 8: 127–150.

Wetzel, P.J. and Woodward, R.H., 1987. Soil moisture estimation using GOES-VISSR infrared data: A case study with a simple statistical method. J. Climate Appl. Meteorol., 26: 107–117.

APPENDIX D

TRANSIENT WATER STRESS IN A VEGETATION CANOPY: SIMULATIONS AND MEASUREMENTS

Toby N. Carlson

James E. Belles

Robert R. Gillies

Department of Meteorology
The Pennsylvania State University
University Park, PA 16802

April 1990

ABSTRACT

TRANSIENT WATER STRESS IN A VEGETATION CANOPY: SIMULATIONS AND MEASUREMENTS

Measurements of evapotranspiration and radiometric surface temperature, supplemented by model simulations, illustrate the effect of transient water stress on the evapotranspiration and radiometric surface temperatures over a corn (Zea Mays L.) canopy. Transient stress is manifested by a plateau in the evapotranspiration and a warmer radiometric temperature of the canopy. The cause of the evapotranspiration plateau is not solely due to reduced soil water content but to excessive atmospheric demand in the face of internal plant constraints. One of these constraints is a threshold epidermal leaf water potential, below which stomatal resistance increases very rapidly with decreasing leaf water potential. Accordingly the evapotranspiration plateau can occur at relatively high soil water content.

The sensitivity of the canopy temperature to changing soil water content is weak at high soil water content. The evapotranspiration plateau and its effect on radiometric surface temperatures would not be detectable until, in this case, the soil water content decreases to about half of field capacity. Since evapotranspiration collapse (wilting) would occur at about 35% of field capacity, it may be possible to remotely monitor the onset of crop water stress over dense vegetation before catastrophic damage occurs.

1. Introduction

A problem in remote sensing is that the infrared temperature of dense vegetation is rather insensitive to soil water content. A current ("root-shoot") controversy amongst plant scientists (Kramer, 1988; Passioura, 1988; Boyer, 1989) may have important implications for solution of this problem.

Let us very briefly summarize the two positions. Adherents of root control cite laboratory evidence showing that stomatal resistance varies according to signals carried in sap from roots to leaves by a hormone (ABA), called abscisic acid. These root signals inform the leaves of the soil water status and allow the stomates to adjust accordingly (Gollan et al, 1986; Schulze et al., 1987; Munns and King, 1988).

A counter - argument in favor of leaf control of stomatal resistance offers evidence that the epidermal cells in the leaf are able to sense water stress. Leaf water stress is more closely related to the leaf turgor and hydraulics of water flow to the leaf than to biochemical signals from the roots (Frensch and Schulze, 1988; Kramer, 1988). Resolution of this issue awaits more research.

Alternately stated, the control of stomatal resistance by the leaf suggests that the former is related to leaf water potential. This implies that the leaf can react to transient periods of water stress brought about by high atmospheric demand and a loss of positive turgor pressure in the leaves (Jones, 1983). Transient periods of water stress could then occur in principle even when the soil is wet, provided that the atmospheric demand exceeds the plant's capability to supply water from its roots. In such a case, transient leaf water stress would be manifested by a midday plateau or dip in the transpiration, with an associated rise in leaf temperature and sensible heat.

The onset of such transient leaf water stress can be modeled by relating epidermal leaf water potential to stomatal resistance and invoking an epidermal leaf water potential threshold (ψ_c), below which stomatal resistance increases rapidly with decreasing leaf water potential.

The concept a leaf water potential threshold originated with Cowan (1965), who defined it in terms of a supply function. Turner (1970; 1974) and many others (e.g. Nizinski and Saugier, 1989) have presented striking observational evidence that such a leaf water potential threshold occurs in a variety of crops. The leaf water potential threshold constitutes an important parameter in the plant component of some boundary layer or climate models (Wetzel and Chang, 1987; Sellers and Dorman, 1987; Lynn and Carlson, 1990).

The purpose of this paper is to [1] present additional observational and modeling evidence of transient water stress, [2] illustrate the effects of the transpiration plateau on the canopy radiometric temperature and [3] describe the factors responsible for the onset of the transpiration plateau, such as soil moisture. This paper also considers the point at which the transient stress can be detected by remote measurement of surface temperature, including the effects of surrounding bare soil, cloud cover and how these can mask the stress signal.

2. Field Measurements

Micrometeorological field measurements were made over a two - year period (1987 - 88) at Rock Springs, a research agricultural site near The Pennsylvania State University. These measurements consist of net radiation, air temperature, wind speed and relative humidity, taken from a tower at approximately 9 meters above the ground. Surface radiometric temperature was measured by a radiometer (Optitherm II) mounted on a second tower and trained towards the surface at an elevation of about 3 meters at an

angle of 20 degrees from the vertical. Surface sensible heat flux was obtained using two methods: [1] Directly from the sonic anemometer and [2] from bulk aerodynamic formulae using measurements of surface radiometric and air temperatures, wind speed and crop height. Surface roughness and displacement height was obtained using standard formulae. Ground heat flux was determined in two ways: A flux plate embedded at a 10 centimeter depth and using temperature profiles obtained from ground thermistors buried up to a depth of 40 centimeters. Soil water content was measured using gypsum blocks buried at 5 substrate levels from 2.5 to 40 centimeters in depth. Instruments operated continually and the measurements were recorded as half - hour averages on computer diskettes.

Surface evapotranspiration was determined from the surface energy budget by subtracting the sum of the ground flux and the surface sensible heat flux from the net radiation flux. During the two growing seasons, there was only one period in which, [1] the measurements functioned continuously for several days under sunny skies, [2] the vegetation was dense enough to permit the assumption that evaporation flux from the underlying soil was relatively small compared to the total evapotranspiration and [3] the sensible heat fluxes measured independently by two methods were in very close agreement. This period was during July 1987 in a corn canopy (Zea Mays L.), which was about 2.5 meters high and had a leaf area index of about 7 (Belles, 1990).

These measurements nonetheless provide good examples of the evapotranspiration plateau. Figure 1 shows this plateau, which is indicated by a sudden change in slope of the evapotranspiration curve. The plateau lengthened progressively between July 18th, when it lasted about two hours, and July 22nd, when it lasted from about 0900 until 1500 local time.

Figure 2 shows the progressive decrease in the evapotranspiration during the

middle part of the day from July 18th to 22th. Differences are slight during the morning and late afternoon before and after the time of the plateau. Measured differences from day to day were also largest near midday. Similarly, the radiometric minus air temperature differences (T_{ir} - T_a) between July 18th and July 22nd were largest (about 3°C) near midday and small during the early morning and late afternoon (Fig. 3).

The increasingly early onset and lengthening duration of the evapotranspiration plateau during these four days is due to a progressive drying of the soil. Indeed, soil water contents (Fig. 4) at both 2.5 and 20 centimeters diminished from values in excess of 0.2 (by volume) to less than 0.1 between July 4th and July 30th, with the surface drying out at a greater rate than that at the deeper level. More precisely, the deeper layer, which we associate with the root zone layer, dried out from 0.74 of field capacity (0.34 by volume for the soil type - Hagerstown loam) on July 4th to 0.5 of field capacity on July 18th to 0.28 of field capacity on July 30th.

3. **Simulations** - *boundary layer model with plant component*

A tool used to interpret our measurements is a boundary layer model with plant component. The model is able to simulate the evapotranspiration plateau from which we can analyze factors responsible for onset and duration of the plateau. The atmospheric boundary layer model has been described by Carlson (1986), its vegetation component by Taconet et al. (1986) and the plant hydraulics by Lynn and Carlson (1990) and Carlson and Lynn (1990). We will restate in this paper, only those aspects of the vegetation model that pertain to the simulation of the plateau.

The model calculates evapotranspiration from a balance between the flow of water from the substrate to the plant (F_w), the transpiration (vapor) flux from the leaves to the surrounding atmosphere (L_eE_f) and the water flux from storage (q_s).

The equation is expressed as:

$$L_e E_f = F_w + q_s \qquad [1a]$$

For steady state ($q_s = 0$) this water balance can be expressed in resistance notation as:

$$\frac{\psi_g - \psi_l - H}{Z_g + Z_p} = \frac{\rho c_p}{\gamma}\left[\frac{e_l(T_l) - e_{af}}{r_s + r_{af}}\right] \qquad [1b]$$

Here, F_w is the flux of liquid water from the soil to the leaf. It is expressed by a drop in water potential from the soil around the roots (ψ_g) to the leaves in the mesophyll (ψ_l) divided by the sum of the soil plus plant resistances ($Z_g + Z_p$). This is equated with transpiration ($L_e E_f$), the flux of water vapor (latent heat) from the leaves to the air. It is given by the vapor pressure drop from the leaf (e_l at the temperature of the leaf T_l) to the surrounding air (e_{af}) divided by the sum of leaf plus its boundary layer resistance ($r_l + r_{af}$). H is the gravitational potential ($H = \rho_w gh$, where ρ_w is the liquid water density, g is the gravitational constant and h represents the height of the leaves above the roots). The psychrometric constant is γ ($\gamma = Pc_p/(0.622L_e)$, where P is the atmospheric pressure, c_p is the specific heat at constant pressure and L_e is the latent heat of condensation.

Leaf resistance consists of stomatal and cuticle resistances, which exist in parallel. Since we set the cuticle resistance to be much larger than the stomatal resistance, we will refer to the leaf resistance r_l as the average stomatal resistance r_s; the latter is defined for a sunlit leaf near the top of the canopy.

Substrate water is accounted for in two layers, a surface layer and a root zone layer. The former controls the evaporation from the soil surface beneath the plant and the latter governs ψ_g and Z_g. In this case since there was dense vegetation cover we made the assumption that evapotranspiration and transpiration are virtually identical quantities. The ground water potential (ψ_g) and the soil resistance (Z_g) are both dependent on the

soil water content and soil type. We calculate the soil water potential and soil resistance using simple formulae given by Cosby et al. (1984). The evaporative flux is computed for the underlying soil layer.

The stomatal resistance (r_s) is assumed to depend on leaf water potential, vapor pressure deficit and sunlight intensity. We use the following relationship to relate these parameters to stomatal resistance:

$$r_s = r_{min} \times f(\psi_e)f(S) \qquad [2]$$

where f(S) and $f(\psi_e)$ are, respectively, functions of incident solar flux and epidermal leaf water potential and r_{min} is a minimum stomatal resistance. The two functions, $f(\psi_e)$ and f(S), vary from one to infinity; r_{min} is the value of r_s when the functions are both equal to one. At f(S) = 1.0, the solar flux is assumed to be a saturation value (S_o), which we assume to be 1000 Wm^{-2}. At $f(\psi_e)$ = 1.0, the leaf is saturated with water and ψ_e = 0.

The effect of vapor pressure deficit on stomatal resistance is accounted for by setting a proportionality between epidermal minus mesophyll water potential difference and the vapor pressure deficit ($e_l(T_l)$ - e_{af}). Lynn and Carlson (1990) show that this formulation realistically captures feedbacks between vapor pressure deficit and stomatal resistance. However, since the stomates in corn are thought to possess a low sensitivity to vapor pressure deficit (B. Choudhury, private communication), we let $\psi_l = \psi_e$.

The functions $f(\psi_e)$ and f(S) are highly exponential, first increasing slowly from a value of one and then much more rapidly with decreasing values of ψ_e or S. To capture this non-linearity in the simplest possible manner consistent with measurements, we separate each exponential function into to two linear regimes, one with a small slope and the other with a large slope. Such a model, called 'linear discontinuous' by Fisher et al. (1981), has also been adopted by Nizinski and Saugier (1989). For the leaf water potential

function, we write:

$$f(\psi_e) = r_{min} \{ r_{min} + b_1\psi_e + b_2(\psi_e - \psi_c)\,\delta_\psi \} \qquad [3]$$

where b_1 and b_2 are constants representing the respective slopes of the two lines and ψ_c is the 'threshold leaf water potential', which lies at the intersection of the two straight lines. The operator δ_ψ is equal to zero when ψ_e is in the sub - threshold (slowly changing) regime, (larger than ψ_c). When ψ_e reaches ψ_c or falls below it, δ_ψ = 1.0 and ψ_e equals ψ_c in the term multiplied by b_1.

We found that the best fit with measurements was to set b_1 equal to zero for all simulations (Table 1). In so doing, we imply that there is no sensitivity of stomatal resistance to leaf water potential until the threshold is reached. Thus, when the leaf water potential is above threshold, substrate water content affects the water balance equation (Eqn. 1b) only by way of the ground water potential ψ_g and the ground resistance Z_g, both of which change very slowly with time. When the leaf water potential decreases below ψ_c, the contribution by the b_2 term is very large (Table 1) and the stomatal resistance increases rapidly with decreasing leaf water potential.

The threshold leaf water potential accompanied by a large magnitude of b_2 produces a transpiration plateau. The dependence of r_s on leaf water potential appears to be necessary for simulating this effect. This is the case even when stomatal resistance is linked to vapor pressure deficit.

A similar linear discontinuous function is used for f(S). Since the threshold solar flux (S_c) is usually rather low (50 Wm^{-2}; Table 1), the behavior of f(S) is unimportant for this study and will not be discussed further.

Water storage also can affect the shape of the transpiration plateau (Carlson and Lynn, 1990). The role of capacitance is relatively minor however, and thus we will not discuss the nature of the flux q_s term (Eqn. 1a) except in passing. Capacitance is calculated in the model but it is omitted in (Eqn. 1a) because a discussion of its mathematics is felt to be unnecessary for this paper.

Equations [1] - [3] constitute a quadratic which can be solved analytically for the leaf water potential (Lynn and Carlson; 1990) and by substitution, the transpiration. These equations form part of a larger boundary layer model. The larger model operates simultaneously in two modes, one for vegetation with underlying bare soil and the other for bare soil without vegetation. Bare soil and vegetation components are blended to account for situations of partial vegetation cover (Carlson et al., 1990). For the most part, we assume full vegetation cover and suppress the separate bare soil component; however some simulations were made for partial vegetation cover with a specified vegetation fraction.

Calculations of r_{af} and e_{af}, T_l and solar flux were made using equations discussed by Taconet et al. (1986). Fluxes computed in the model pertain to a single leaf. Extension of these fluxes from a leaf to a canopy is currently undergoing considerable scrutiny (Baldocchi et al., 1990; Rochette et al., 1990; Mascart et al., 1990). Our method for scaling from a leaf to a canopy is to multiply the individual leaf fluxes by a shelter factor to leaf area index ratio. The shelter factor accounts for the fact that not all leaves transpire at the sunlit amount due to fact that solar radiation decreases with height beneath the top of the canopy. For dense vegetation, the shelter factor to leaf area index ratio approaches two. The reader is referred to Taconet et al. (1986) and Lynn and Carlson (1990) for a more detailed discussion of our scaling factor.

4. The transpiration plateau

Simulations of evapotranspiration were made for July 18th, 21st and 22nd, 1987 (Fig. 1) using values of the vegetation parameters shown in Table 1; these are similar to values adopted by Lynn and Carlson (1990) for their corn simulations. Soil water contents for the surface and root zone are given in Figure 4. Except for the soil water contents and the initial atmospheric conditions, the model parameters are identical for all three days.

The purpose in performing these simulations is to demonstrate that the model is capable of reproducing the transpiration plateau during the period 18th to 22nd July. We obtained close agreement with the measurements for values of threshold leaf water potential and other parameters in Table 1. The threshold water potential of ψ_c = -15 bars is typical for temperate latitude crops (Nizinski and Saugier, 1989). Agreement between measurement and model results depends upon the choice of Z_p, which was 0.06 bars $(Wm^{-2})^{-1}$ (Table 1). A smaller value of Z_p would have required our using a smaller value of the threshold leaf water potential. Lynn and Carlson (1990) determined a threshold leaf water potential of -13 bars and Z_p = 0.04 bars $(Wm^{-2})^{-1}$ for corn.

The evapotranspiration plateau tends to slope downward with time. We can simulate this slope in two ways: [1] By the inclusion of plant capacitance and [2] by relating stomatal resistance to vapor pressure deficit. Since the vapor pressure deficit effect was suppressed in the simulations, the slope in the modeled plateau was due to capacitance.

A primary objective of this paper is to show how the plateau would have evolved during a period of soil drying, such as between the 4th and 30th of July, 1987. To accomplish this, we used the soil water contents obtained from inspection of Figure 4 for seven days during the drying period (July 4th, 10th, 18th, 21st, 22nd, 26th and 30th). We further assume that these days were clear, which was generally not the case except for July

18^{th}, 21^{st} and 22^{nd}. Initial atmospheric conditions for these three days were obtained from the Pittsburgh upper air sounding (200 km from the measurement site) and from local surface weather observations.

Results proved to be insensitive to initial atmospheric conditions but highly sensitive to initial deep layer soil water content. In view of the uncertainty in specifying initial atmospheric conditions (due to the absence of local rawinsonde measurements), we used the initial atmospheric conditions for July 22^{nd} in all simulations except for July 18^{th} and 21^{st}, when field measurements existed for testing the model. Our intention is to investigate the transpiration plateau, showing its evolution on clear days in response to a progressive drying of the soil.

Figure 5 is an example of a simulated decrease in the evapotranspiration as a function of soil water content, which we specify as a function of surface (f) and deep soil (fsub) water contents, expressed as fractions of the field capacity. Note that the two wettest cases are almost identical. Lynn and Carlson (1990) also demonstrated that very little change occurs in the transpiration over corn until the soil water content decreases to half of field capacity. In these simulations an obvious plateau occurs when the root zone soil water content is decreased below 59% of field capacity, which appears after the 18^{th}. A collapse in the transpiration happens when the ground water potential ψ_g is reduced to the threshold leaf water potential ψ_c (-15 bars), which is equivalent to a soil water content of 0.12 by volume (fsub = 0.35).

Evapotranspiration for the two wettest days in Figure 5 also shows a slight flattening near midday as the leaf water potential briefly reaches the threshold potential. Figure 6 suggests that a small plateau was present some time prior to the 18^{th}, possibly as early as July 4^{th}, when the soil water content was 74% of field capacity. Thus, the threshold potential may be reached in relatively well - watered vegetation providing the

atmospheric demand is sufficiently large.

An important aspect of both Figures 2 and 5, which has also been pointed out by Lynn and Carlson (1990), is that the variation in transpiration and radiometric surface temperature of the corn crop canopy is small from day to day when there is no plateau. Once the plateau forms, changes in evapotranspiration and radiometric temperature from one day to the next increase during the time when the plateau is present. By setting b_1 to a value of zero in Eqn. 3 the evapotranspiration curves are virtually identical until the onset of the plateau. Stated alternately, the curves of Figure 5 are all alike before the onset of the plateau because leaf water potential is decoupled from stomatal resistance in the sub - threshold regime ($\psi_e > \psi_c$).

5. Radiometric temperature of the canopy

Radiometric surface temperatures reflect the presence of the transpiration plateau. To remove the variable effects of the atmosphere on radiometric surface temperature, we compute the radiometric surface and ambient air temperature difference. Simulations (Fig. 7) and measurements (Fig. 3) of the T_{ir} - T_{air} differences increase most rapidly with decreasing soil water content during the period of the transpiration plateau. We are unable to explain the reason for the higher and more rapid increase in the measured versus simulated surface minus air temperature differences during this four - day period. While the measured values seem somewhat large, being 1 - 2 °C positive at radiation sunset and sunrise (Fig. 3), it should be noted that measured sensible heat fluxes for both the aerodynamic method and sonic anemometer were in close agreement. The important point, however, are that measurements and simulations exhibit similar response to soil drying, particularly with regard to the midday increase of radiometric surface temperature.

This response of leaf temperature to threshold leaf water potential is evident in simulated T_{ir} - T_{air} throughout the entire drying period (Fig. 8). Largest increases from

day to day occur after the plateau has formed. The two wettest cases, corresponding to 4^{th} and 10^{th} July, show virtually no differences at any time during the day. In the driest case, T_{ir} - T_{air} is at a maximum and corresponds to the evapotranspiration collapse (re: Fig. 5).

As the length of the plateau increases, so does the midday radiometric surface temperature. Figure 9a demonstrates a radiometric temperature increase almost linearly with plateau length. The increase in radiometric surface temperature following July 4^{th} remains less than a degree during the first two weeks. When the plateau length exceeds about 200 minutes, the increase in midday radiometric surface temperature with decreasing soil water content becomes noticeably more rapid with time. Similar behavior is exhibited in the measurements (Fig. 9b), although T_{ir} - T_{air} is larger and the plateau length somewhat shorter than for the simulations.

Simulated and measured T_{ir} - T_{air} versus soil water content are given in Figure 10. Again, the measured radiometric surface temperatures are higher than those simulated, but more importantly, the midday surface radiometric temperature first increases gradually and then considerably more rapidly after July 18^{th}. If one concedes that a reasonable measurement uncertainty for radiometric measurement of a vegetation canopy is at least plus or minus 1°C, Figures 9 and 10 suggest that one is unable to detect a reduction in soil water content below field capacity for a period of at least two weeks after July 4^{th}, by which time the soil water content diminished to about half of its field capacity.

6. Effects of vegetation cover soil and cloud cover

(a) *Vegetation cover*

The effect of bare soil patches is to mask the evapotranspiration plateau. We made simulations in which fractional vegetation cover was varied, while maintaining the same surface and root zone water content values obtained from Figure 4 (Figs. 11a & b).

Increasing the fraction of exposed bare soil causes the plateau to decrease and subsequently vanish when the vegetation cover is reduced to 50% of full cover (Fig. 11a). At 50% vegetation cover, $T_{ir} - T_{air}$ is larger and exhibits a steeper increase with decreasing soil water content than for full vegetation cover (Fig. 11b). Although these changes in temperature for partial vegetation cover are more easily detectable by a radiometer, they represent a mixed signal from both surface and root zone.

(b) *Cloud cover*

In addition, cloud cover also affects the transpiration plateau. A reduction of solar flux due to cloud cover does not produce a corresponding reduction in the transpiration flux. Decreasing the solar flux by as little as 25 %, simulating scattered cloud cover, effectively eliminates the plateau (Fig. 12) and the corresponding rise in $T_{ir} - T_{air}$ (Fig. 13). The disappearance of the water stress signal occurs as a result of a reduction in the solar flux and therefore in the atmospheric demand. Katerji and Hallaire (1984) also show that a reduction in solar demand reduces the decrease in the leaf water potential. A further decrease in soil water content, however, would cause the plateau to reappear for scattered and eventually for broken sky cover, provided that ψ_g is sufficiently low.

7. Conclusions

Although soil moisture limitation constitutes an underlying cause of the evapotranspiration plateau, its onset, duration and shape are determined by a combination of factors, particularly those of atmospheric demand and internal plant constraints. Demand constitutes the incident solar flux and the vapor pressure deficit. The important plant constraint is the threshold leaf water potential, which is necessary for simulating the evapotranspiration plateau. Given that stomatal resistance increases rapidly for decreasing leaf water potential below the threshold, simulations with the plant model indicate an increase in the intensity of solar radiation, a decrease in the ambient relative

humidity or a decrease in soil moisture contribute to an earlier formation and longer duration of the evapotranspiration plateau. Therefore, the evapotranspiration plateau may occur when the soil is relatively moist, providing the atmospheric and solar demand are high. It may not occur when the soil is dry if the demand is weak.

Onset of the evapotranspiration plateau is manifested by an increase in the leaf (radiometric surface) temperature and sensible heat flux. Our simulations suggest that the largest changes in radiometric surface temperatures occur during the period of the plateau, notably near 1300 local time. We show that an increase in radiometric canopy temperature with decreasing soil water content below field capacity is detectable by a radiometer only when the plateau lasts for more than a couple of hours. In the case of a dense corn canopy, detectability begins when the soil water content decreases to about 50% of its field capacity. Since the true wilting point for the corn was about 35% of field capacity (essentially the point at which the soil water potential reaches the threshold leaf water potential), remotely sensing the onset of severe crop water stress may be possible using radiometric surface temperatures.

Finally, we surmise that the evapotranspiration plateau operates to protect the plant against excessive water loss. However, the plateau implies an increase in the leaf temperature, likewise in the vapor pressure deficit between leaf and air, and in stomatal resistance. This would lead to a further destructive escalation in leaf temperature. In view of the adverse effects of such a positive feedback, it seems reasonable to suppose that the evapotranspiration plateau may not constitute a routine and optimum protective strategy for a plant under normal conditions. Rather, we feel that plants have evolved such a survival mechanism in response to their indigenous habitat such that they experienced the evapotranspiration plateau only under conditions of abnormal soil or atmospheric dryness.

Table 1

List of some parameters used in the simulations

Parameter	Value	Units
r_{min}	25	s m^{-1}
ψ_c	-15	bars
b_1	0	s m^{-1} $bars^{-1}$
b_2	500	s m^{-1} $bars^{-1}$
S_c	50	s m^{-1} W^{-1} m^2
Z_p	0.06	bars $(Wm^{-2})^{-1}$

Acknowledgements

The authors would like to thank Jasser El Salem and Richard Thompson for their assistance in taking and processing the measurements. We are also grateful to the following agencies for sponsoring this research, which has tied together three avenues of research, -- surface hydrology, remote sensing and plant science. These agencies are The United States Geological Service, under grant number 14-08-0001-G1490, the National Aeronautics and Space Administration, under grant number NAG 5-919, and the United States Department of Agriculture, Agricultural Research Service, under grant number 58-32U4-8-27.

References

Baldocchi, D.D., R.J. Luxmoore and J.L. Hatfield, 1990: Canopy stomatal conductance discerning the forest from the trees: An essay on scaling canopy stomatal conductance. Ag. and Forest Meteor. (in press).

Belles, J.E., 1990: Calculation of the surface sensible heat flux from the bulk aerodynamic method using a thermal radiometer. M.S. Thesis, Dept. of Meteorology, Penn State University, 80 pp.

Boyer, J.S., 1988: Water potential and plant metabolism: Comments on Dr. J.P. Kramer's article Changing concepts regarding plant water relations. Vol. II, No. 7, pp. 565-568 and Dr. J.B. Passioura's response, pp. 569-571, Plant, Cell and Environment, 12, 213-216.

Carlson, T.N., 1986: Regional-scale estimates of surface moisture availability and thermal inertia using remote thermal measurements. Remote Sensing Reviews, 1, 197-247.

Carlson, T.N., E.M. Perry, T.J. Schmugge, 1990: Remote estimation of soil moisture availability and fractional vegetation cover for agricultural fields. Ag. and Forest Meteor. (in press).

Carlson, T.N. and B. Lynn, 1990: The effects of plant capacitance in a boundary layer model. Submitted to Ag. and Forest Meteor.

Cosby, B.J., G.M. Hornberger, R.B. Clapp and T.R. Ginn, 1984: A statistical exploration of the relationships of soil moisture characteristics to the physical properties of soils. Water Resources Res., 20, 682-690.

Cowan, I.R., 1965: Transport of water in the soil-plant-atmosphere system. J. Appl. Ecol., 2, 221-239.

Fisher, M.J., D.A. Charles Edwards and M. Ludlow, 1981: An analysis of the effects of repeated short-term soil water deficits on stomatal conductance to carbon dioxide and leaf photosynthesis by the legume macroptilium atropurpureum cv. stratro. Aust. J. Plant Physiol., 8, 347-357.

Frensch, J. and E.-D. Schulze, 1988: The effect of humidity and light on cellular water relations and diffusion conductance of leaves of Tradescantia Virginiana L., Planta, 173, 554-562.

Gollan, T., J.B. Passioura and R. Munns, 1986: Soil water stratus affects the stomatal conductance of fully turgid wheat and sunflower leaves. Aust. J. Plant Physiol., 13, 459-464.

Jones, H.G., 1983: Plants and Microclimate, Cambridge University Press, New York, 323 pp.

Katerji, N. and M. Hallaire, 1984: Les grandeurs de reference utilisables dans l'etude de l'alimentation en eau des cultures, Agronomie, 4, 999-1008.

Kramer, P.J., 1988: Changing concepts regarding plant/water relations. Plant, Cell and Environment, 11, 565-568.

Lynn, B. and T.N. Carlson, 1990: A model illustrating plant versus external control of transpiration. Ag. and Forest Meteor. (in press).

Mascart, P., O. Taconet, J.-P. Pinty and M. Ben Hebrez, 1990: Canopy resistance formulation and its effect on mesoscale models: A HAPEX perspective. Ag. and Forest Meteor. (in press).

Munns, R. and R.W. King, 1988: Abscisic acid is not the only stomatal inhibitor in the transpiration stream of wheat plants. Plant Physiol., 88, 703-708.

Nizinski, J. and B. Saugier, 1989: A model of transpiration and soil-water balance for a mature oak forest. Ag. and Forest Meteor., 47, 1-17.

Passioura, J.B., 1988: Response to Dr. P.J. Kramer's article Changing concepts regarding plant water relations, Vol. 11, No. 7, pp. 565-568, Plant, Cell and Environment, 11, 569-571.

Rochette, P., E. Pattey, R.L. Despardius, L.M. Dwyer and D.W. Stewart, 1990: Estimation of maize (zea mays L.) canopy conductance by scaling-up leaf stomatal conductance. Ag. and Forest Meteor. (in press).

Schulze, E.,D., N.C. Turner, T. Gollan and K.A. Shackel, 1987: Stomatal response to air humidity and to soil drought. Stomatal function, Zeiger, Farquhar and Cowan (eds.), Stanford University Press, Ch. 14, 311-321.

Sellers, P.J. and J.L. Dorman, 1987: Testing the simple biosphere model (SiB) using point micrometeorological biophysical data. J. Clim. and Appl. Meteor., 26, 622-651.

Taconet, O., T.N. Carlson, R. Bernard, D. Vidal-Madjar, 1986: Evaluation of a surface/vegetation model using satellite infrared surface temperatures. J. Clim. Appl. Meteor., 25, 1752-1767.

Turner, N.C., 1970: Response of adaxial and abaxial stomata to light. New Phytol., 69, 647-653.

Turner, N.C., 1974: Stomatal behavior and water status of maize, sorghum and tobacco under field conditions. II at low-soil water potential. Plant Physiol., 53, 360-365.

Wetzel, P.J. and J.-T. Chang, 1987: Concerning the relationship between evapotranspiration and soil moisture. J. Clim. and Appl. Meteor., 26, 18-27.

LIST OF FIGURES

Figure 6. Volumetric root zone water content (fsub; fraction of field capacity) versus length of the evapotranspiration plateau (min) for simulations of hypothetical clear sky days (squares) and for measurements (crosses). Numbers aside data points denote the dates in July 1987.

Figure 7. Simulated surface radiometric minus air temperature differences (°C) versus time for three days in July 1987 (see legend) for soil water contents obtained from Figure 4.

Figure 8. Simulated radiometric surface minus air temperatures differences (°C) with time for the five idealized clear sky days shown in Figure 5.

Figure 9a. Surface radiometric air temperature differences (°C) at 1300 local time versus length of the evapotranspiration plateau (min) for simulations (solid line and squares). Numbers refer to dates of hypothetical clear sky days in July 1987.

Figure 9b. Same as Figure 9a but a comparison of measured (dashed line and crosses) and simulated (solid line and squares) evapotranspiration plateau lengths.

Figure 10. Radiometric surface minus air temperature differences (°C) at 1300 local time versus root zone volumetric water content (cm^3/cm^3) for simulations (lower curve) and measurements (upper curve).

Figure 11a. Simulated variation of evapotranspiration fluxes (Wm^{-2}) versus time for differing fractional vegetation cover.

Figure 11b. Radiometric surface minus air temperature differences (°C) at 1300 local time versus root zone volumetric water content (cm^3/cm^3) for full vegetation cover (lower curve) and 50% vegetation cover (top curve). Numbers refer to dates of idealized clear sky days in July 1987.

Figure 12. Radiometric surface minus air temperature differences (°C) versus fractional root zone water content (fsub) simulated for 100% and 50% fractional vegetation cover using initial atmospheric conditions of 22nd July 1987.

Figure 13. Simulated evapotranspiration fluxes (Wm^{-2}) versus time for clear, scattered and broken sky cover; these conditions correspond, respectively, to full sun, 25% and 40% reduction in solar flux using initial atmospheric conditions of 22nd July 1987.

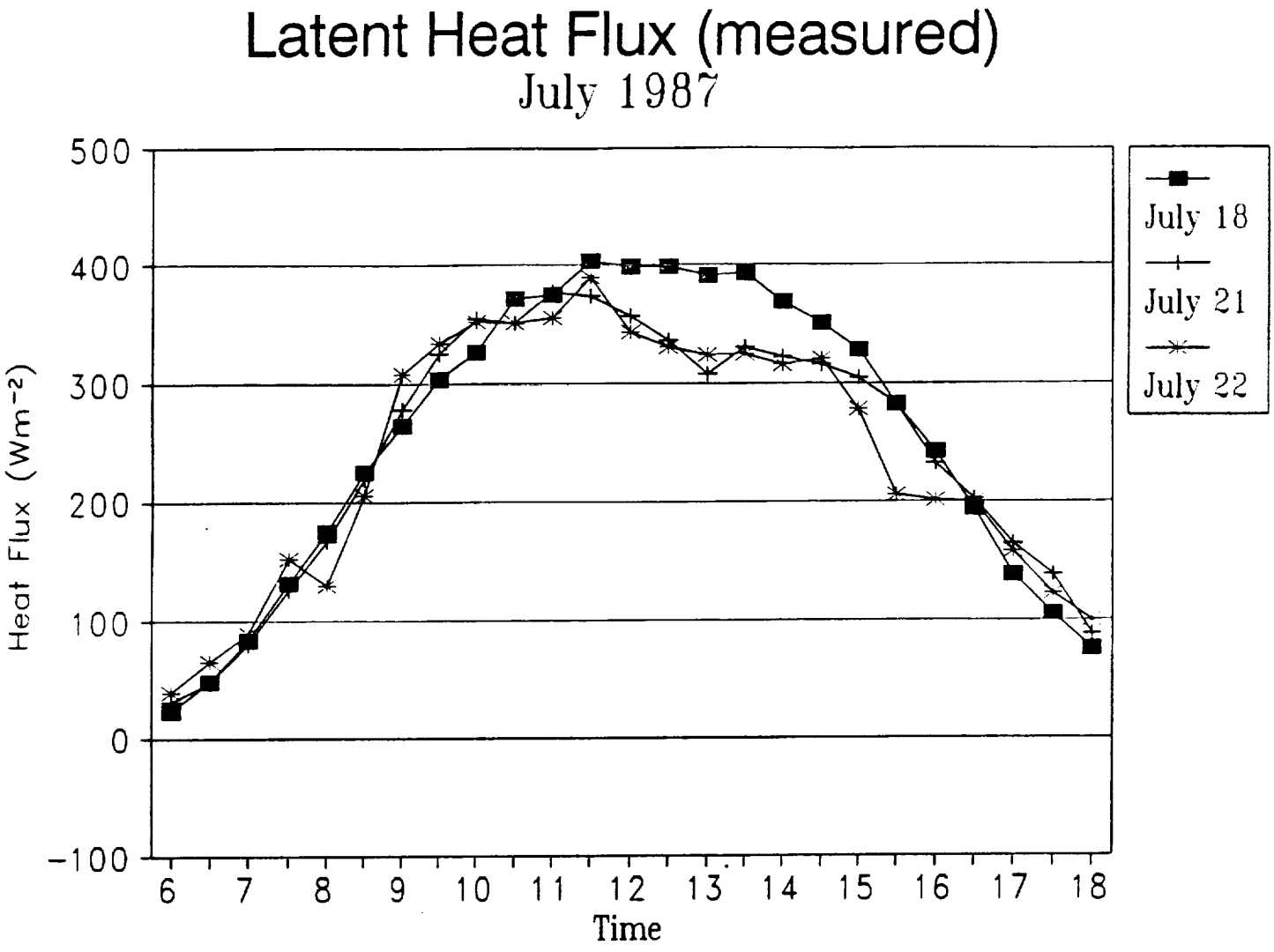

Figure 2. Measured evapotranspiration fluxes (Wm^{-2}) versus time for 18th, 21st and 22nd July, 1987.

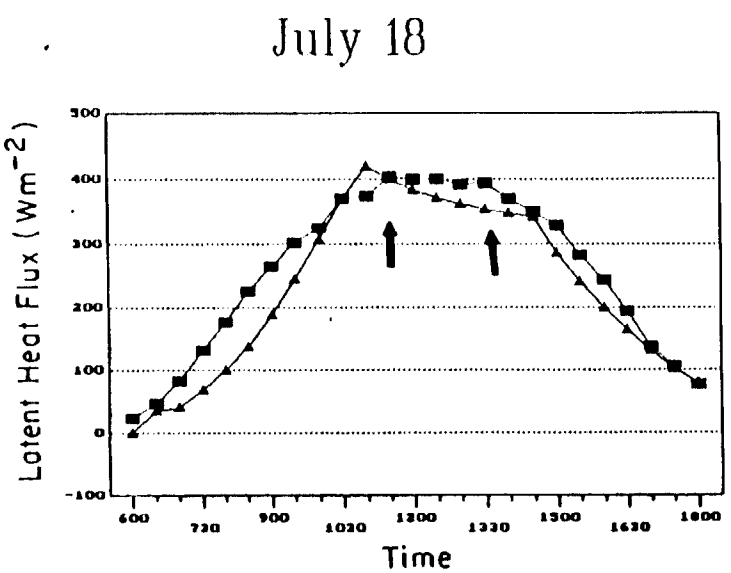

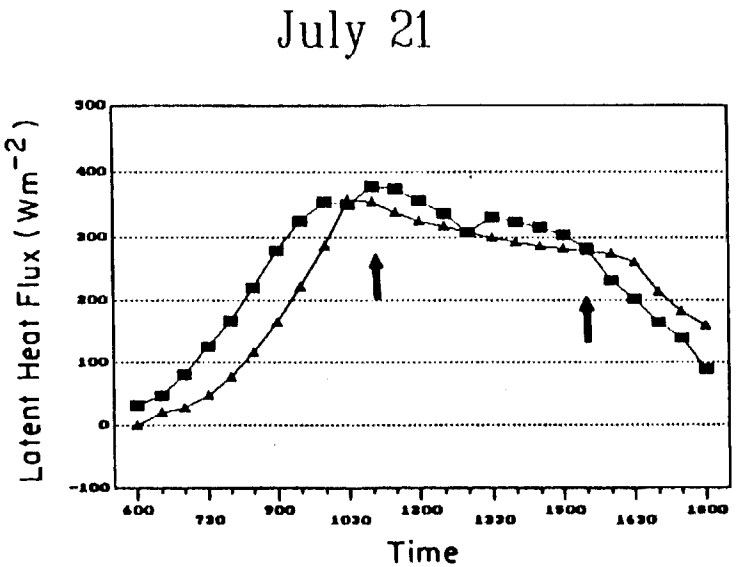

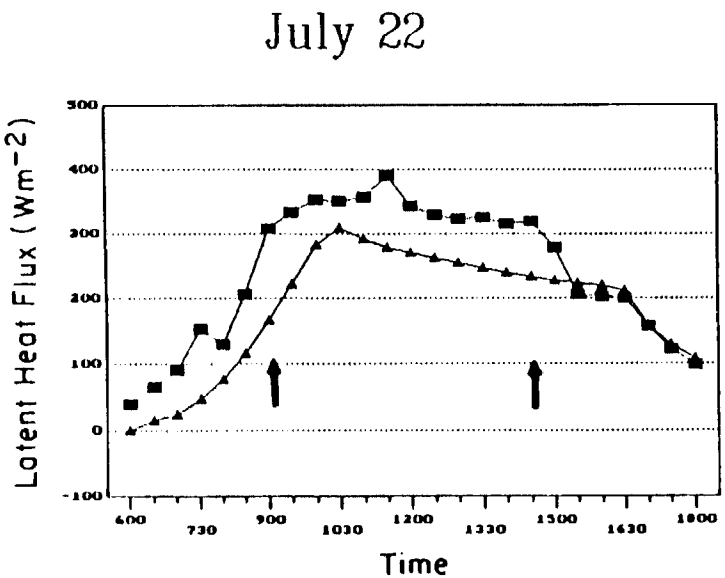

Figure 1. The measured latent heat (evapotranspiration) fluxes (Wm^{-2}; squares) from aerodynamic method (over corn; leaf area index = 7.19) based on the surface radiometric temperatures at Rock Springs, 18th, 21st and 22nd July, 1987 and the simulated fluxes (triangles) for the same days. Vertical arrows denote duration of the evapotranspiration plateau in the measurements.

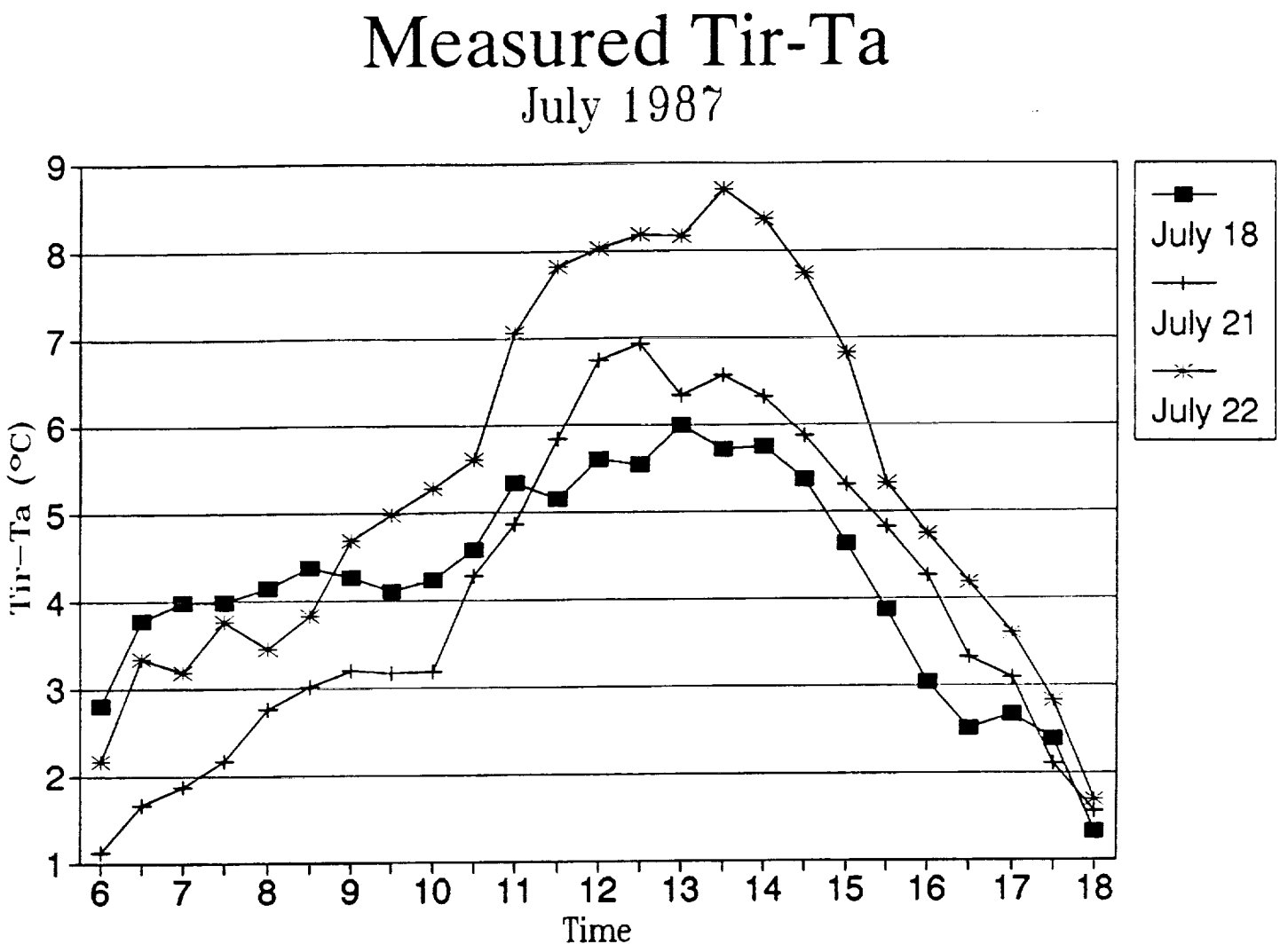

Figure 3. Measured surface radiometric minus air temperature differences (°C) versus time for 18th, 21st and 22nd July, 1987.

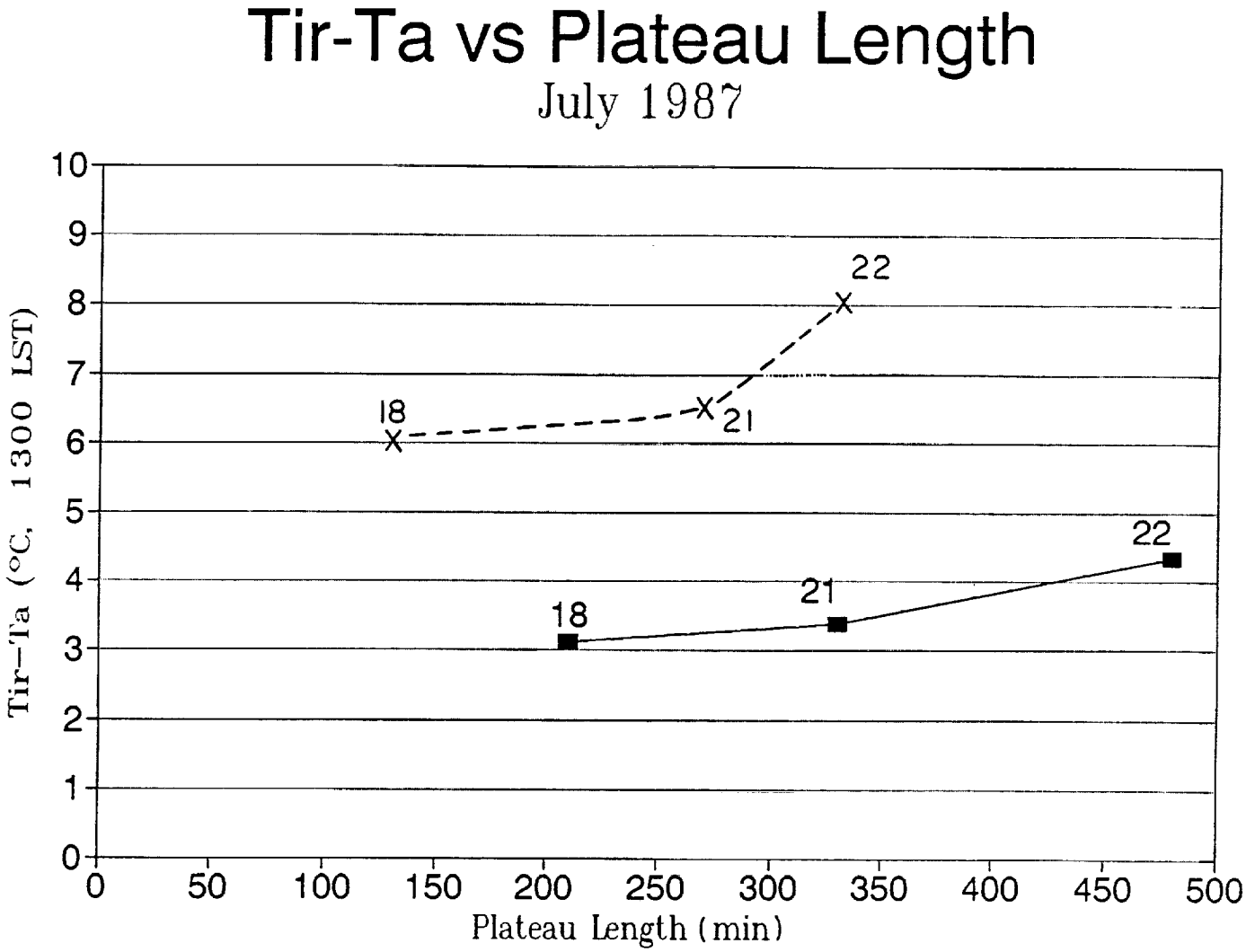

Figure 9b. Same as Figure 9a but a comparison of measured (dashed line and crosses) and simulated (solid line and squares) evapotranspiration plateau lengths.

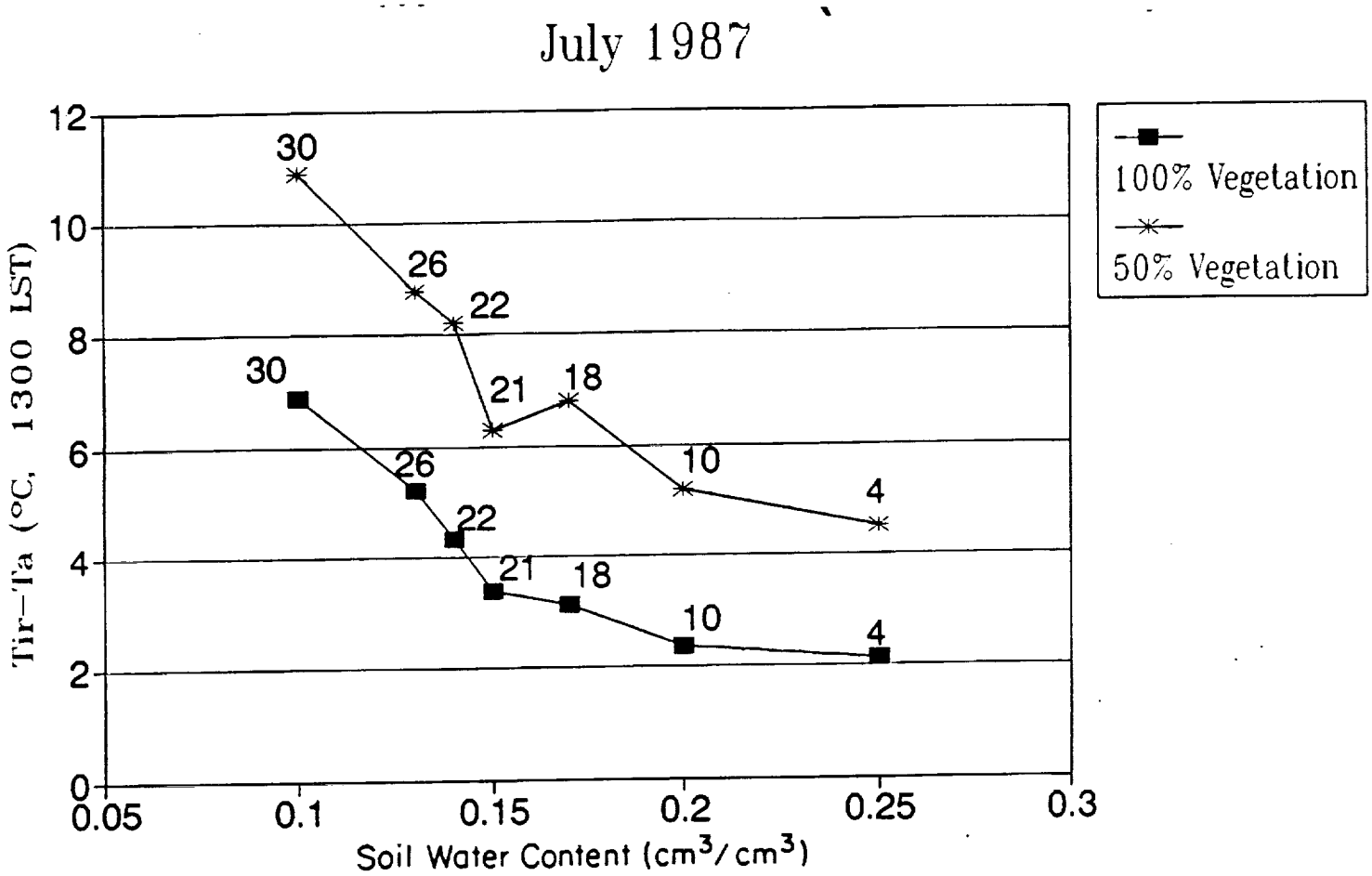

Figure 11b. Radiometric surface minus air temperature differences (°C) at 1300 local time versus root zone volumetric water content (cm^3/cm^3) for full vegetation cover (lower curve) and 50% vegetation cover (top curve). Numbers refer to dates of idealized clear sky days in July 1987.

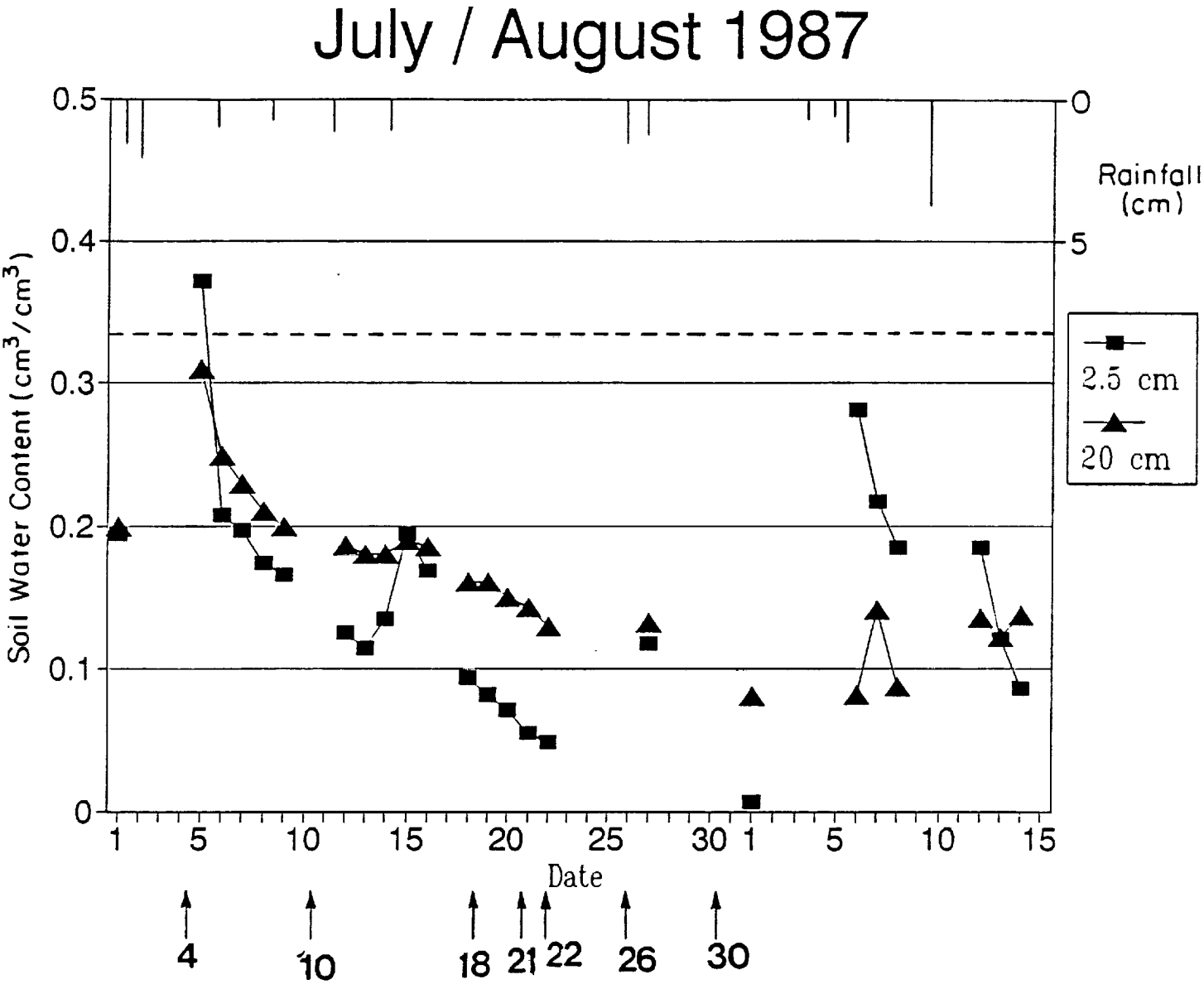

Figure 4. Volumetric soil water content at 0700 local time during July 1987 as measured by gypsum blocks at depths of 2.5 cm (squares) and at 20 cm (triangles). The dashed horizontal line denotes the volumetric field capacity for the soil and the hanging bars are proportional to the daily rainfall, which is measured against the scale in centimeters at the right. Vertical arrows along horizontal scale indicate dates in July as referred to in the text.

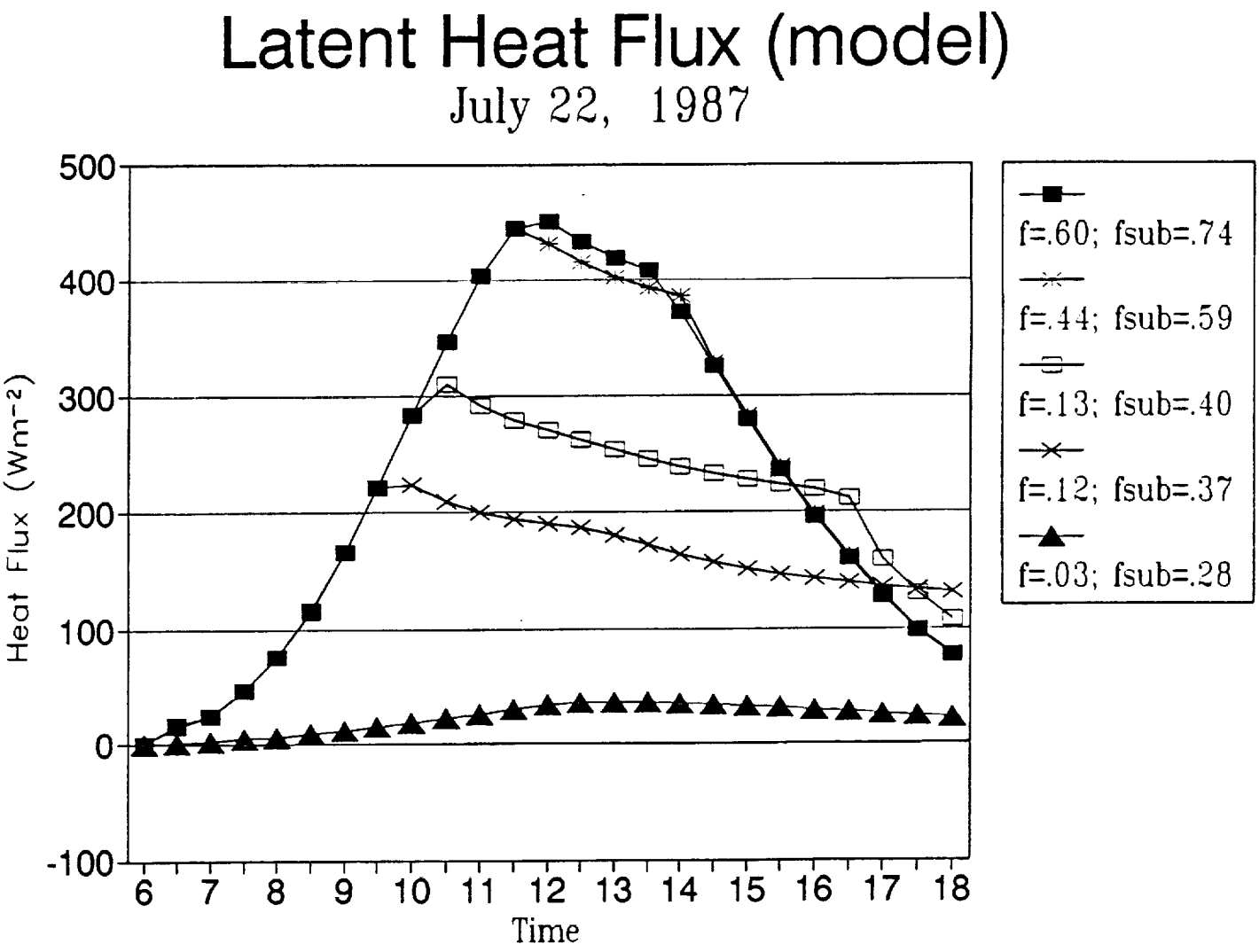

Figure 5. Simulated evapotranspiration fluxes (Wm^{-2}) versus time but for differing surface and root zone soil water concentrations obtained from Figure 4 (legend shows surface (f) and root zone (fsub) water contents expressed as fractions of the field capacity, which is 0.34 by volume). From top to bottom these curves represent hypothetical clear sky days: July 4th, 10th, 22nd, 26th and 30th. (All initial atmospheric conditions pertain to July 22nd.)

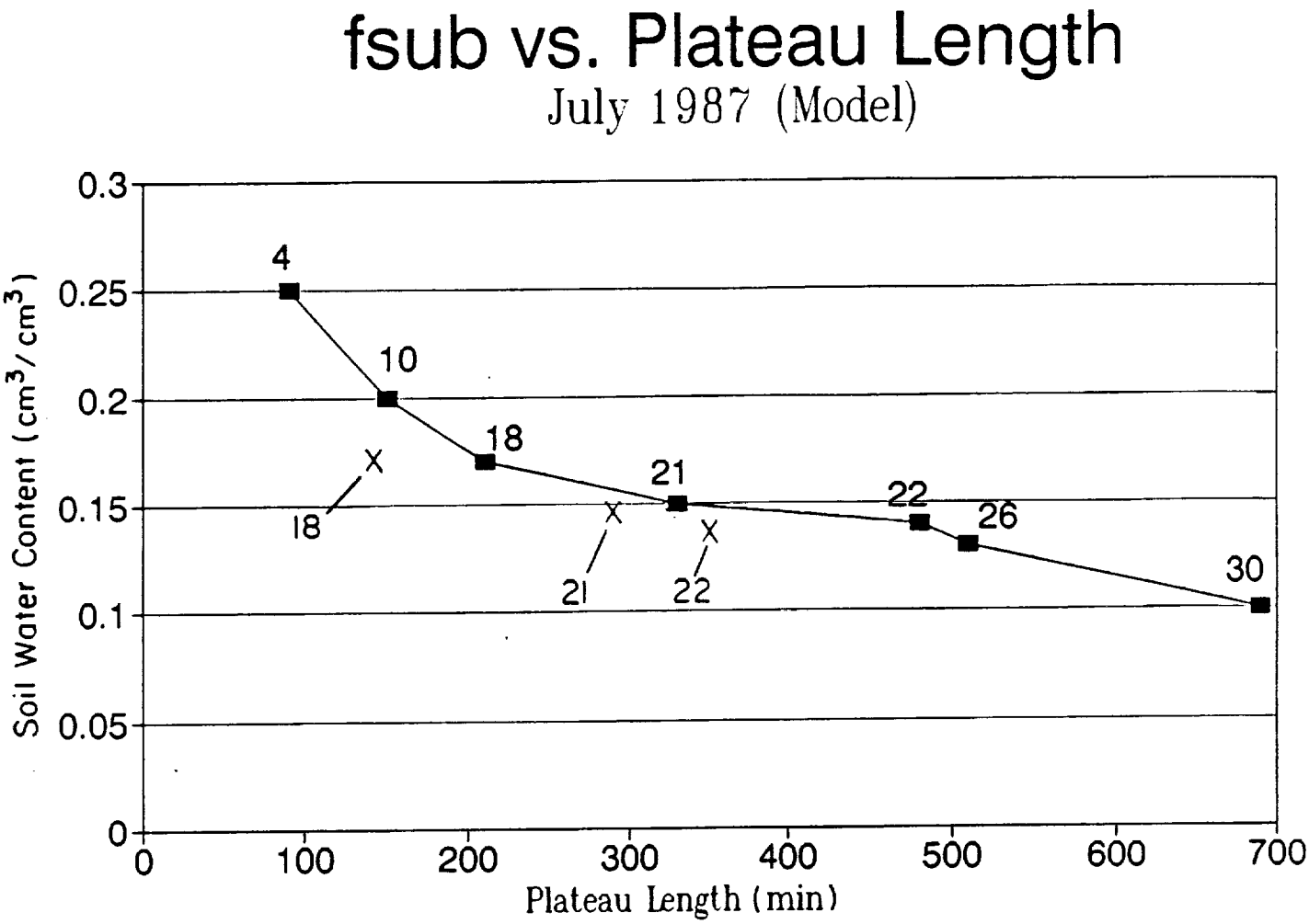

Figure 6. Volumetric root zone water content (fsub; fraction of field capacity) versus length of the evapotranspiration plateau (min) for simulations of hypothetical clear sky days (squares) and for measurements (crosses). Numbers aside data points denote the dates in July 1987.

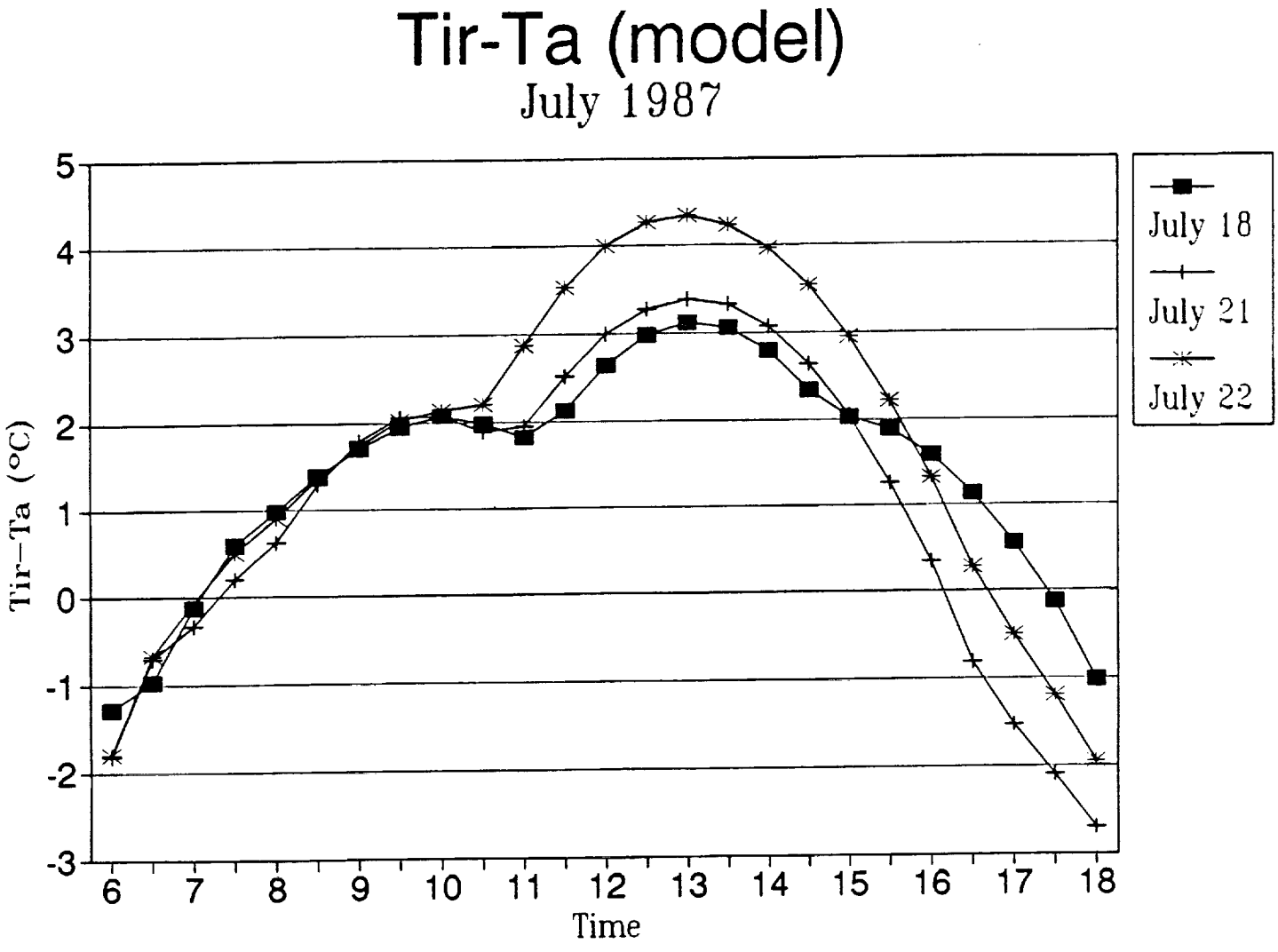

Figure 7. Simulated surface radiometric minus air temperature differences (°C) versus time for three days in July 1987 (see legend) for soil water contents obtained from Figure 4.

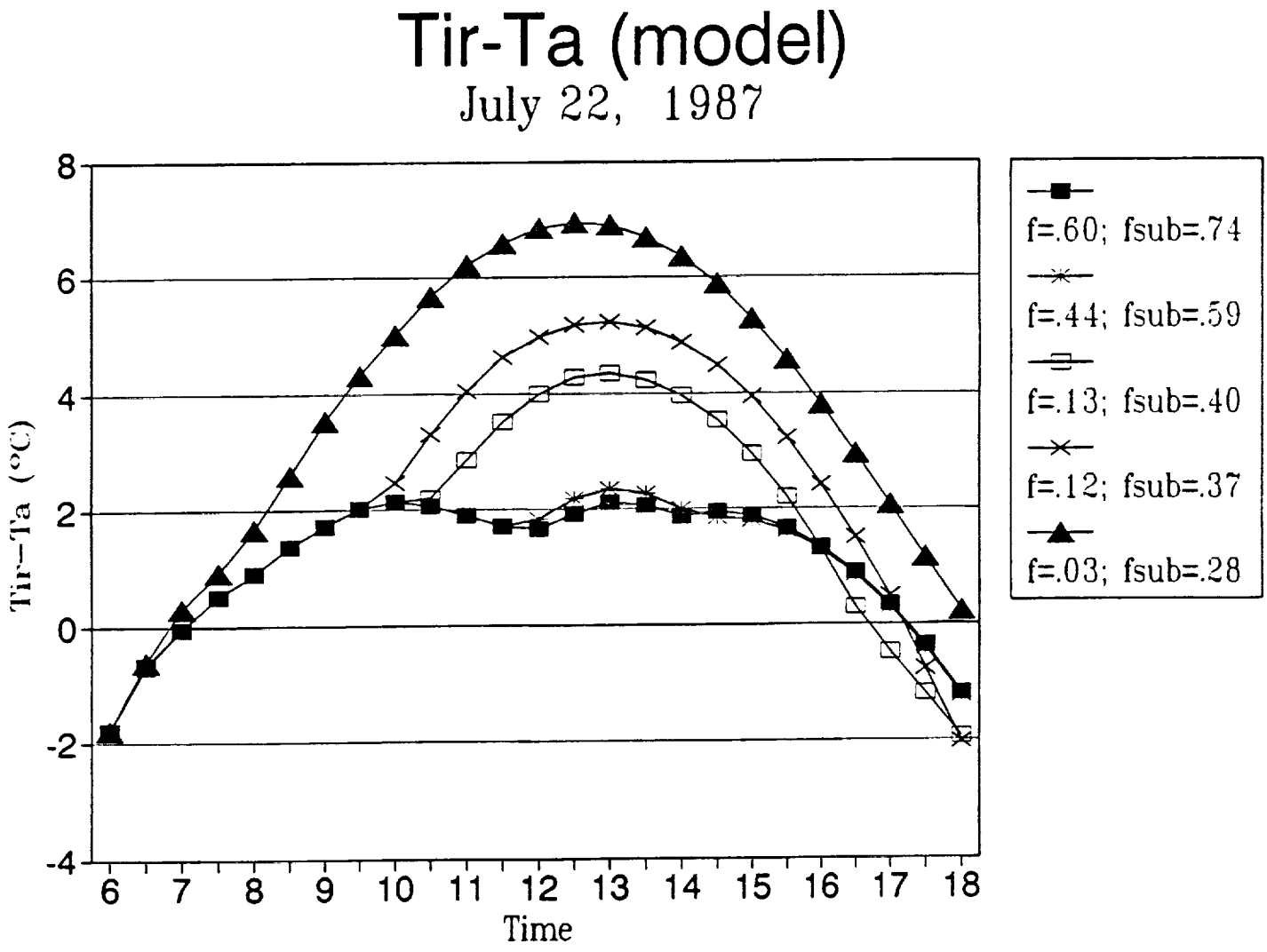

Figure 8. Simulated radiometric surface minus air temperatures differences (°C) with time for the five idealized clear sky days shown in Figure 5.

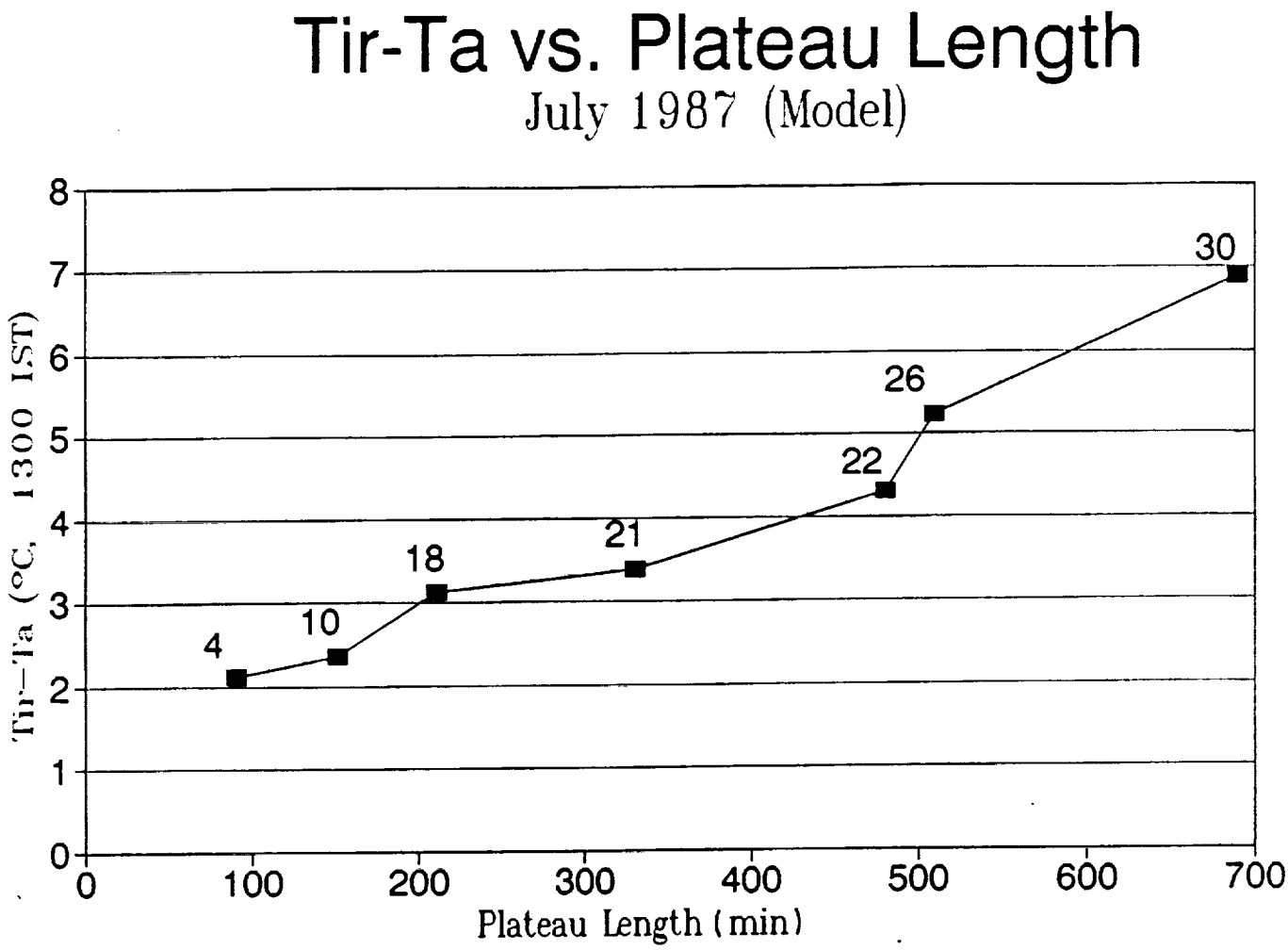

Figure 9a. Surface radiometric air temperature differences (°C) at 1300 local time versus length of the evapotranspiration plateau (min) for simulations (solid line and squares). Numbers refer to dates of hypothetical clear sky days in July 1987.

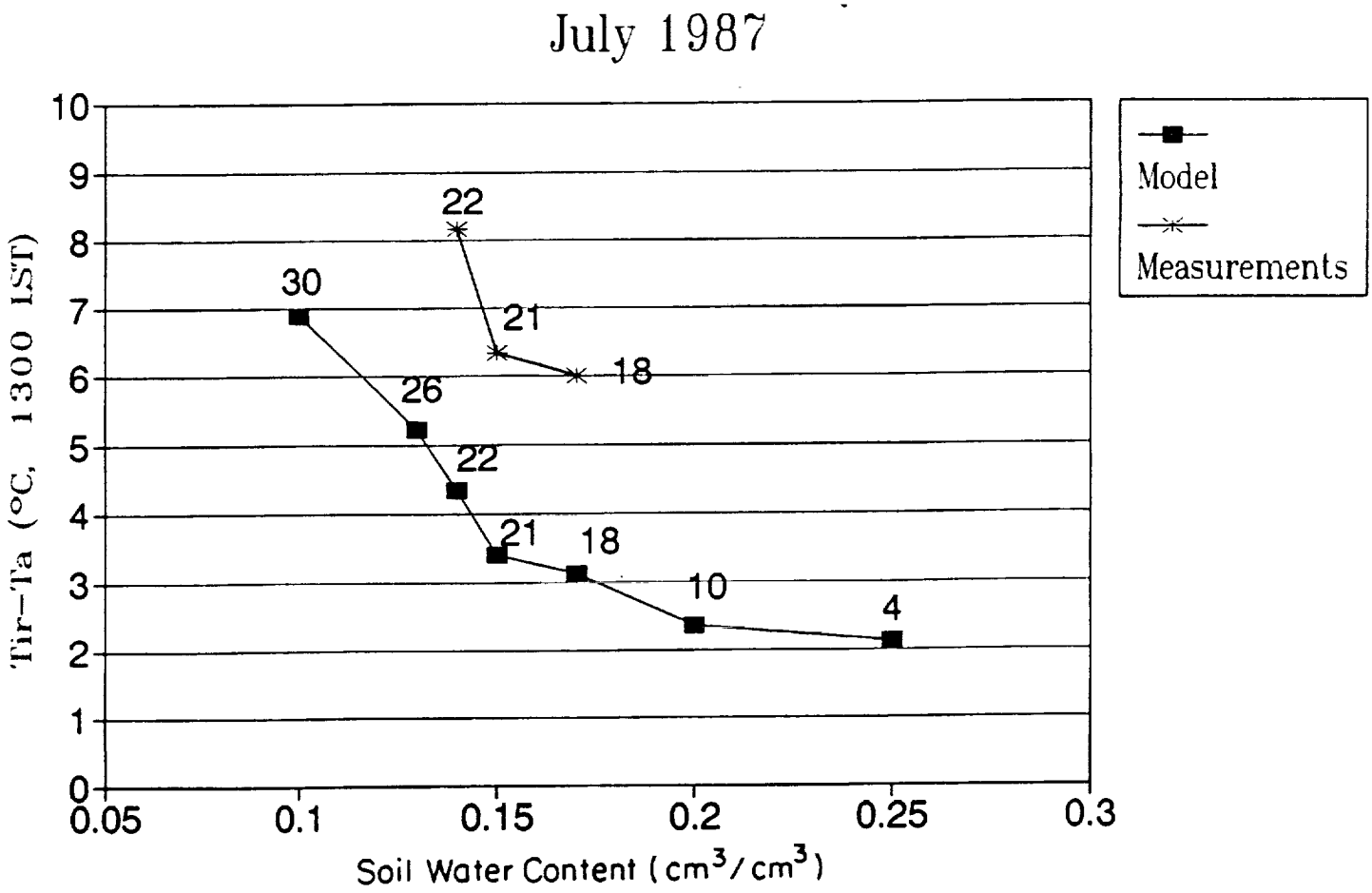

Figure 10. Radiometric surface minus air temperature differences (°C) at 1300 local time versus root zone volumetric water content (cm^3/cm^3) for simulations (lower curve) and measurements (upper curve).

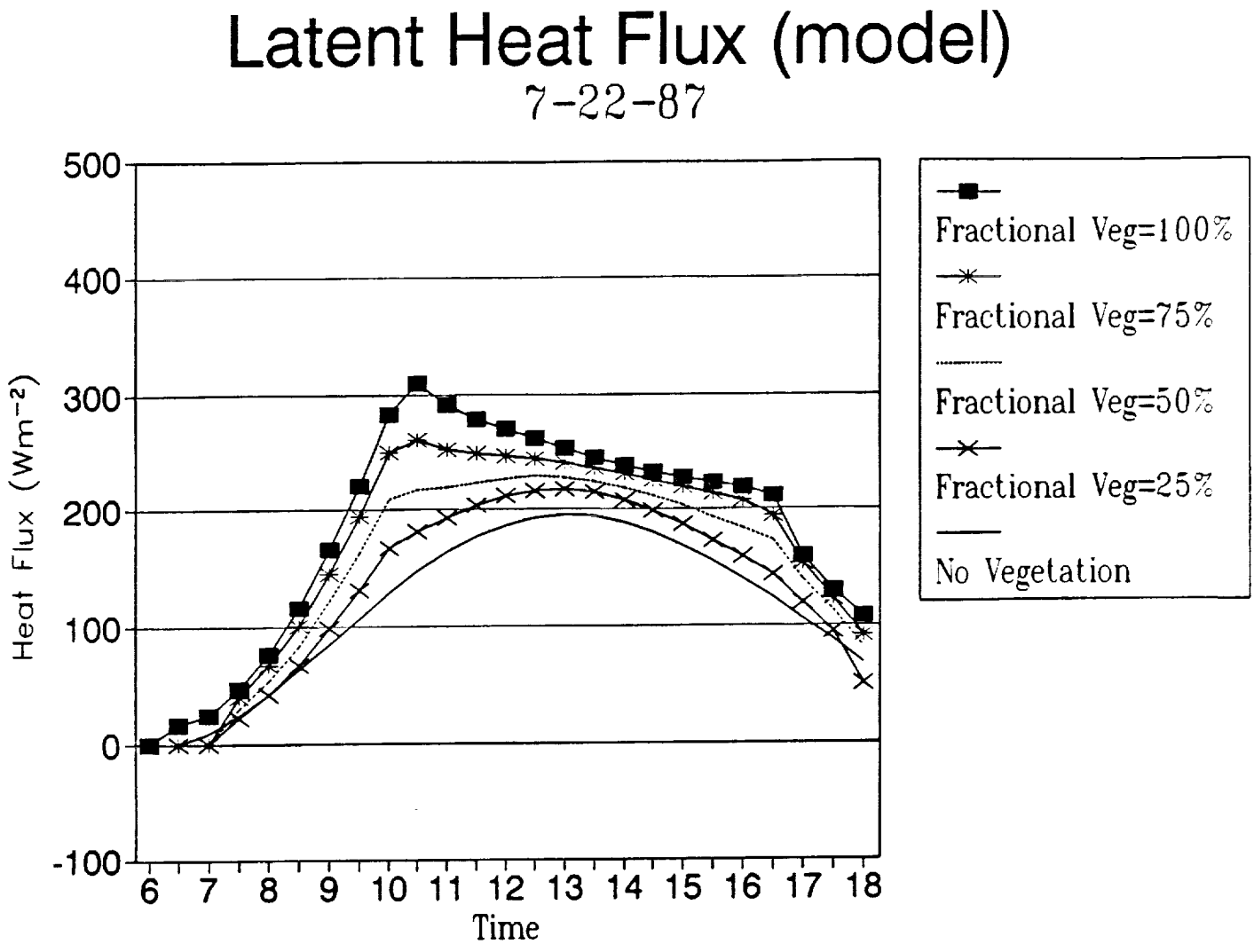

Figure 11a. Simulated variation of evapotranspiration fluxes (Wm^{-2}) versus time for differing fractional vegetation cover.

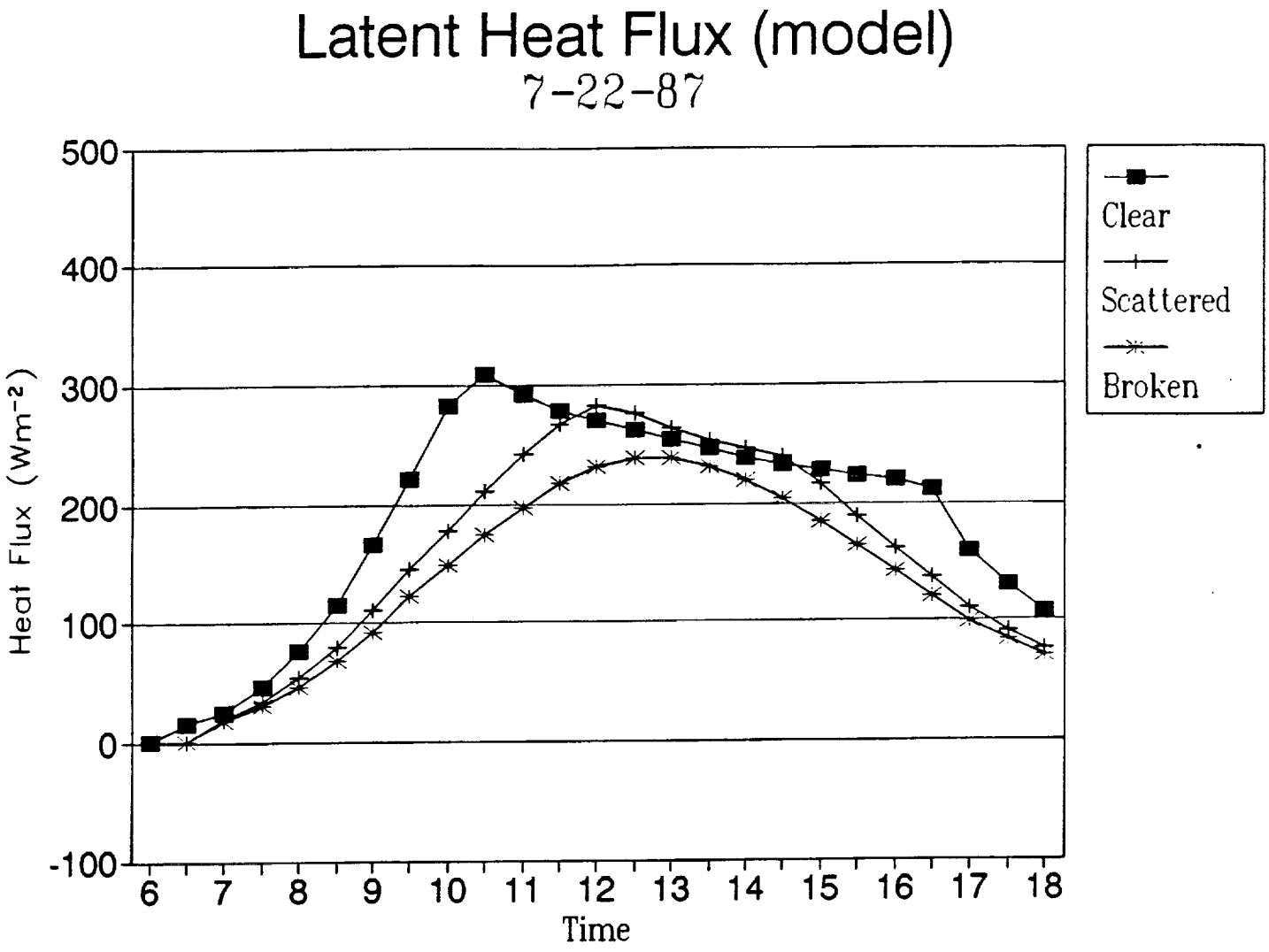

Figure 12. Radiometric surface minus air temperature differences (°C) versus fractional root zone water content (fsub) simulated for 100% and 50% fractional vegetation cover using initial atmospheric conditions of 22nd July 1987.

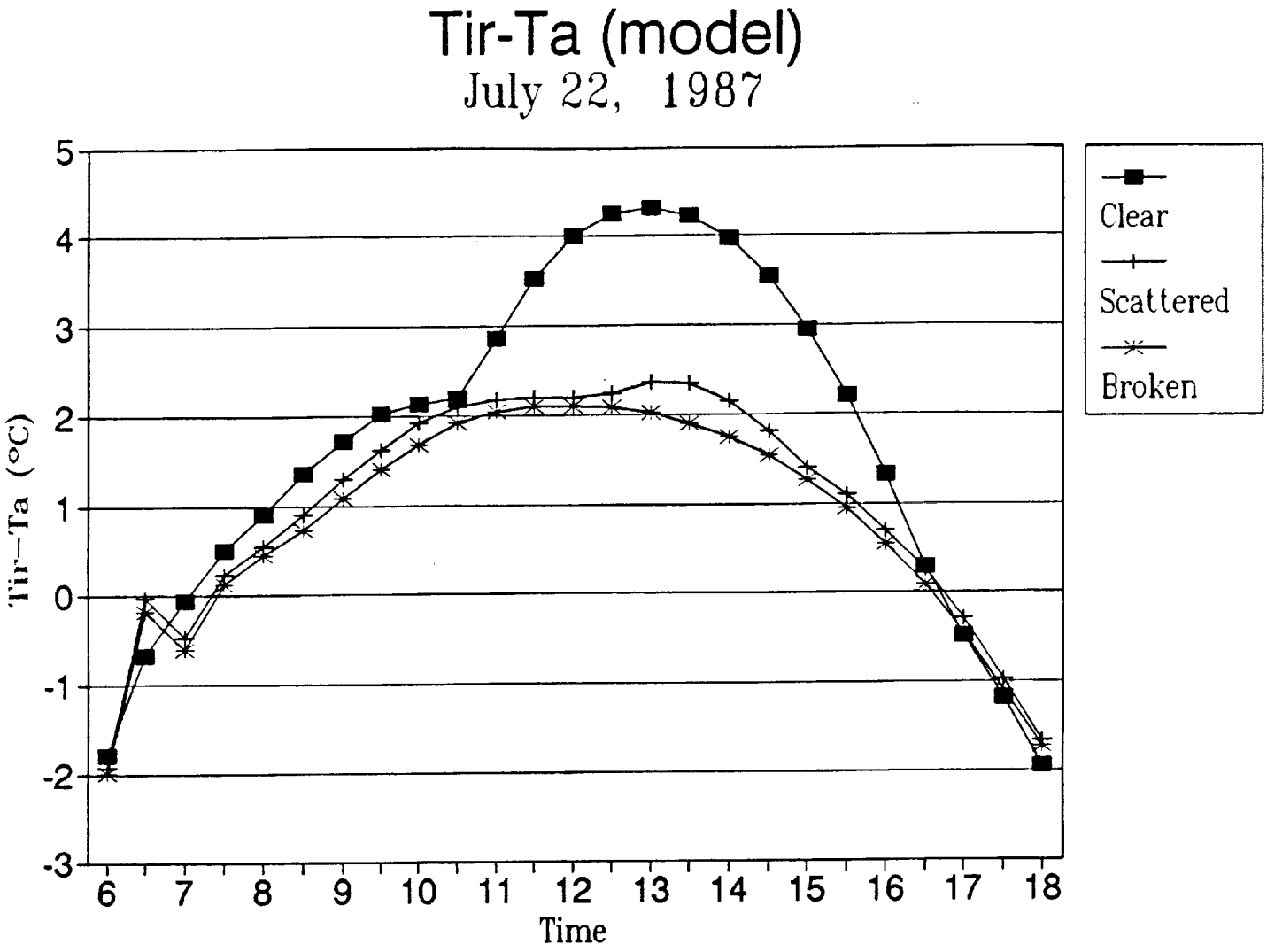

Figure 13. Simulated evapotranspiration fluxes (Wm^{-2}) versus time for clear, scattered and broken sky cover; these conditions correspond, respectively, to full sun, 25% and 40% reduction in solar flux using initial atmospheric conditions of 22nd July 1987.